SYNTHESIS OF NEW, SINGLE-ISOMER QUATERNARY AMMONIUM DERIVATIVES OF β-CYCLODEXTRIN FOR ELECTROPHORETIC ENANTIOMER SEPARATIONS

A Dissertation

by

KINGSLEY C. I. NZEADIBE

Submitted to the Office of Graduate Studies of
Texas A&M University
in partial fulfillment of the requirements for the degree of

DOCTOR OF PHILOSOPHY

May 2006

Major Subject: Chemistry

SYNTHESIS OF NEW, SINGLE-ISOMER QUATERNARY AMMONIUM DERIVATIVES OF β-CYCLODEXTRIN FOR ELECTROPHORETIC ENANTIOMER SEPARATIONS

A Dissertation

by

KINGSLEY C. I. NZEADIBE

Submitted to the Office of Graduate Studies of
Texas A&M University
in partial fulfillment of the requirements for the degree of

DOCTOR OF PHILOSOPHY

Approved by:

Chair of Committee,	Gyula Vigh
Committee Members,	Manuel P. Soriaga
	Ronald D. Macfarlane
	Suryakant Waghela
Head of Department,	Emile A. Schweikert

May 2006

Major Subject: Chemistry

ABSTRACT

Synthesis of New, Single-Isomer Quaternary Ammonium Derivatives of β-Cyclodextrin
for Electrophoretic Enantiomer Separations. (May 2006)
Kingsley C. I. Nzeadibe, B.S., University of Oklahoma;
M.S., Louisiana Tech University
Chair of Adversory Committee: Dr. Gyula Vigh

The isolation of individual enantiomers of drugs is an important subject of interest in the pharmaceutical and medical fields, because stereochemistry can have a significant effect on the biological activity of the drug. Therefore, it is important to develop enantiomeric separation methods for the determination of the optical purity of drugs, since the undesired enantiomer is regarded as one of the impurities.

The available single isomer anionic cyclodextrins (CD) can resolve the enantiomers of only a few weakly acidic analytes. To rectify this problem, the chloride salts of heptakis(6-deoxy-6-morpholinio)-cyclomaltoheptaose (HMBCD), and mono(6-deoxy-6-*N,N,N′,N′,N′*-pentamethylethylenediammonio)-cyclomaltoheptaose (PEMEDA-BCD), the first members of the permanently charged, single-isomer cationic cyclodextrin family, have been synthesized. The purity of process intermediates and final products was determined by HPLC-ELSD and indirect UV-detection capillary electrophoresis. Structural identity was verified by 1D and 2D NMR and mass spectrometry.

Both cationic CD derivatives have been used for the separation of the enantiomers of strong acid, weak acid, weak base, ampholytic, and neutral analytes by capillary electrophoresis. Because the charge state of these cationic chiral resolving agents is independent of the pH of the buffer, separation could be performed in both low and high pH buffers without compromising the charge density of the resolving agent. Contrary to expectation, the multiply charged HMBCD showed poor complexation with the newly synthesized strong electrolyte test analytes. The weak binding between the analytes and HMBCD resulted in separation of enantiomers of only three strong electrolyte analytes. Strong complexation was observed between PEMEDA-BCD and the anionic and nonionic analytes in both low and high pH buffers, though complexation was stronger in the high pH buffer. Due to strong complexation between the anions and PEMEDA-BCD, only low concentrations of the resolving agent were required to effect good enantiomer resolutions.

To my wife Chinyere, whose unwavering support has helped me to accomplish this work, and my three children for their unprecedented understanding through the duration of this work. To my mother, Felecia, for the sacrifices you made to put me through secondary school, and to my late father, Benjamin, for instilling values of education in me.

ACKNOWLEDGEMENTS

First of all, I thank God for all his blessings. I thank all the people from the chemistry department who helped me to make this work possible. Steven Silber, Shane Tichy, and Vanessa Santiago will always be remembered for their enormous help. Thanks to my friend and colleague Shulan Li, and the rest of my group members, Ivan Spanik, Brent Busby, Adriana Salinas, Silvia Sanchez-Vindas, Sanjiv Lalwani, Ann Hwang, Evan Shaves. Peniel Lim, Omar Maldonando, Neillie Fleisher, Brian Sinajon, Roy Estrada, Edward Tutu, and Robert North, without whom this work may not have been completed. I would like to thank members of my graduate committee, Dr. Soriaga, Dr. Macfarlane, Dr. Waghela, and Dr. Rathore, for your time, interest and encouragement. Finally, without reservation, I express my gratitude to my advisor Dr. Gyula Vigh for his time and patience, and everything he did for me to realize my dreams.

TABLE OF CONTENTS

Page

ABSTRACT iii

DEDICATION v

ACKNOWLEDGEMENTS vi

TABLE OF CONTENTS vii

LIST OF FIGURES x

LIST OF TABLES xv

CHAPTER

I INTRODUCTION 1

1.1 Chirality 1
1.2 Principles of Capillary Electrophoresis 2
1.3 Enantioresolution and Cyclodextrins 4
1.4 Single-isomer Charged Cyclodextrins 7
1.5 Enantioseparation with Cationic Cyclodextrins 10

II SYNTHESIS AND CHARACTERIZATION 17

2.1 Materials and General Methods 17
2.2 Synthesis and Characterizations of HMBCD 19
  2.2.1 Heptakis(6-deoxy-6-iodo)-β-cyclodextrin 19
  2.2.2 Heptakis(6-deoxy-6-morpholino)-β-cyclodextrin 28
  2.2.3 Heptakis(6-deoxy-6-morpholinio)-β-cyclodextrin Iodide 37
  2.2.4 Heptakis(6-deoxy-6-morpholinio)-β-cyclomaltoheptaose Chloride (HMBCD) 40
2.3 Synthesis and Characterization of PEMEDA-BCD 46
  2.3.1 Synthesis of *p*-Toluenesulfonyl Anhydride (Ts_2O) 46
  2.3.2 Mono(6-*O*-tosyl)-β-cyclodextrin 47
  2.3.3 Mono(6-deoxy-6-pyridinium)-β-cyclodextrin (CDP) 56
  2.3.4 Mono(6-deoxy-6-*N,N,N’,N’,N’*-pentamethylethylenediamino)-β-cyclodextrin 61
  2.3.5 Mono(6-deoxy-6-*N,N,N’,N’,N’*-pentamethylethylenediammonio)-β-cyclodextrin Iodide 67

CHAPTER Page

- 2.3.6 Mono(6-deoxy-6-*N,N,N',N',N'*-pentamethylethylenediammonio)-cyclomaltoheptaose Chloride (PEMEDA-BCD) 74
- 2.4 Synthesis of Anionic Analytes 76
- 2.5 Summary of Synthesis Methods 83

III SEPARATION OF ENANTIOMERS 84

- 3.1 Separations with HMBCD 85
  - 3.1.1 Materials 85
  - 3.1.2 CE Conditions 86
  - 3.1.3 Methods 86
  - 3.1.4 Results and Discussion 91
    - 3.1.4.1 Separation of the Enantiomers of Strong Electrolyte Analytes with HMBCD 103
    - 3.1.4.2 Separation of the Enantiomers of Weak Acids with HMBCD 105
- 3.2 Separations with PEMEDA-BCD 108
  - 3.2.1 Materials 108
  - 3.2.2 Capillary Electrophoretic Methods 109
  - 3.2.3 Results and Discussion 113
    - 3.2.3.1 Separation of the Enantiomers of Strong Electrolyte Analytes with PEMEDA-BCD in Low pH BEs 114
    - 3.2.3.2 Separation of the Enantiomers of Weak Acid Analytes with PEMEDA-BCD in Low pH BEs 122
    - 3.2.3.3 Separation of the Enantiomers of Nonionic Analytes with PEMEDA-BCD in Low pH BEs 124
    - 3.2.3.4 Separation of the Enantiomers of Weak Base Analytes with PEMEDA-BCD in Low pH BEs 129
    - 3.2.3.5 Separation of the Enantiomers of Weak Acid Analytes with PEMEDA-BCD in High pH BEs 134
    - 3.2.3.6 Separation of the Enantiomers of Ampholytic Analytes with PEMEDA-BCD in High pH BEs 142
    - 3.2.3.7 Separation of the Enantiomers of Nonionic Analytes with PEMEDA-BCD in High pH BEs 150
  - 3.2.4 Comparison of Separation of Enantiomers with HMBCD and PEMEDA-BCD BEs 156

IV CONCLUSIONS 159

REFERENCES 164

Page

APPENDIX 171

VITA 183

LIST OF FIGURES

FIGURE Page

1 Peak resolution surfaces for 7-charged and 14-charged cyclodextrins as a function of separation selectivity and normalized electroosmotic flow 11

2 Synthesis scheme for heptakis(6-deoxy-6-morpholinio)-β-cyclodrxtrin chloride (HMBCD) 21

3 Chromatograms of intermediate compound (2) 22

4 ^{1}H NMR spectra in DMSO-d_6, using a 500 MHz NMR spectrometer, during purification of intermediate compound (2) 23

5 ^{1}H-^{1}H COSY of intermediate compound (2) in DMSO-d_6, using a 500 MHz NMR spectrometer 25

6 ^{1}H-^{13}C HMQC of intermediate compound (2) in DMSO-d_6, using a 500 MHz NMR spectrometer 26

7 The Na$^+$ ion-adduct portion of the high resolution MALDI-TOF-MS spectrum of intermediate compound (2) 27

8 Indirect UV-detection electropherogram of intermediate compound (3) 29

9 ^{1}H NMR spectrum of intermediate compound (3) in CDCl$_3$, using a 500 MHz NMR spectrometer 32

10 ^{1}H NMR spectrum of intermediate compound (3) in pyridine-d_5, using a 500 MHz NMR spectrometer 33

11 ^{1}H-^{1}H COSY of intermediate compound (3) in pyridine-d_5, using a 500MHz NMR spectrometer 34

12 ^{1}H-^{13}C HMQC of (3) in pyridine-d_5, using a 500 MHz NMR spectrometer 35

13 Part of the high resolution MALDI-TOF-MS spectrum of intermediate compound (3) 36

14 Indirect UV-detection electropherogram of intermediate (4) 38

FIGURE Page

15 ^{1}H NMR spectrum of intermediate compound (4) in D_2O, using a 500 MHz NMR spectrometer 41

16 ^{1}H-^{1}H COSY of intermediate compound (4) in D_2O, using a 500 MHz NMR spectrometer 42

17 ^{1}H-^{13}C HMQC of intermediate compound (4) in D_2O, using a 500 MHz NMR spectrometer 43

18 Portions of the high resolution ESI-TOF-MS spectrum of intermediate compound (4) for 3, 4, and 5 charge states 44

19 Portions of the high resolution ESI-TOF-MS spectrum of HMBCD for 3, 4, and 5 charge states after ion exchange 45

20 Synthesis scheme for mono(6-deoxy-6-*N,N,N',N',N'*-pentamethylethylenediammonio)-β-CD (PEMEDA-BCD) 48

21 ^{1}H NMR spectrum of *p*-toluenesulfonyl anhydride in $CDCl_3$, using a 500 MHz NMR spectrometer 49

22 High resolution ESI-TOF-MS spectrum showing the fragment ions of *p*-toluenesulfonyl anhydride 50

23 Chromatogram of intermediate compound (2) 52

24 ^{1}H-^{1}H COSY of intermediate compound (2) in DMSO-d_6, using a 500 MHz NMR spectrometer 53

25 ^{1}H-^{13}C HMQC of intermediate compound (2) in DMSO-d_6, using a 500 MHz NMR spectrometer 54

26 A portion of MALDI-TOF-MS spectrum of intermediate compound (2) 55

27 UV-detection electropherogram of CDP 58

28 ^{1}H-^{1}H COSY of CDP in D_2O, using a 500 MHz NMR spectrometer 59

29 A portion of high resolution MALDI-TOF-MS spectrum of CDP 60

30 Indirect UV-detection electropherogram of intermediate compound (3) 63

FIGURE Page

31 ^{1}H-^{1}H COSY of intermediate compound (3) in DMSO-$d_{6,}$ using a 500 MHz NMR spectrometer 64

32 ^{1}H-^{13}C HMQC of intermediate compound (3) in DMSO-$d_{6,}$ using a 500 MHz NMR spectrometer 65

33 A portion of the high resolution MALDI-TOF-MS spectrum of intermediate compound (3) 66

34 Indirect UV-detection electropherogram of intermediate compound (4) 68

35 ^{1}H NMR spectrum of intermediate compound (4) in D_2O, obtained by using 500 MHz NMR spectrometer 69

36 ^{1}H-^{1}H COSY of intermediate compound (4) in D_2O, using a 500 MHz NMR spectrometer 71

37 ^{1}H-^{13}C HMQC of intermediate compound (4) in D_2O, obtained by using a 500 MHz NMR spectrometer 72

38 A portion of the high resolution ESI-TOF-MS spectrum of intermediate compound (4) 73

39 A portion of the high resolution ESI-TOF-MS spectrum of PEMEDA-BCD 75

40 Direct UV-detection electropherogram of 1-phenyl-2-*O*-sulfo-propane 77

41 A portion of the high resolution ESI-TOF-MS spectrum of 1-phenyl-2-*O*-sulfo-propane 78

42 A portion of the high resolution ESI-TOF-MS spectrum of 1-phenyl-2-*O*-sulfo-butane 79

43 A portion of the high resolution ESI-TOF-MS spectrum of 1-phenyl-2-*O*-sulfo-pentane 80

44 A portion of the high resolution ESI-TOF-MS spectrum of 1-phenyl-1,2-di-*O*-sulfo-ethane monosodium salt 81

45 A portion of the high resolution ESI-TOF-MS spectrum of trans-2-phenyl-1-*O*-sulfo-cyclohexane 82

FIGURE Page

46 UV-detector traces of DMSO 89

47 Ohm's plot obtained with a 50mM HMBCD BE 90

48 Names and structures of strong electrolytes (all sodium salts), weak base, weak acid, neutral, and ampholytic analytes 92

49 Typical effective mobilities and separation selectivities for the enantiomers of selected strong electrolytes with HMBCD in pH = 9.3 BEs 104

50 Effective mobilities of the enantiomers of weak acid analytes in pH = 9.3 BEs with HMBCD 107

51 UV-detector traces of DMSO 111

52 Indirect UV-detection electropherograms of a 50 mM PEMEDA-BCD solution 112

53 Effective mobilities (top portion) and separation selectivities (bottom portion) for enantiomers of strong electrolyte analytes 118

54 Typical effective mobility and separation selectivity curves for the enantiomers of weak acid analytes with PEMEDA-BCD in pH = 2.5 BEs 123

55 Effective mobility and separation selectivity curves for the enantiomers of nonionic analytes with PEMEDA-BCD in pH = 2.5 BEs 128

56 Typical electropherograms for enantiomers of weak acid and neural analytes with PEMEDA-BCD in pH = 2.5 BEs 132

57 Typical electropherograms for the enantiomers of strong electrolytes with PEMEDA-BCD in pH = 2.5 BEs 133

58 Effective mobilities and separation selectivities for the enantiomers of weak acids with PEMEDA-BCD in pH = 9.3 BEs 140

59 Typical electropherograms for the enantiomers of weak acid analytes with PEMEDA BCD in pH = 9.3 BEs 141

60 Effective mobility and separation selectivity curves for the enantiomers of ampholytic analytes with PEMEDA-BCD in pH = 9.3 BEs 148

FIGURE Page

61 Typical electropherograms for the enantiomers of ampholytic analytes with PEMEDA-BCD in pH = 9.3 BEs 149

62 Effective mobility and separation selectivity curves for the enantiomers of nonionic analytes with PEMEDA-BCD in pH = 9.3 BEs 154

63 Typical electropherograms for the enantiomers of nonionic analytes with PEMEDA-BCD in pH = 9.3 BEs 155

64 Comparison of separation of enantiomers with HMBCD (block and triangle) and PEMEDA-BCD (circle and cross) BEs 158

LIST OF TABLES

TABLE Page

1 Separation data for the strong electrolyte analytes as a function of HMBCD concentration in pH = 9.3 BE ... 98

2 Separation data for weak acid analytes as a function of HMBCD concentration in pH = 9.3 BE ... 101

3 Separation data for strong electrolytes analytes as a function of PEMEDA-BCD concentration in pH = 2.5 BE ... 115

4 Separation data for weak acid analytes as a function of PEMEDA-BCD concentration in pH = 2.5 BE ... 119

5 Separation data for neutral analytes as a function of PEMEDA-BCD concentration in pH = 2.5 BE ... 125

6 Separation data for weak base analytes as a function of PEMEDA-BCD concentration in pH = 2.5 BE ... 130

7 Separation data for weak acid analytes as a function of PEMEDA-BCD concentration in pH = 9.3 BE ... 135

8 Separation data for ampholytic analytes as a function of PEMEDA-BCD concentration in pH = 9.3 BE ... 143

9 Separation data for nonionic analytes as a function of PEMEDA-BCD concentration in pH = 9.3 BE ... 151

CHAPTER I

INTRODUCTION

1.1 Chirality

Chirality describes the relationship between two molecules that have the same atom to atom connectivity, but are non-superimposable. These molecules are mirror images, and are called enantiomers. The isolation of individual chiral forms of drugs is an important subject of interest in the pharmaceutical and medical fields, because stereochemistry can have a significant effect on the biological activity of the drug [1]. There is a large number of currently used drugs that contain at least one chiral center, and one enantiomer of a given drug may not have equivalent therapeutic value, or potentially could cause unwanted side effects relative to the other enantiomer [1,2].

Enantiomers of pharmaceuticals have been predominantly separated by chromatographic techniques such as GC, HPLC and SFC [3-6]. The limitation of GC to volatile compounds gives the liquid chromatographic techniques advantage over the former. SFC has shown distinct advantage over HPLC due to the higher separation efficiencies and shorter run times observed in SFC. Currently, the most powerful method for separation of drug enantiomers is CE, owing to its high separation efficiency in small diameter capillaries [7-11].

This dissertation follows the style and format of Journal of Chromatography A.

1.2 Principles of Capillary Electrophoresis

In CE, charged molecules migrate under the influence of an electric field, with a certain electrophoretic velocity, ν. This velocity is proportional to the electric field strength, E.

$$\nu = \mu E \qquad (1)$$

The magnitude of the proportionality factor, μ, the mobility, is dependent on the charge of the separand, and the frictional drag:

$$\mu = z/6\pi\eta r, \qquad (2)$$

where z is the charge of the ion, η is the viscosity of the buffer solution (background electrolyte, BE), and r is the hydrated ionic radius of the separand. Separation in CE is achieved by differences in the electrophoretic mobility of charged molecules.

During electrophoresis, there is partial dissociation of the silanol groups at the surface of the fused silica capillary in contact with the BE. The extent of the dissociation of the silanol groups depends on the pH of the BE. Thus, immobilized negative charges are created on the inner wall of the capillary. In order to establish electroneutrality, some of the positive ions in the BE are strongly attracted to the wall, thus a compact or Stern layer is formed. The remaining cations from the BE are loosely held further out in the diffuse or Gouy-Chapman layer. Therefore, a double layer is created with a shear plane between the two layers. The potential at the shear layer is known as zeta potential. When voltage is applied along the length of the capillary, the solvated cations in the diffuse layer migrate toward the cathode at a constant velocity, dragging along with them solvent molecules. Thus, a bulk flow of the BE, electroosmotic flow, is obtained in the capillary. However, differential adsorption of positively charged molecules from the BE can cause the silica surface to acquire positive charges [12]. In this case the bulk flow will migrate toward the anode, and its magnitude is dependent on the concentration of the adsorbing molecule.

The electroosmotic velocity (v^{eo}), depends on the permittivity of the medium (ε), the dielectric constant (ε_0), the zeta potential (ξ), the dynamic viscosity of the medium (η), and the applied electric field (E):

$$v^{eo} = -\xi\varepsilon_0\varepsilon E/\eta = \mu^{eo}E \qquad (3)$$

The negative sign is an indication of the direction of flow, to the cathode.

When the thickness of the double layer (which is a reciprocal of the Debye-Huckel parameter, 1/k), is much smaller than the radius of the capillary, r, a plug flow profile is obtained for the bulk flow [12]. When the thickness of the double layer is about equal to the inner radius of the capillary, the electroosmotic velocity is much reduced, and consequently, the flow profile becomes parabolic [12, 13]. During a CE run the electroosmotic flow can carry cations, anions, and uncharged molecules in the same direction, past the detector, allowing them to be detected. Therefore, charged molecules migrate with the combination of the non-selective EOF mobility and their effective mobility, μ^{eff}. This sum is defined as the observed mobility, μ^{obs}:

$$\mu^{obs} = \mu^{eff} + \mu^{eo} \qquad (4)$$

The effective mobility of the separand is dependent on the ionic strength of the BE, and for an organic ion with a charge, z, it can be expressed by the equation:

$$\frac{\mu^{eff}}{\mu_0} = \exp(-0.77)(zI)^{1/2} \tag{5}$$

where μ_0 is the ionic mobility at infinite dilution. The ionic strength of the BE, I, is defined as

$$I = 1/2\Sigma cz^2 \tag{6}$$

where c, is the concentration the ionic species of the BE.

Because of the flat flow profile of EOF, and efficient heat dissipation in the capillary, CE offers a greater separation efficiency (over 1 million theoretical plate) than the pressure-driven methods, in which the flow profile is parabolic. As an analytical tool, CE has developed rapidly as one of the most powerful techniques for separation of a wide range of compounds including enantiomers. This is as a result of its speed of analysis, low operating cost, and the ease of modifying the BE with additives to improve separation selectivity.

1.3 Enantioresolution and Cyclodextrins

Enantiomers of a chiral compound can not be resolved without a chiral selector since both the EOF and the effective mobility of the analyte are identical for the enantiomers [14,15]. What may distinguish enantiomers in a chiral CE is their differential interaction with a chiral selector that leads to formation of diastereomeric complexes in a dynamic equilibrium process. If the complexation constants of the enantiomers with the chiral selector or the ionic mobilities of the diastereomeric complexes are different, then, enantiomer separation in CE can be obtained.

Among the different chiral selectors used in CE, cyclodextrins (CD) are the most popular [16]. This can be attributed to their previous successful applications in GC and HPLC [17-19], their ability to differentially interact with a large number of analytes, and their relatively high water solubility [20-23]. CDs are chiral, neutral, cyclic oligosaccharides composed of glucopyranose units connected to each other through α-(1-4) glycosidic linkages, and having the shape of a hallow, truncated cone. There are two generally accepted requirements for chiral recognition of enantiomers by CDs in CE separation. First, the analyte must have a proper structural fit, which can result in the formation of inclusion complexes. Secondly, the groups on the rim of the CD cavity must interact with a substituent group near or on the stereogenic center of the molecule [24]. Differences in the properties of the diastereomeric complexes, especially their hydrodynamic volume, enable the separation of the enantiomer by CE.

Properties of the parent cyclodextrin can be modified by replacement of one or more of the primary or secondary hydroxyl groups with suitable moieties. These derivatized CDs can provide potentially useful interaction sites, and unique selectivity for CE separations by altering the charge and solubility of the native cyclodextrin. Derivatization of the hydroxyl groups present at the rim may also cause changes in the size and depth of the cyclodextrin cavity [25]. Since the only restriction to derivatization of cyclodextrins is the type and number of functional groups that can be substituted on the hydroxyl groups on the rim of CD, a large and diverse group of derivatized cyclodextrins is available now.

Derivatized cyclodextrins that are commonly used in CE can be classified as neutral, anionic, cationic, and zwitterionic. Monosubstituted, polysubstituted, and persubstituted cyclodextrins are now available. The degree of substitution of the cyclodextrin derivative has been shown to have significant effect on the resolution of the enantiomers [26,27 and 28]. For example, hydroxypropyl-derivatized cyclodextrins and methylated cyclodextrins are commercially sold as mixtures of isomers, but are not labeled as such [28]. Other neutral, derivatized cyclodextrins such as naphthylethylcarbamoylated [29], and mono-3-O-phenylcarbamoylated cyclodextrins are available for chiral CE separation. The major problem with neutral CDs, like with the native CDs, is that they can only be used for the separation of charged analytes.

In the last few years, CDs bearing charged functional groups have aroused great interest for the following reasons. (i) Only charged analytes may be resolved in CE with neutral CDs, whereas charged CDs allow the separation of neutral analytes as well as charged ones [30-33]. (ii) Being more soluble in water, it is possible to obtain highly concentrated solutions in the background electrolyte (BE). (iii) The guest-host electrostatic interactions between the oppositely charged selectors and selectrands increase the stability of the inclusion complexes, and alter the selectivity in the host-guest interaction [33].

1.4 Single-isomer Charged Cyclodextrins

Some anionic and cationic CDs are commercially available, generally as mixtures of randomly derivatized components with different degrees of substitution. Obviously, random substitution produces a number of isomers that leads to batch-to-batch variations in the composition of the mixture. Because each CD isomer has a unique binding characteristics for a given enantiomer pair, it is difficult to predict the outcome of interactions with a particular analyte [34]. This complexity creates difficulty in performing a systematic study of chiral CE separations, and prevents the development of a molecular-level separation. Therefore, it is necessary to synthesize single-isomer substituted CDs that will allow a better understanding of the different factors involved in enantiorecognition.

Selectively modified anionic [35,36], and cationic CD derivatives have been synthesized which allow good understanding of the different factors involved in the chiral recognition process [37, 38]. Single-isomers sulfated α-, β-, and γ-CDs have recently been synthesized, and characterized by both NMR and mass spectrometry [39-48]. Each of these single-isomer CDs has been effectively used to separate some cationic enantiomers, and the results obtained are in agreement with the predictions of the Charged Resolving Agent Migration (CHARM) model [49].

The secondary equilibra-based CHARM model was introduced specifically to simplify the development of chiral CE separation methods by determining resolution and separation selectivity as a function of the concentration of the charged single-isomer chiral selector (CCD) and pH of the BE. For a 1:1 complex between the CCD and the analyte, the resulting effective mobility of one of the enantiomers can be written as:

$$\mu_R^{eff} = \frac{\mu_R^0 + \mu_{RCD}^0 K_{RCD}[CD] + K[H_3O](\mu_{HR}^0 + \mu_{HRCD}^0 K_{HRCD}[CD]}{1 + K_{RCD}[CD] + K[H_3O](1 + K_{HRCD}[CD]} \qquad (7)$$

where μ^o_R and μ^o_{RCD}, μ^o_{HR} and μ^o_{HRCD} are the ionic mobilities of the uncomplexed and fully complexed species, K_{RCD} and K_{HRCD} are the complexation coefficients for the non-protonated and the protonated forms of the enantiomer complexes, K is the acid dissociation constant for the enantiomer, and $[H_3O]$ and $[CD]$ are the concentrations of the hydronium ion and the resolving agent. For a given enantiomer pair, the separation selectivity, α, obtained at a particular CD concentration is:

$$\alpha = \frac{\mu_1^{eff}}{\mu_2^{eff}} \qquad (8)$$

The peak resolution expression for an ideal CE system with longitudinal diffusion as the major contributor to peak dispersion [49] is described as:

$$R_s = \sqrt{\frac{Ele^0}{8kT}} \times \frac{abs(\alpha - 1)\sqrt{abs(\alpha + \beta)}\sqrt{abs(1 + \beta)}\sqrt{z_1^{eff}}\sqrt{z_2^{eff}}}{\sqrt{abs((\alpha + \beta)^3)z_1^{eff}} + \sqrt{\alpha \cdot abs((1 + \beta)^3)z_2^{eff}}} \qquad (9)$$

where *l* is the length of the capillary, e^o is the electric charge, k is Boltzman's constant, T is the absolute temperature, z^{eff} is the effective charge of the analyte complex, α is the separation selectivity. The normalized electroosmotic mobility (β), which is given by the expression μ^{eo} / μ_2^{eff} can easily be adjusted to obtain better resolution for the enantiomer separations so long as α is not equal to unity. The subscript 2 refers to the slower of the two migrating enantiomers.

According to the CHARM model, peak resolution for weak electrolytes depends on the pH of the BE. This leads to three types of enantiomer separations using CCDs: desionoselective, ionoselective, and duoselective separations. For desionoselective separation of weak acids and ionoselective separation of weak bases, peak resolution is high at low pH. For ionoselective separation of weak acids, and desionoselective separation of weak bases, peak resolution is high at high pH. For duoselective separation of both weak acids and weak bases, resolution is high at both low and high pH. On the other hand, peak resolution values for both neutral and strong electrolyte analytes are similar at all pH values. From a practical point of view, the most efficient approach to developing a rugged method for chiral CE separations is the use of two BEs: one at low pH, and the other at high pH [49]. It is important to note that the development of enantiomer separations lies in optimizing the β term through the use of coated capillaries and /or appropriate background electrolyte constituents. By optimizing β and knowing the dependence of α, z_1^{eff}, and z_2^{eff} on the composition of the BE, resolution can be achieved. According to equation 9, when all other parameters are equal, resolution increases with the square root of z. Therefore, under identical conditions, increase in the

z^{eff} will lead to increase in resolution. Thus, the three-dimensional resolution surface in Figure 1 demonstrates that, under identical α, and β conditions, resolution increases with the effective charge. When β and z^{eff} are constant, resolution increases linearly with α. Under identical α and z, resolution increases towards infinitely high value as β approaches –1. As long as the cyclodextrin shows some selectivity for the enantiomers, one can improve resolution by optimizing β, though this comes at the expense of increased analysis time.

1.5 Enantioseparation with Cationic Cyclodextrins

More anionic than cationic CDs are currently used in chiral CE separations, and the available single-isomer anionic CDs can only resolve few of the anionic analytes. Most of the previously synthesized cationic cyclodextrins were not often used for separation of enantiomers in CE. For example, an amino-functionalized cyclodextrin was used as a model for studying enzymatic biological processes involving a positively charged group in the vicinity of the active site [50]. Mono-6-(alkylamino)-β-cyclodextrins [51, 52] were used to study the degree of cooperative binding between organic quest and aggregated amphipathic cyclodextrins. Recently, three positional isomers of β-cyclodextrin derivatives bearing two trimethylammonio groups on two of the C-6 atoms of cyclodextrin [53,54], were made by alkylation of the corresponding regioisomers of diamino β-CD compounds [55] with methyl iodide in the presence of potassium hydrogen carbonate. However, these cationic CDs were not used for chiral

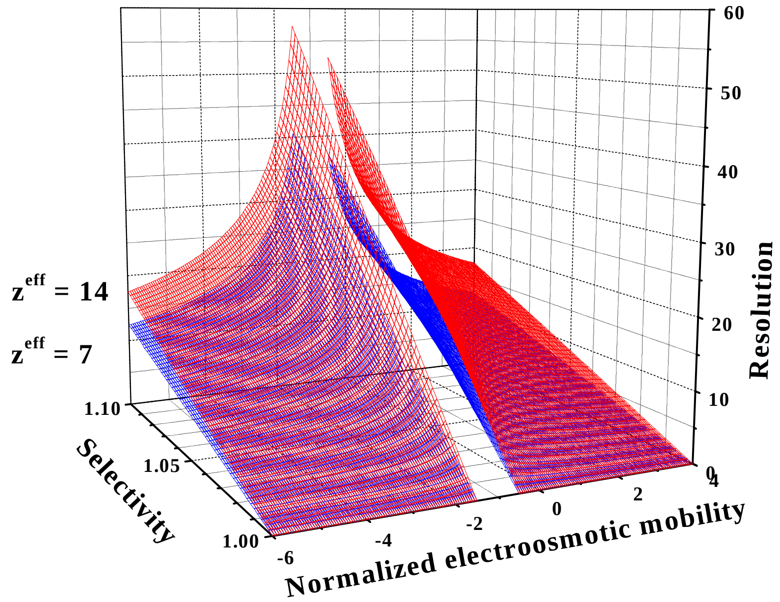

Figure 1. Peak resolution surfaces for 7-charged and 14-charged cyclodextrins as a fuction of separation selectivity and normalized electroosmotic flow.

CE separation studies. Rather chiral guest recognition was performed by calorimetric studies using the regioisomer, quaternary ammonio CDs.

The earliest cationic cyclodextrin derivative that was used for CE separation was the mono-(6-β-aminoethylamino-6-deoxy)-β-cyclodextrin [37]. However its use was limited to the separation of a few dansylated amino acid. Following this, some monosubstituted, strong electrolyte, and weak electrolyte, cationic CDs have been synthesized and applied to CE enantiomer separations [56-67]. Typically, these monocationic, single-isomer CDs are prepared from CD intermediates bearing a good leaving group such as tosyl and iodo, at carbon six of one of the glucose units. The final products are obtained by reaction of the intermediates with an amine or quaternary ammonium group under suitable conditions (usually at elevated temperature). For example, 6^A-methylamino-β-cyclodexrin was synthesized through tosylated β-cyclodextrin intermediate [54], followed by substitution of the tosyl group with methylamine [68]. Enantiomers of 2-hydroxy acids (mandelic acid, MA, m-hydroxymandelic acid, m-MA, p-hydroxymandelic acid, p-MA, and 3,4-di-hydroxymandelic acid, 3,4-di-MA) were separated by Nerdi et al., using the 6^A-methylamino-β-cyclodexrin [69]. It was found from these studies that all the compounds migrated anodically on a bare fused silica capillary, and the order of complexation was p-MA > MA > 3,4-di-MA > m-MA. 3,4-di-MA and m-MA showed lesser complexation with the cationic CD because of the hindering effect of the OH group on the aromatic ring.

Dicationic CDs have also been synthesized and used for separation of enantiomers by CE. For example, 6-ethylenediamine-derivatized -β-cyclodextrin was effectively used to separate some anionic compounds [70]. Under the conditions the CD was used, cathodic EOF was observed, and all the analytes were detected at the cathode. All the analytes separated, contained at least one aromatic ring and a carboxylic acid functionality. Also, in most cases, the carboxylic acid group was one of the groups at the chiral center, which lies within one to two bond distances from the aromatic ring. Selectively modified 6,6'-didoexy-6,6'-diamino-cyclodextrins, having the amine group directly attached onto two glucose units of the cyclodextrins have been prepared, and used for separation of enantiomers of hydroxy acids, and carboxylic acids [71]. The relative distance between the two positive charges on the rim of these cationic CDs greatly influenced their enantio-recognition ability. For a dicationic CD derivative, there is an optimum distance between the two charges that leads to good enantiomer separation. Selectively functionalized, dicationic CD, 6-deoxy-6-(N-histamino)-β-cyclodextrin, bearing a histamine moiety linked to the C-6 atoms of a glucose unit via the amino group, was synthesized by treating mono substituted iodo-β-CD with histamine under very harsh conditions [72]. Following a similar synthetic method, its analog, 6-deoxy-[4-(2-aminoethyl)imidazolyl]-β-cyclodextrin, bearing the histamine moiety linked to the C-6 atoms via the imidazolyl group was also synthesized [73]. Both CDs have been used for the separation of enantiomers of dansylated amino acids, hydroxy acids, and carboxylic acids [74, 75]. Here again the pKa of the protonated groups varied according to the relative distance from the CD cavity, and as a consequence the two chiral selectors exhibited different enantiorecognition characteristics. The effect of pH on selectivity and resolution was studied for both CDs in the range of 4.0 to 9.0. Because of the differences in the pKa values of the protonated groups, the number of net positive charges on the CDs changed as the pH of the BE was varied. As the pH value increased, selectivity decreased, and after pH 7.5, there was practically no separation of the enantiomers. The best enantioseparation was observed at pH 5.

Using either pertosylated or perhalogenated CDs [76,77] as precursors, a few primary, secondary and persubstituted, amino CDs have been synthesized [78-83]. Heptakis(6-deoxy-6-methoxyethylamine)-β-cyclodextrin was used to separate the enantiomers of non-steroidal, anti-inflamatory drugs (NSAID), and phenoxy propionic acids [84]. The positively charged CD did not only cover the inner wall of the bare fused silica capillary, but also produced a reversed, stable EOF under the conditions it was used. It was also observed that in addition to the ionic and hydrogen-bonding contributions to chiral recognition, steric interactions also contributed to the overall complexation between the multiply charged CD and the NSAIDs [84]. At pH 5, where the CD was fully protonated and the analytes were all anionic, no separation of the enantiomers of ketoprofen was observed. However, the enantiomers of suprofen which is structurally similar to ketoprofen were resolved at pH 5. It was noted that the propionic acid moiety of suprofen is in the para position while that of ketoprofen is in the meta position indicating that suprofen can more favorably orient within the cavity of the CD than ketoprofen [84]. Here again it was observed that the EOF, the charge, and the chiral recognition properties of both the analytes and the CD depended on the pH of the BE.

Two randomly substituted, commercially available, quaternary ammonium β-CDs have been used for the separation of the enantiomers of various acidic analytes [70,85]. A quaternary ammonium β-CD, having the quaternary groups linked to the C_6 atoms through a 2-hydroxypropylene ether, and quaternary ammonium hydroxypropyl β-CD, having the quaternary ammonium group directly attached to the C_6 atoms are sold commercially as multiple-isomer CDs. When compared to neutral CDs, both CDs were effective for the separation of enantiomers at low CD concentrations due to the strong electrostatic interaction between the cationic CDs and anionic analytes. Following a similar synthetic scheme, some other randomly substituted quaternary ammonium CDs have been made, and used for the separation of racemic mixtures [86]. The best advantage of this set of chiral selectors is that they allow for the adjustment of the pH of the BE according to the requirements of the particular analyte because the charges on the CDs are independent of the pH of the BE. However, because they consist of multi-components having different degrees of substitution, good reproducible enantiomer separations are more difficult to obtain with them.

From the foregoing analysis of CE enantiomer separation, it is clear that having a system in which the effective mobilities of the uncomplexed analyte and the complexed analyte have opposite signs will be most desirable as predicted by the CHARM model [49]. From the practical point of view, it is also desirable to have systems in which the pH of the BE can be freely adjusted, according to the type of the separation involved (desionoselective, ionoselective or duoselective separation [49]), without changing the charge state of the resolving agent used. For the anionic analytes, multiply charged, quaternary ammonium CDs would be preferable.

In order to satisfy these requirements, the objective of this dissertation is to synthesize cationic cyclodextrins that are (*i*) single-isomers, (*ii*) multi-cationic derivatives that carry (*iii*) closely spaced, (i*v*) permanent charges and (*v*) can be made readily available in large quantities to permit their widespread use in CE. Since most anionic analytes of interest are single-charged, the lowest and highest charge numbers on the permanently cationic, single-isomer, resolving agent that fulfill this requirement are two and seven respectively, in the case of beta cyclodextrin. Therefore, this dissertation will discuss the synthesis, analytical characterization of heptakis(6-deoxy-6-morpholinio)-cyclomaltoheptaose (HMBCD), and mono(6-deoxy-6-*N,N,N',N',N'*-pentamethylethylenediammonio)-cyclomaltoheptaose, (PEMEDA-BCD), and their applications in capillary electrophoretic separation of enantiomers.

CHAPTER II

SYNTHESIS AND CHARACTERIZATION

A very small number of anionic chiral compounds have been resolved with the available single-isomer sulfated cyclodextrins. In this work, the first single-isomer, persubstituted quaternary ammonium β-CD, the chloride salt of heptakis(6-deoxy-6-morpholinio)-cyclomaltoheptaose (HMBCD), and the first single-isomer, quaternary diammonio β-CD, the chloride salt of mono(6-deoxy-6-pentamethylethylenediammonio)-cyclomaltoheptaose (PEMEDA-BCD) have been synthesized on a large scale and analytically characterized.

2.1 Materials and General Methods

All chemicals used in this work were purchased from Aldrich Chemical Company (Milwaukee, WI, USA), except native β-CD, which was purchased from Cerastar (Cedar Rapids, IA). Progress of the reaction for the β-CD intermediates was monitored by thin layer chromatography (TLC), using Silica-60 plates (E. M. Science, Gibbstown, NJ). The developed plates were visualized by dipping them into an ethanolic α-naphthol staining solution (made by combining 26.25 g of α-naphthol, 315 mL of 100% ethanol, 105 mL of concentrated sulfuric acid, and 66 mL of distilled water) and heating for 10 min at 100°C. The purity of the intermediates was determined by analytical isocratic HPLC using a system containing a Programmable Solvent Module

126 (Beckman-Coulter, Fullerton, CA), a Sedex Model 55 evaporative light scattering detector (S.E.D.E.R.E., Alfortville, France), and an AD 406 data acquisition system operated under Gold 8.1 software control (Beckman-Coulter) running on a 486DX4 personal computer (Computer Associates, College Station, TX). The separations were obtained on a 4.6 mm I. D. × 250 mm column packed with a 5μm Zorbax ODS stationary phase (Agilent, Newport, DE). The purity values reported in this dissertation were calculated with the assumption that the response factors of the evaporative light scattering detector were the same for all CD isomers. Since the products of the amination and quaternarization reactions are charged, the progress of these reactions, and the purity of β-CD derivatized with morpholine, and that of the quaternary ammonio β-CD were determined by indirect UV-detection CE, using a P/ACE 2000 system (Beckman-Coulter), at 214 nm and 10 kV applied potential, on a 26.4 / 19.6 cm long, 25 μm I. D. bare fused silica capillary column (Polymicro Technologies, Phoenix, AZ). The cartridge coolant of the P/ACE 2000 was thermostated at 20^{o}C.

The molecular mass of the intermediates was obtained by high resolution MALDI-TOF-MS. A Voyager Elite XL TOF mass spectrometer equipped with delayed extraction capability (PerSeptive Biosystems, Framingham, MA) in reflectron mode, with an acceleration voltage of 25 kV, 70% grid voltage, 0.035% guide wire voltage, and a delay time of 180 μs, was used to collect the high-resolution mass spectra. The analytes were spotted onto a Teflon target using the dried droplet method [87]. The matrix was prepared by dissolving 10 mg 2,4,6-trihydroxyacetophenone in 1 mL acetonitrile [88]. The molecular mass of the final products, HMBCD and PEMEDA-

BCD was obtained by ESI-TOF-MS with a Vestec Model 201-A single quadrupole mass spectrometer equipped with a Vestec electrospray ion source (PerSeptive Biosystems). The sample was prepared at a concentration of 4 mg/mL in an acetonitrile : water 1:1 (v/v) solvent mixture. ^{1}H and ^{13}C NMR spectra were measured on UnityPlus 300 and 500 spectrometers with a quad nucleus (^{1}H / ^{13}C /^{19}F / ^{31}P) probe, operated under Solaris 2.4 and Vnmrx 5.3 b software control. The proton (H) and carbon (C) assignments were based on the ^{1}H-^{1}H 2D COSY (Correlation Spectroscopy), ^{1}H-^{13}C HETCOR NMR (Heteronuclear Correlation Spectroscopy), and ^{1}H-^{13}C HMQC (Heteronuclear Correlation Through Multiple Quantum Coherence) experiments.

2.2 Synthesis and Characterization of HMBCD

The synthesis scheme used for preparation of heptakis(6-deoxy-6-morpholinio)-cyclomaltoheptaose (HMBCD) is shown in Figure 2. The details of the synthetic procedures are outlined in the Appendix.

2.2.1 Heptakis(6-deoxy-6-iodo)- β-cyclodextrin

Selective substitution of the hydroxy groups at the primary positions of native β-CD with iodine was performed, as reported in the literature [89, 90], by direct halogenation with bromine or iodine, in the presence of triphenylphosphine (Ph_3P) and DMF [91].

Thus, native β-CD (1) was treated with I_2 and Ph_3P in DMF at 70 °C for 18 hours to obtain heptakis(6-deoxy-6-iodo)-β-CD, intermediate compound (2). Because the reported workup procedures that used either water to precipitate the product or Soxhlet extraction to clean up the product, did not yield a pure product, a recrystallization method involving a DMF/water mixture was developed and used to obtain intermediate compound (2). The progress of the purification process, and the purity of intermediate compound (2) was monitored by isocratic aqueous reversed phase HPLC, using a 4.6 mm I.D. × 250 mm Zorbax C18 column and a 95: 5 CH_3OH: water mobile phase at 1.8 mL/min at 45 °C. Intermediate compound (2) was obtained with an isomeric purity > 99% at 65% yield for a 46 g scale. Figure 3 shows the chromatograms obtained by aqueous, reversed-phase HPLC separation of intermediate compound (2) before and after recrystallization from the DMF/water mixture. Figure 4 shows the ^1H NMR spectra of intermediate compound 2 before and after recrystallization from the DMF/water mixture.

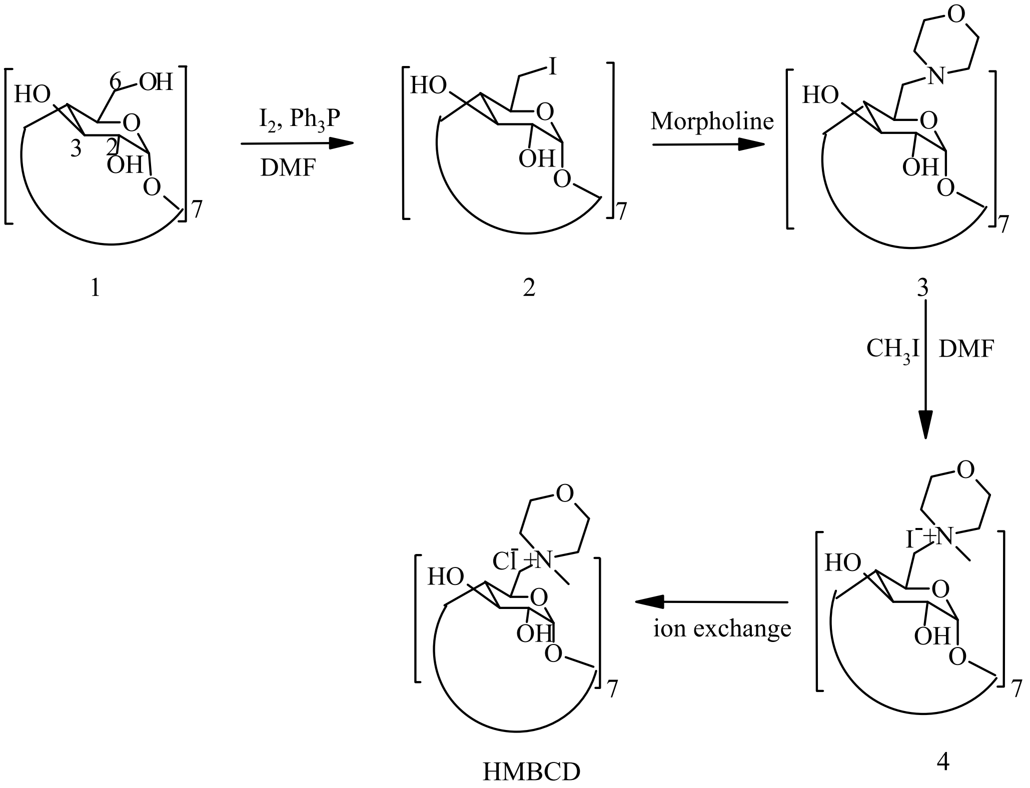
HO
6
OH
O
3
2
OH
O
7
1
I2, Ph3P
DMF
HO
I
O
OH
O
7
2
Morpholine
HO
O
N
O
OH
O
7
3
CH3I
DMF
HO
O
I-
+N
O
OH
O
7
4
ion exchange
HO
O
Cl-
+N
O
OH
O
7
HMBCD

Figure 2. Synthesis scheme for heptakis(6-deoxy-6-morpholinio)-β-cyclodextrin chloride (HMBCD).

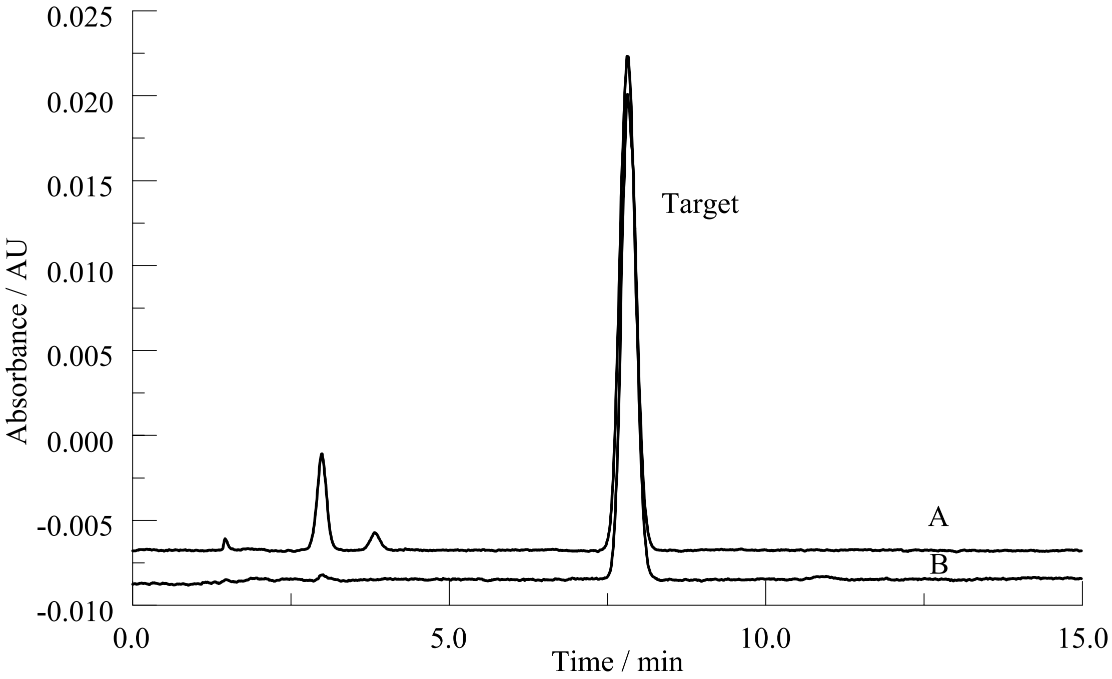

Figure 3. Chromatograms of intermediate compound (2). (A) before recrystallization, (B) after recrystallization. Conditions: RP HPLC, C-18, 95 : 5 CH_3OH : H_2O. Flow rate = 1.8mL/min at 45°C.

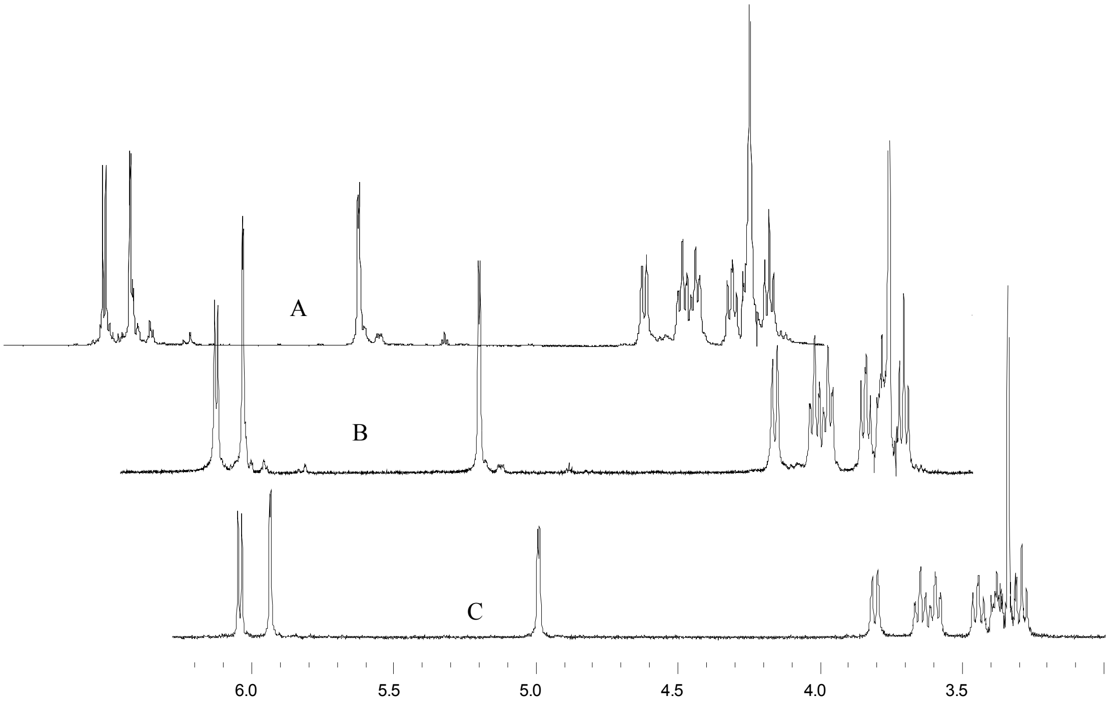

Figure 4. ^{1}H NMR spectra in DMSO-d_6, using a 500 MHz NMR spectrometer, during purification of intermediate compound (2). (A) reaction mixture, (B) after the first purification step, (C) after the final purification step.

The structure of intermediate compound (2) was verified by high-resolution ^{1}H and ^{13}C NMR spectroscopy. The peak assignments were determined from the 1-dimensional ^{1}H and ^{13}C NMR spectra, coupled with 2-dimensional ^{1}H-^{1}H COSY and ^{1}H-^{13}C HMQC NMR spectroscopy. ^{1}H NMR data in CD_3SOCD_3: δ 6.05 (doublet, 7 O**H**, J = 6.5 Hz); δ 5.94 (doublet, 7 O**H**, J = 2 Hz); δ 4.99 (doublet, 7 H-1, $J_{1\text{-}2}$ = 3.5 Hz); δ 3.80 (doublet, 7 H-6, $J_{6\text{-}6'}$ = 9.5 Hz); δ 3.65 (triplet, 7 H-3, $J_{3\text{-}2}$ = 9.0 Hz, $J_{3\text{-}4}$ = 9.5 Hz); δ 3.59 (triplet, 7 H-5, $J_{5\text{-}4}$ = 9.0 Hz, $J_{5\text{-}6'}$ = 9.0 Hz);); δ 3.44 (triplet, 7 H-6′, $J_{6'\text{-}5}$ = 9.0 Hz, $J_{6'\text{-}6}$ = 9.5 Hz); δ 3.38 (multiplet, 7 H-2); δ 3.291 (triplet, 7 H-4, $J_{4\text{-}3}$ = 9.5 Hz, $J_{4\text{-}5}$ = 9.0 Hz); ^{13}C NMR data in CD_3SOCD_3: δ102.80 (C-1); δ 86.2 (C-4); δ 72.85 (C-2); δ 72.59 (C-3); δ 71.64 (C-5); δ 10.17 (C-6). ^{1}H - ^{1}H COSY and ^{1}H - ^{13}C HMQC NMR spectra in Figures 5 and 6 show the proton and carbon contours that were used for assignment of the signals.

High resolution MALDI-TOF-MS was used to determine the molecular mass of intermediate compound (2). The Na^+ ion-adduct portion of the mass spectrum of intermediate compound (2) is shown in Figure 7. The calculated molecular mass value of the Na^+ ion-adduct of the parent molecule, 1681.43, agrees well with the value obtained using MALDI-TOF-MS, 1680.89, indicating the presence of seven iodine atoms on intermediate compound (2).

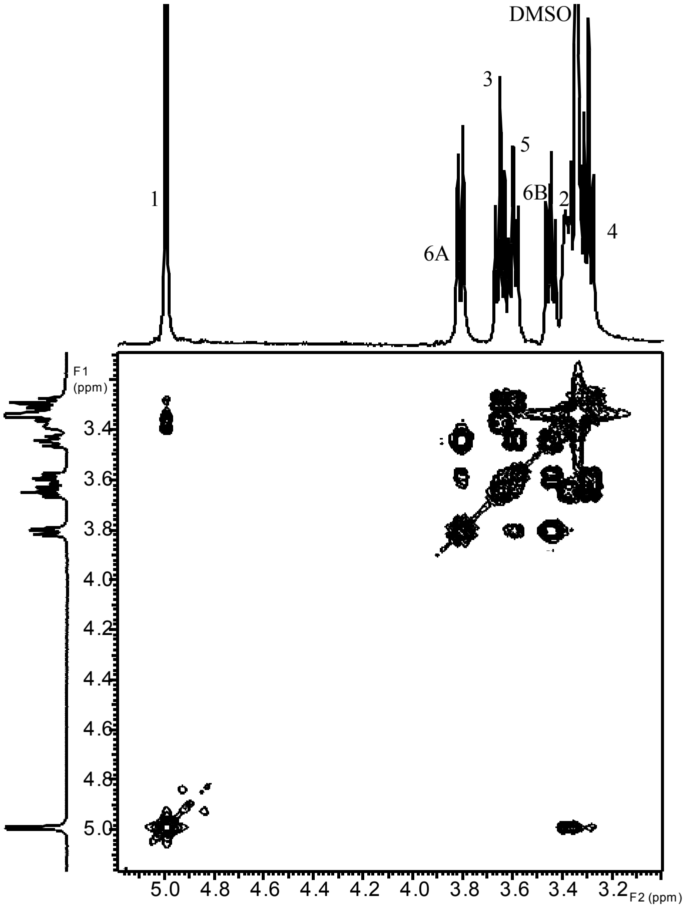

Figure 5. ^{1}H-^{1}H COSY of intermediate compound (2) in DMSO-d_6, using 500 MHz NMR spectrometer.

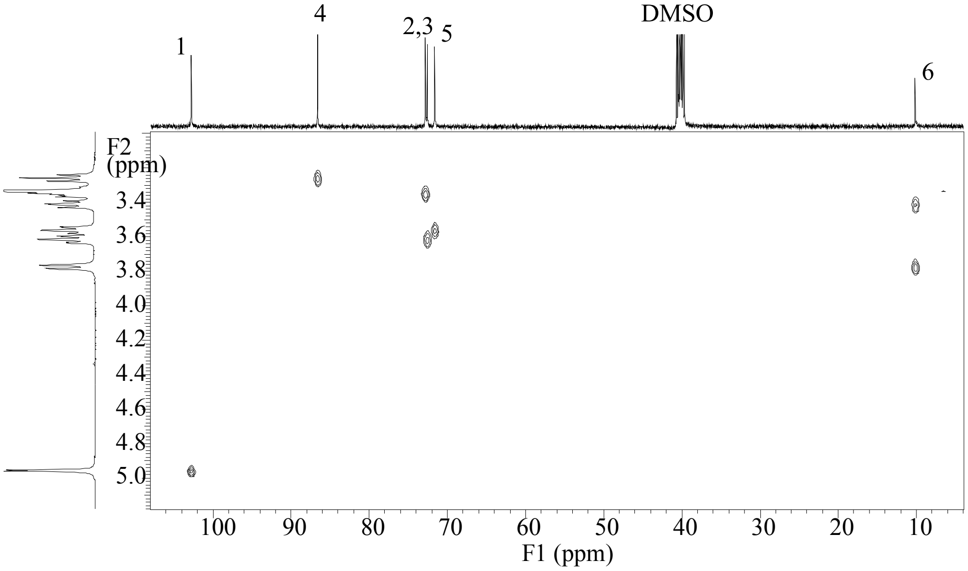

Figure 6. ^1H-^{13}C HMQC of intermediate compound (2) in DMSO-d_6, using a 500 MHz NMR spectrometer.

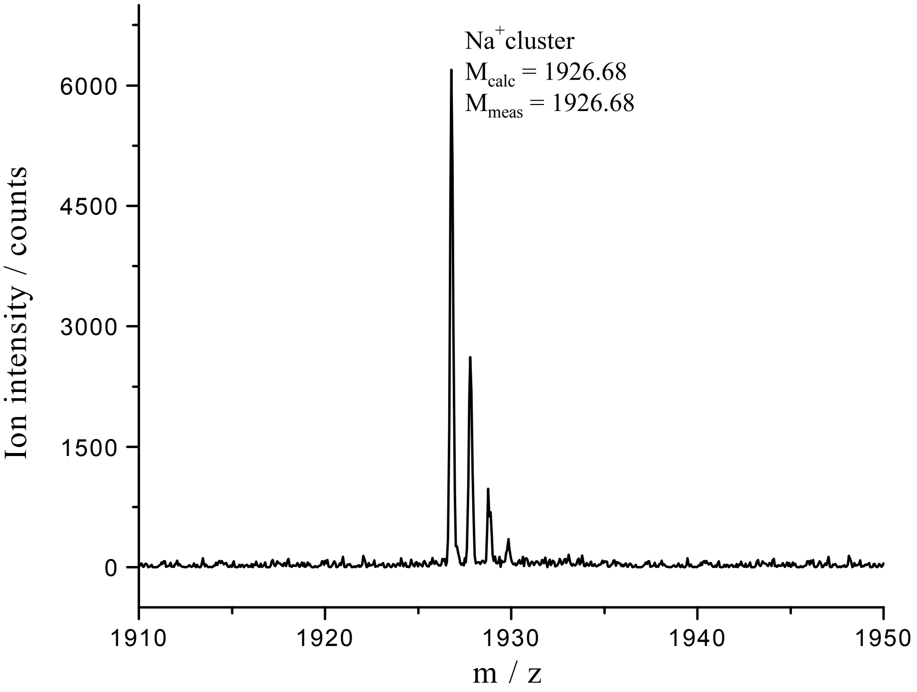

Figure 7. The Na$^+$ ion-adduct portion of the high resolution MALDI-TOF-MS spectrum of intermediate compound (2).

2.2.2 Heptakis(6-deoxy-6-morpholino)-β-cyclodextrin

Intermediate compound (2) was converted to heptakis(6-deoxy-6-morpholino)-β-cyclodextrin, intermediate compound (3), having all the iodine atoms at the primary positions substituted with morpholine by reacting (2) in excess morpholine at 65 °C for 18 hours. Since the pKa of a substituted tertiary amine moiety is typically lower than that of the secondary amine precursor [92], it was expected that free morpholine will deprotonate the tertiary amine β-CD to give intermediate compound (3). Intermediate compound (3) is protonoted in a buffer with a pH lower than its pKa, and become charged, allowing for the monitoring of the progress of the reaction and the determination of the purity of intermediate compound (3) by indirect UV-detection CE. CE was performed, using a 20 mM acetic acid buffer titrated to pH 4.55 with imidazole as the BE, with the detector placed at the cathode. The reaction was stopped when the normalized target peak area relative to the other minor components was over 98%. The workup involved the evaporation of the reaction solvent under reduced pressure at 50 °C, leaving a brown solid material, which was repeatedly digested with ethanol to obtain intermediate compound (3) in its pure form. The isomeric purity of the final product was determined to be greater than 98% as shown in Figure 8.

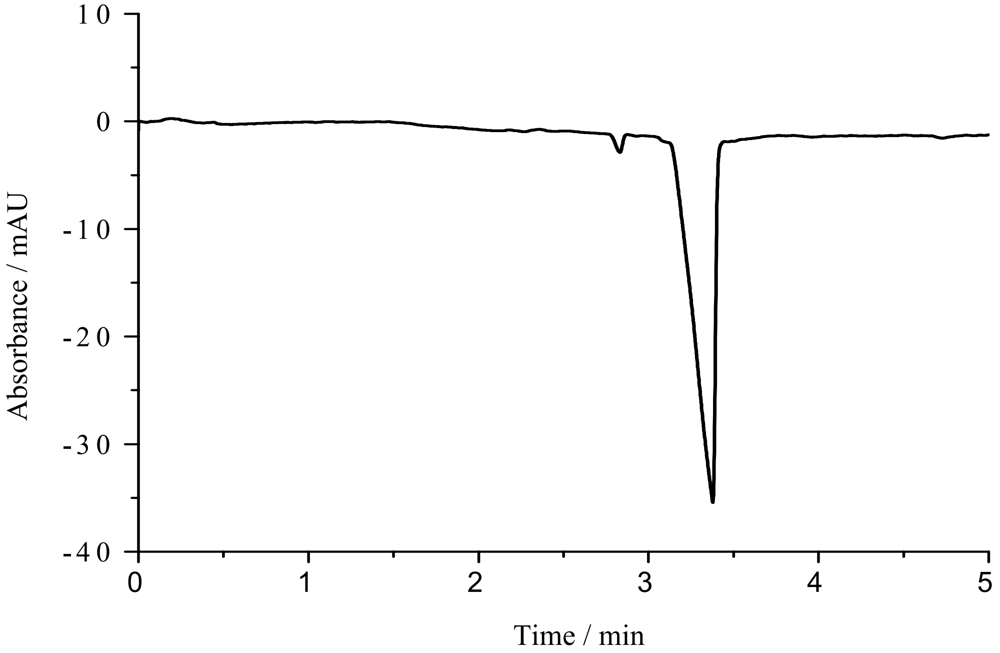

Figure 8. Indirect UV-detection electropherogram of intermediate compound (3). Conditions: 25 µm I. D. fused silica capillary, 20 mM acetic acid / imidazole BE, pH = 4.6, (+) to (-) polarity.

The structure of intermediate compound (3) was verified by high-resolution ^1H and ^{13}C NMR spectroscopy. Two solvents were used to obtain the ^1H NMR spectra of intermediate compound (3). Originally, the first ^1H NMR spectrum obtained in $CDCl_3$ showed that protons at C-2, C-3 and C-5 of the CD, and the protons on the morpholinio substituent could not be resolved. Even though the $CDCl_3$ solvent allowed for the observation and identification of the hydroxy protons at C-2 and C-3, there was a need to resolve the other proton signals, and check for the presence of impurities. Because of the poor resolution of the proton signals with $CDCl_3$, a second ^1H NMR spectrum was obtained in deuterated pyridine. Figures 9 and 10 show the two ^1H NMR spectra of intermediate compound (3) obtained in $CDCl_3$ and deuterated pyridine, respectively. Comparison of the two spectra also facilitated the characterization of intermediate compound (3). The peak assignments were determined from the 1-dimensional ^1H and ^{13}C NMR spectra, coupled with 2-dimensional ^1H-^1H COSY and ^1H-^{13}C HMQC NMR spectroscopy. ^1H NMR data in $CDCl_3$: δ 6.83 (singlet, 7 O**H**); δ 5.29 (singlet, 7 O**H**); δ 5.00 (doublet, 7 H-1, J_{1-2} = 3.5 Hz); δ 3.99 (triplet, 7 H-3, J_{3-4} = 9.0 Hz, J_{3-2} = 9.0 Hz); δ 3.74 – 3.60 (multiplet, 49 H-2, H-4, H-5, and morpholine); δ 2.75 (doublet of doublets 7 H-6, $J_{6-6'}$ = 4.2 Hz, J_{6-5} = 3.7 Hz); δ 2.64 (multiplet, 14 (C$\underline{\mathbf{H}_2}$C); δ 2.51 – 2.38 (multiplet, 7 (C$\underline{\mathbf{H}_2}$C), 7 H-6). ^1H NMR data in pyridine-d_5: δ 4.44 (doublet, 7 H-1, J_{1-2} = 3.5 Hz); δ 3.48 (triplet, 7 H-3, J_{3-2} = 9.5 Hz, J_{3-4} = 9.5 Hz); δ 3.26 (doublet of doublets, 7 H-5, J_{5-4}

= 6.0 Hz, J_{5-6} = 6.0 Hz); δ 3.04 – 2.98 (multiplet 7 H-2 and 7 H-4); δ 2.64 (broad singlet, 7 (C$\mathbf{H_2}$C); δ 2.07 (doublet of doublets, 7 H-6, J_{6-5} = 6.0 Hz, $J_{6-6'}$ = 13.0 Hz); δ 1.77 (doublet, 7 H-6′, $J_{6'-6}$ = 13.0 Hz); δ 1.68 (broad singlet, 7 (C$\mathbf{H_2}$C)); δ1.55 (broad singlet, 7 (C$\mathbf{H_2}$C)); ^{13}C NMR data in Pyridine-d_5: 104.0 (C-1); δ 85.1 (C-2); δ 75.1 (C-3); δ 74.5 (C-4); δ 72.0 (C-5); δ 67.7 ($\mathbf{C}$H$_2$C); δ 59.2 (C-6); δ 55.7 ($\mathbf{C}$H$_2$C). ^{1}H - ^{1}H COSY and ^{1}H - ^{13}C HMQC NMR spectra in Figures 11 and 12 show only those proton and carbon contours that were used for signal assignment.

High resolution MALDI-TOF-MS was used to determine the molecular mass of intermediate (3). A portion of the mass spectrum (the H$^+$, Na$^+$ and K$^+$ ion-adduct portion) of intermediate (3) is shown in Figure 13. The calculated molecular mass values of the H$^+$, Na$^+$ and K$^+$ ion-adducts of the parent molecule, 1618.78, 1640.76, and 1656.74 agree well with the values obtained using MALDI-TOF-MS, 1618.63, 1640.62 and 1656.57 respectively, indicating the presence of seven morpholine moieties in intermediate compound (3).

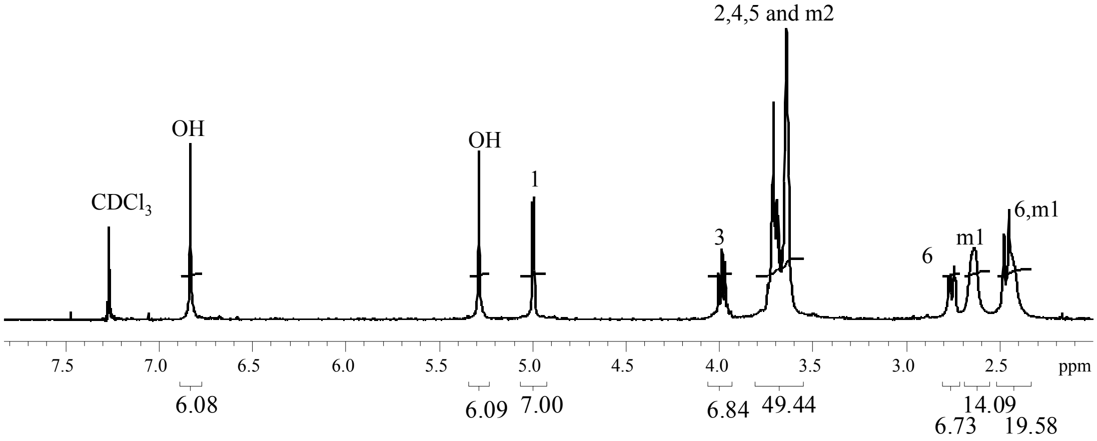

Figure 9. ^{1}H NMR spectrum of intermediate compound (3) in $CDCl_3$, using a 500 MHz NMR spectrometer.

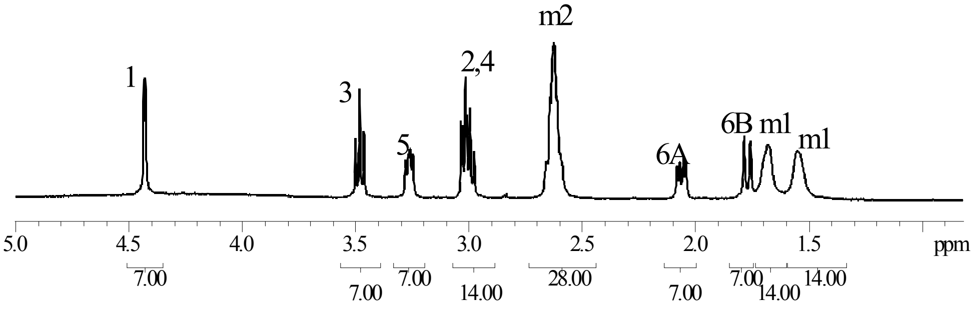

Figure 10. ^{1}H NMR spectrum of intermediate compound (3) in pyridine-d_5, using a 500 MHz NMR spectrometer.

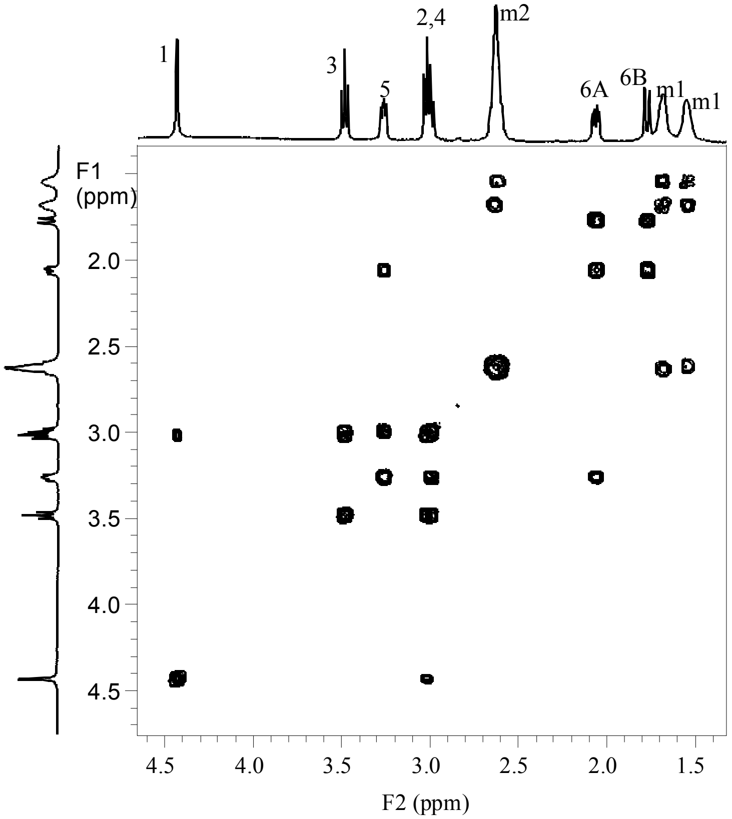

Figure 11. ^1H-^1H COSY of intermediate compound (3) in pyridine-d_5, using a 500 MHz NMR spectrometer.

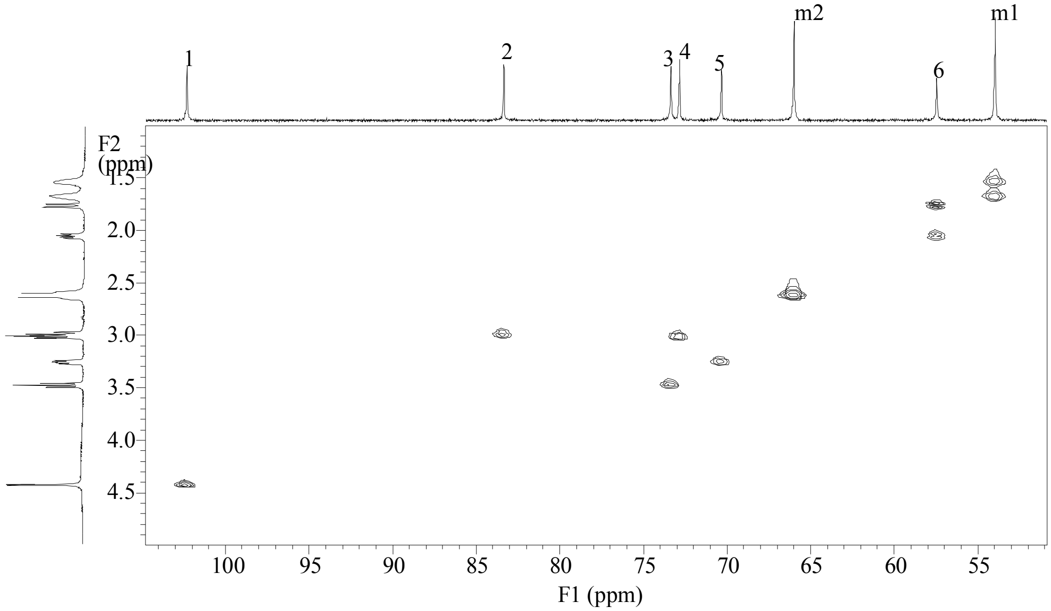

Figure 12. ^{1}H-^{13}C HMQC of (3) in pyridine-d_5, using a 500 MHz NMR spectrometer.

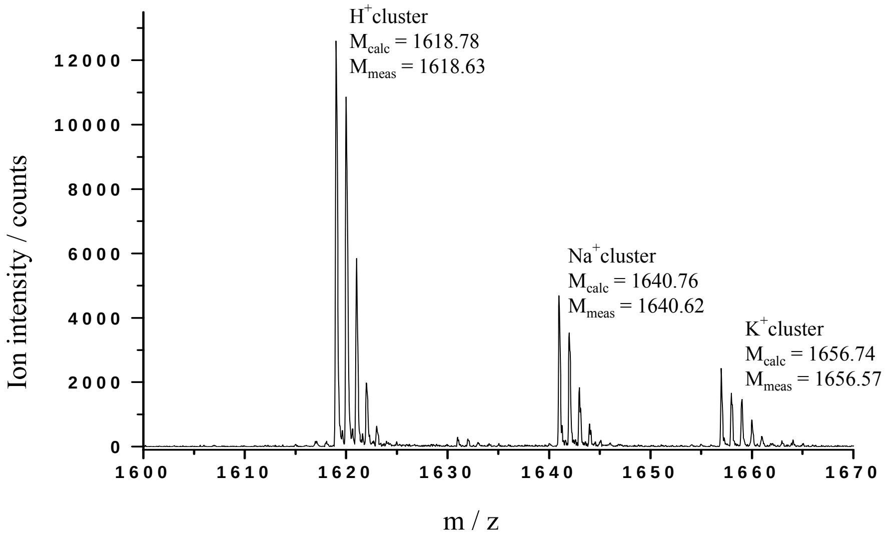

Figure 13. Part of the high resolution MALDI-TOF-MS spectrum of intermediate compound (3).

2.2.3 Heptakis(6-deoxy-6-morpholinio)-β-cyclodextrin Iodide

The most common procedure for the quaternarization of tertiary amines involves the addition of excess methyl iodide to the amine in DMF. Therefore, methyl iodide was added to a solution of intermediate (3) in 1-methyl-2-pyrrolidinone (NMP), and refluxed at 45 °C for 24 hours to give heptakis(6-deoxy-6-morpholinio)- β-cyclodextrin iodide, intermediate compound (4). NMP was used instead of DMF because NMP is a dipolar aprotic solvent that has been shown to be superior to DMF for nucleophilic substitution, and it is more stable than DMF under acidic or basic conditions [92]. Methyl iodide had to be added to the reaction solution in the presence of Na_2CO_3 to release of the free amines from their hydrohalide salts to permit complete alkylation. The progress the reaction was monitored in D_2O by ^1H NMR. The workup involved the evaporation of the reaction solvent under reduced pressure at a temperature of 60 °C, which produced a brownish paste that dissolved readily in water. The off-white solid, intermediate (4), was precipitated from the aqueous solution with acetone, and subsequently recrystallized from a methanol-ethanol mixture to produce pure intermediate compound (4). The isomeric purity of the final product was determined to be greater than 98% by indirect UV-detection CE. Figure 14 depicts the electropherogram of intermediate compound (4) obtained by using 20 mM formic acid, titrated to pH 3.4 with aniline as BE.

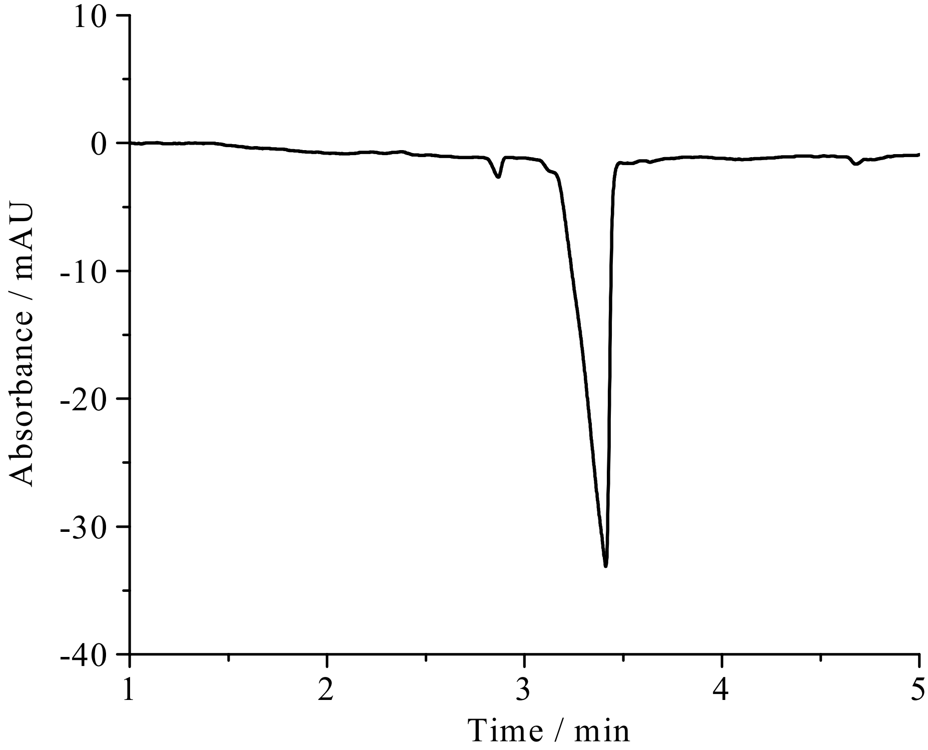

Figure 14. Indirect UV-detection electropherogram of intermediate (4). Purity > 97%. Conditions: 20 mM formic acid / aniline, pH = 3.4, (+) to (-) polarity, Lt/Ld = 26.4 / 19.6 cm, 18 kV, 214 nm, T = 22 °C.

The structure of intermediate compound (4) was verified by high-resolution ^1H and ^{13}C NMR spectroscopy. The initial ^1H NMR spectrum that was acquired at 22 °C showed unusually broad line widths for the cyclodextrin proton signals as well as the proton signals of the morpholinio substituents, suggesting the presence of impurities in the intermediate product. To investigate this possibility, ^1H NMR of intermediate compound (4) was acquired at different temperatures in the 22 °C to 70 °C range. Figure 15 depicts the ^1H NMR spectra of intermediate compound (4) at 22 °C and 60 °C with decrease in the peak line width for the proton signals at higher temperature, indicating that intermediate compound (4) exists in different conformations that interconvert rapidly as the viscosity of the sample solution is decreased with an increase in temperature. The peak assignments were determined from the 1-dimensional ^1H and ^{13}C NMR spectra, coupled with 2-dimensional ^1H-^1H COSY and ^1H-^{13}C HMQC NMR spectroscopy. ^1H NMR data in D_2O. 60 °C: δ 5.59 (doublet, 7 H-1, $J_{1\text{-}2} = 3.0$ Hz); δ 5.03 (triplet, 7 H-5, $J_{5\text{-}4} = 8.0$ Hz, $J_{5\text{-}6} = 8.0$ Hz); δ 4.42 (triplet, 7 H-3, $J_{3\text{-}2} = 8.0$ Hz, $J_{3\text{-}4} = 8.0$ Hz); δ 4.40 – 4.25 (multiplet, 7 H-6, 14 ($C\underline{\mathbf{H}_2}$)); δ 4.07 (triplet, 7 H-4, $J_{4\text{-}3} = 8.0$ Hz, $J_{4\text{-}5} = 8.0$ Hz); δ 4.02 (doublet of doublets, 7H-2, $J_{2\text{-}1} = 3.0$ Hz, $J_{2\text{-}3} = 8.0$ Hz); δ 4.00 – 3.94 (multiplet, 7 ($C\underline{\mathbf{H}_2}$)); δ 3.93 – 3.84 (multiplet, 7 H-6, 7 ($C\underline{\mathbf{H}_2}$)); δ 3.66 (singlet, 7 ($C\underline{\mathbf{H}_3}$)). ^{13}C NMR data in D_2O: 98.58 (C-1); δ 79.0 (C-4); δ 71.1 (C-2); δ 70.7 (C-3); δ 68.4 (C-5); δ 65.7 (C-6); δ 61.3 ($\underline{\mathbf{C}}H_2$); δ 60.6 ($\underline{\mathbf{C}}H_2$); δ 48.0 ($\underline{\mathbf{C}}H_3$). ^1H - ^1H COSY and ^1H - ^{13}C HMQC NMR spectra in Figures 16 and 17 show only those proton and carbon contours that were used for the assignment of the signals.

High resolution ESI-TOF-MS was used to determine the molecular mass of intermediate (4). Figure 18 shows a portion of the mass spectrum of the (M+I$^-$) ion-adducts of intermediate compound (4). The calculated m/z values agree well with the measured ones indicating the existence of the desired product.

2.2.4 Heptakis(6-deoxy-6-morpholinio)-β-cyclomaltoheptaose Chloride (HMBCD)

Next, the iodide counter ion of intermediate compound (4) was exchanged with chloride, using a strong anion exchanger. Heptakis(6-deoxy-6-morpholinio)-β-cyclodextrin iodide was dissolved in a minimum volume of water, and applied to a bed of strong anion exchanger (Amberlite IRA-400, OH form), and eluted with water. The collected effluent was then titrated with HCl to a neutral pH. Evaporation of the solvent provided the pure final product as off-white crystals.

High resolution ESI-TOF-MS was used to determine the molecular mass of the final product. Figure 19 shows a portion of the mass spectrum of the (M+Cl$^-$) of the final product), HMBCD. The calculated m/z values agree well with the measured ones confirming that the desired final material, HMBCD, was synthesized, and exists in the chloride form.

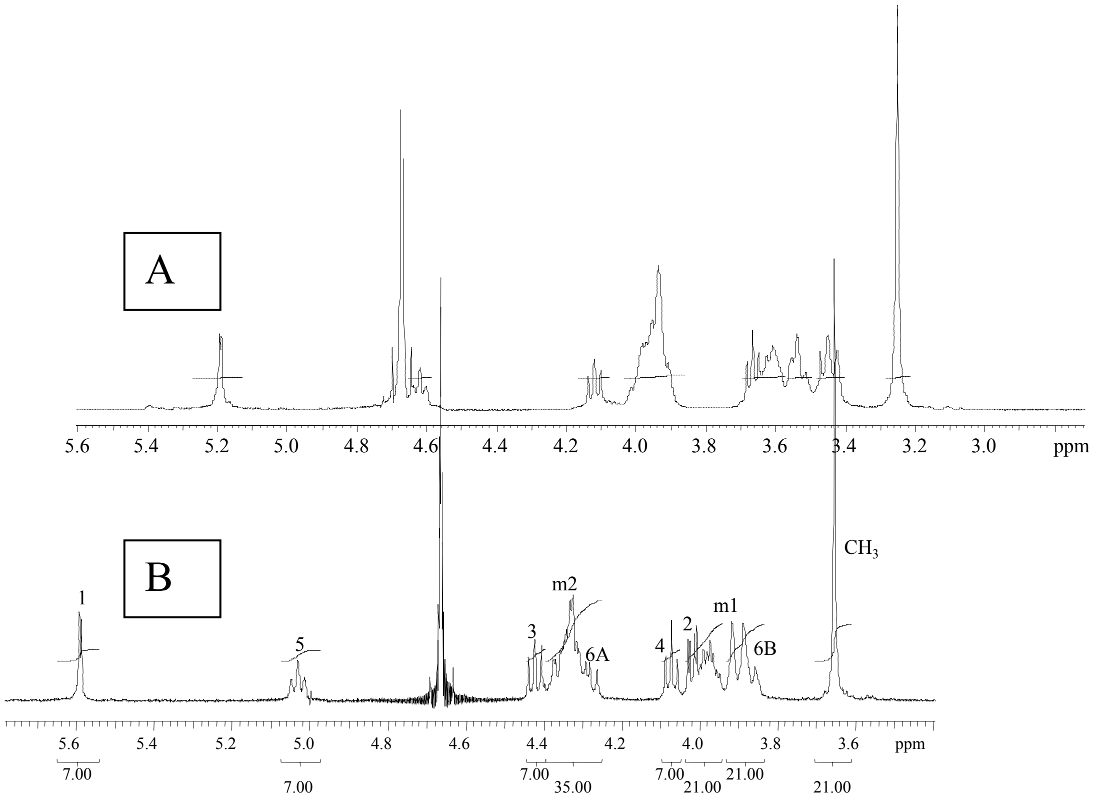

Figure 15. ^{1}H NMR spectra of intermediate compound (4) in D_2O, using a 500 MHz NMR spectrometer. (A) Temperature = 22 °C, (B) Temperature = 60 °C.

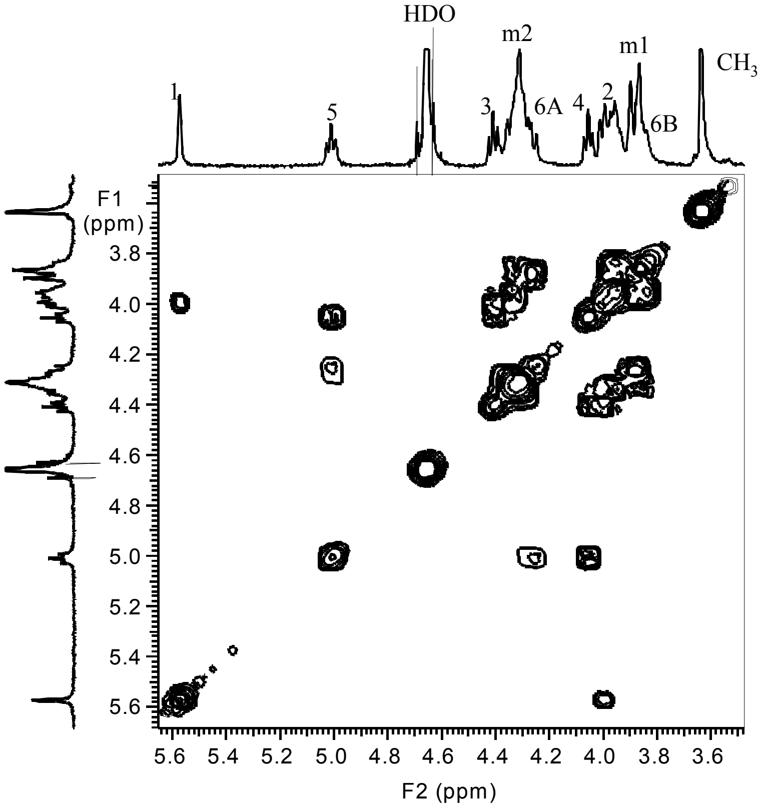

Figure 16. ^1H-^1HCOSY of intermediate compound (4) in D_2O using a 500 MHz NMR spectrometer.

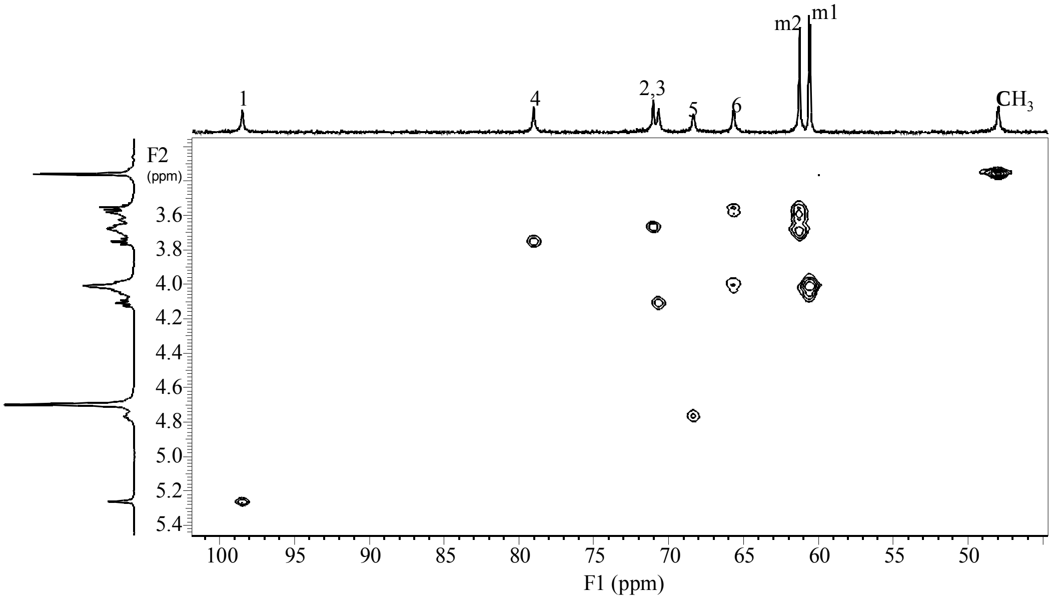

Figure 17. ^1H-^{13}C HMQC of intermediate compound (4) in D_2O, using a 500 MHz NMR spectrometer.

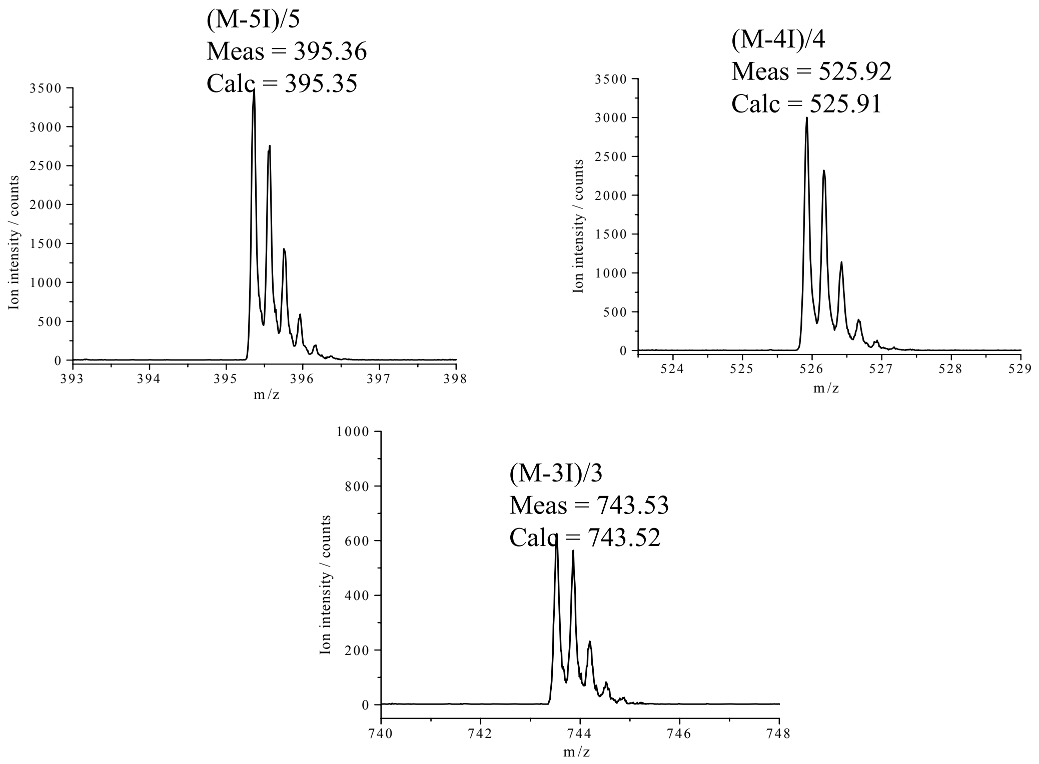

Figure 18. Portions of the high resolution ESI-TOF-MS spectrum of intermediate compound (4) for 3, 4, and 5 charge states. Measured vales are in agreement with the calculated values.

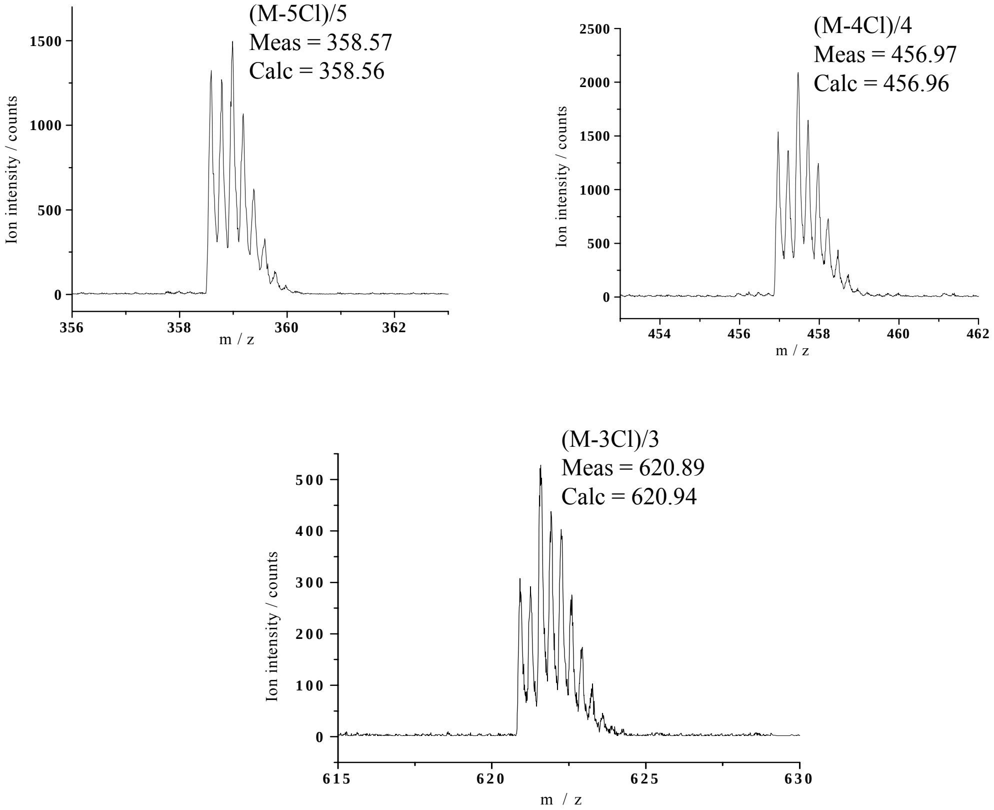

Figure 19. Portions of the high resolution ESI-TOF-MS spectrum of HMBCD, after ion exchange, for 3, 4, and 5 charge states. Measured values are in agreement with the calculated values.

2.3 Synthesis and Characterization of PEMEDA-BCD

Mono-quaternarized single-isomer cyclodextrins have been obtained only by having CDs that were selectively derivatized with a good leaving group in one of the glucose units of the CD, and having insignificant amounts of multiply substituted isomers at the other primary or secondary hydroxy group positions. The synthetic scheme used for the preparation of mono(6-deoxy-6-N, N, N', N', N'-pentamethylethylenediammonio)-cyclomaltoheptaose (PEMEDA-BCD) is shown in Figure 20. The details of the synthetic procedures are outlined in the Appendix.

2.3.1 Synthesis of *p*-Toluenesulfonyl Anhydride (Ts_2O)

p-Toluenesulfonyl anhydride was prepared by adding *p*-toluenesulfonic acid into a solution of *p*-toluenesulfonyl chloride in dichloromethane, and stirring for 24 hours as reported in the literature [93]. This was followed by filtration of the reaction mixture, through silica gel. The filtrate was then concentrated to 30% of the initial volume by evaporation. The pure, white crystals of Ts_2O were precipitated from the solution with hexane, and collected by filtration.

The structure of Ts_2O was verified by high-resolution ^{1}H and ^{13}C NMR spectroscopy. Figure 21 shows the ^{1}H NMR spectrum. ^{1}H NMR data in $CDCl_3$: δ 7.95 (doublet, 4 CH, $J_{1\text{-}2}$ = 8.7 Hz); δ 7.43 (doublet, 4 CH, $J_{2\text{-}1}$ = 8.7 Hz); δ 2.52 (singlet, 6 CH_3);. ^{13}C NMR data in $CDCl_3$: 130.2 (C-1); δ 126.9 (C-2); δ 21.8 (C-3). The peak assignments for ^{1}H and ^{13}C NMR were determined from the 1-dimensional ^{1}H and ^{13}C NMR spectra.

High resolution ESI-TOF-MS was used to determine the molecular mass of Ts_2O. Figure 22 shows portions of the mass spectrum obtained for the (M-Ts), and (M-TsO) fragments of Ts_2O. The calculated m/z values, 171.01and 155.02 agree well with the measured values, 171.01 and 155.01 respectively, indicating that the desired product was obtained.

2.3.2 Mono(6-*O*-tosyl)-β-cyclodextrin

Monotosylated β-CD, intermediate compound (2), was obtained following the procedure published by Zhong et al. [93]. Native β-CD and freshly made tosyl anhydride were suspended in deionized water and stirred for two hours. Then, a 10% NaOH solution was added to the reaction flask. After 10 minutes, the reaction mixture was filtered using a sintered glass funnel to remove unreacted tosyl anhydride. Then, ammonium chloride crystals were added to the filtrate, allowing pure intermediate compound (2) to precipitate from the solution, without the need for further purification. The precipitate was washed 2 times with deionized water and acetone, and collected by filtration. The reaction progress was monitored by TLC, using aluminum-backed Silica 60 plates and n-propanol : water : ethylactate : ammonium hydroxide; 5:3:1:1 as running solvent, giving an $R_f = 0.68$ for intermediate compound (2). The purity of intermediate compound (2) was determined by an isocratic normal phase HPLC separation, using a 4.6 mm I. D. × 250 mm Zorbax silica column and a 30 : 70,

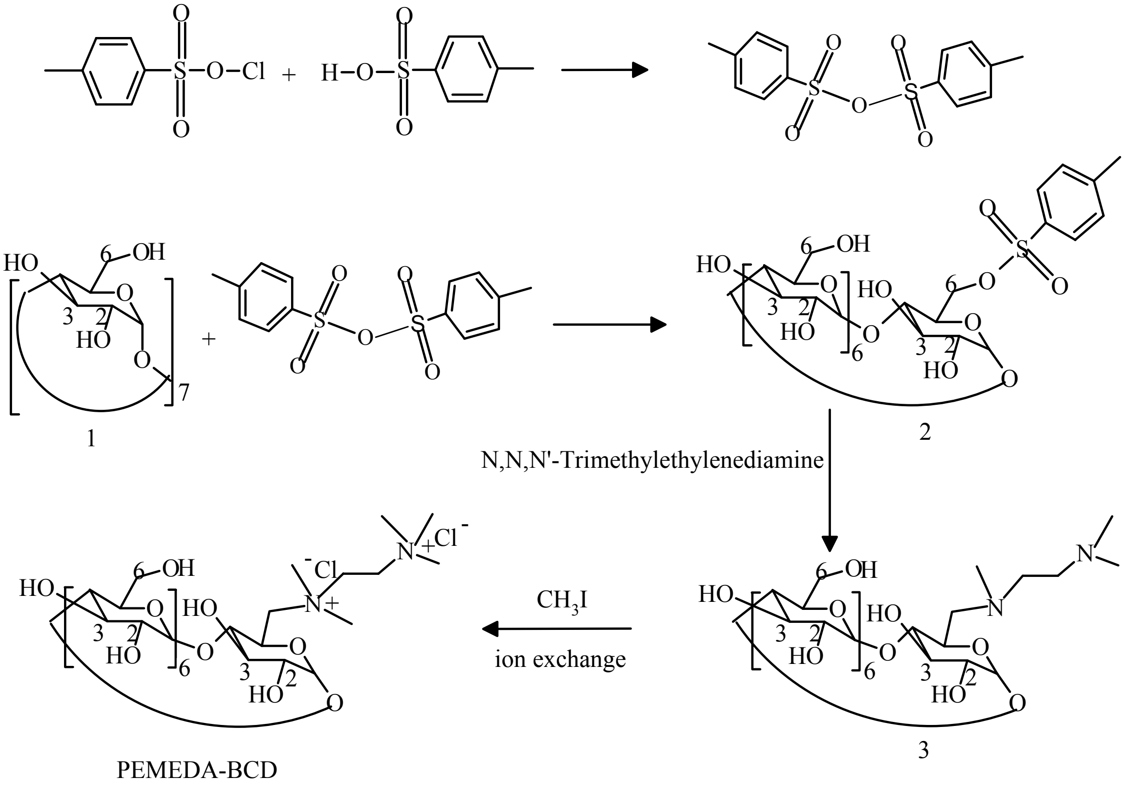
+
+
1
2
N,N,N'-Trimethylethylenediamine
3
CH₃I
ion exchange
PEMEDA-BCD

Figure 20. Synthesis scheme for mono(6-deoxy-6-*N,N,N′,N′,N′*-pentamethylethylendiammonio)-β-CD (PEMEDA-BCD).

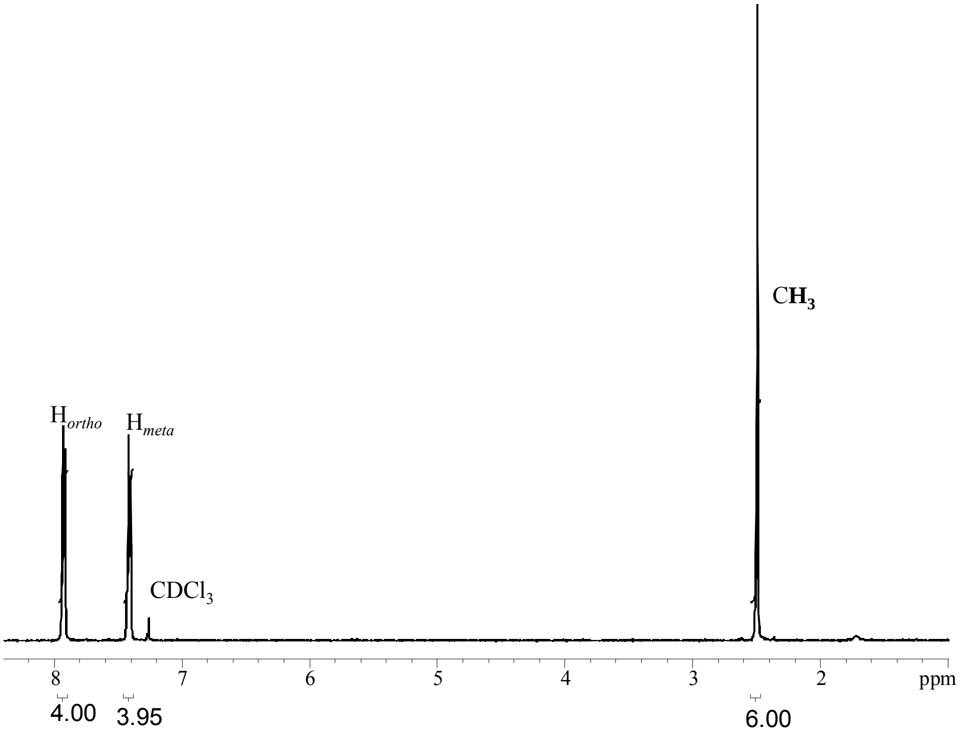

Figure 21. ^{1}H NMR spectrum of *p*-toluenesulfonyl anhydride in $CDCl_3$, using a 500 MHz NMR spectrometer.

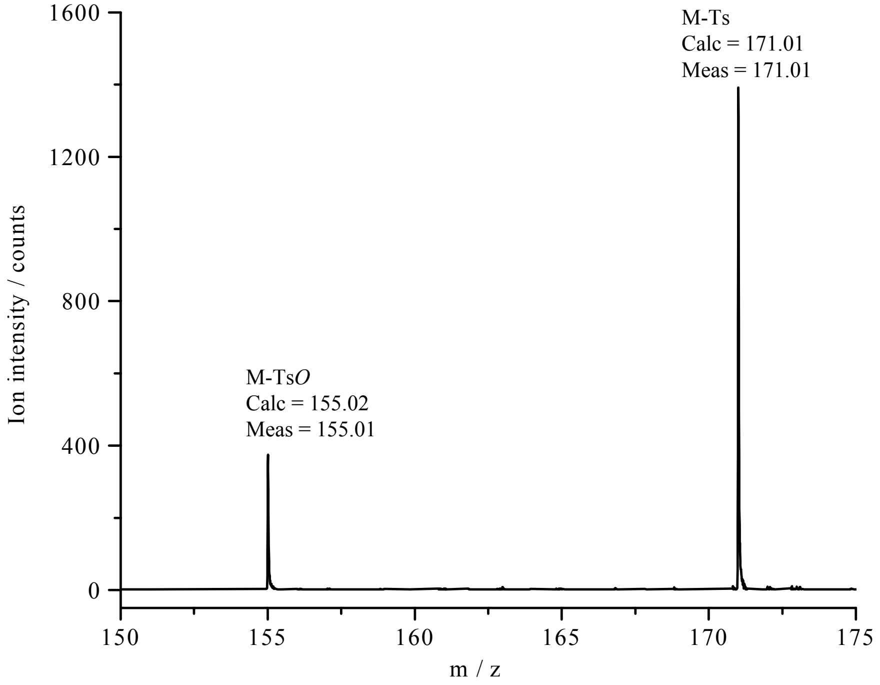

Figure 22. High resolution ESI-TOF-MS spectrum showing the fragment ions of *p*-toluenesulfonyl anhydride.

ethylacetate : methanol binary mobile phase at 2.0 mL / min, at ambient temperature. The chromatogram of intermediate (2), after washing with deionized water and acetone, is shown in Figure 23. An isomeric purity > 98% was obtained for intermediate compound (2).

The structure of intermediate compound (2) was verified by high-resolution ^{1}H and ^{13}C NMR spectroscopy. The peak assignments were determined from the 1-dimensional ^{1}H and ^{13}C NMR spectra, coupled with 2-dimensional ^{1}H-^{1}H COSY and ^{1}H-^{13}C HMQC NMR spectroscopy. ^{1}H NMR data in CD_3OSCD_3 : δ 7.75 (doublet, 2 CH$_{\textit{meta}\text{Ts}}$, J = 8.5 Hz); δ 7.42 (doublet, 2 CH$_{\textit{ortho}\text{Ts}}$, J = 8.5 Hz); δ 5.81 (doublet, 1 O**H** of the monosubstituted glucopyranose unit, J = 6.5 Hz); δ 5.79 – 5.61 (multiplet, 12 O**H**); δ 4.89 – 4.73 (multiplet, 7 H-1); δ 4.52 – 4.12 (multiplet, 7 O**H**); δ 3.72 – 3.19, (multiplet, 42 H); δ 2.42, (singlet, 3 (C$\underline{\mathbf{H_3}}$)). ^{13}C NMR data in CD_3OCD_3: δ 145.4 (C$_{\text{Ts}}$); δ 137.5 (C$_{\text{Ts}}$); δ 128.0 (C$_{\text{Ts}}$); δ 125.4 (C$_{\text{Ts}}$); δ 102.3 – 101.3 (m, C-1); δ 81.5 –80.8 (m); δ 73.1 – 72.0 (m); δ 69.7; δ 68.9; δ 59.9 – 59.3 (m); δ 21.2 (CH$_{3\text{Ts}}$). ^{1}H - ^{1}H COSY and ^{1}H - ^{13}C HMQC NMR spectra in Figures 24 and 25 show only those proton and carbon contours that are related to the glucose unit.

High resolution MALDI-TOF-MS was used to determine the molecular mass of intermediate compound (2). A portion of the MALDI-TOF-MS spectrum (the Na^+ and K^+ ion-adduct portions) of intermediate compound (2) is shown in Figure 26. The calculated m/z value of the Na^+ ion-adduct of the parent molecule, 1311.37 and agrees well with the value obtained using MALDI-TOF-MS, 1327.34, indicating the presence of the β-cyclodextrin bearing a single tosyl group.

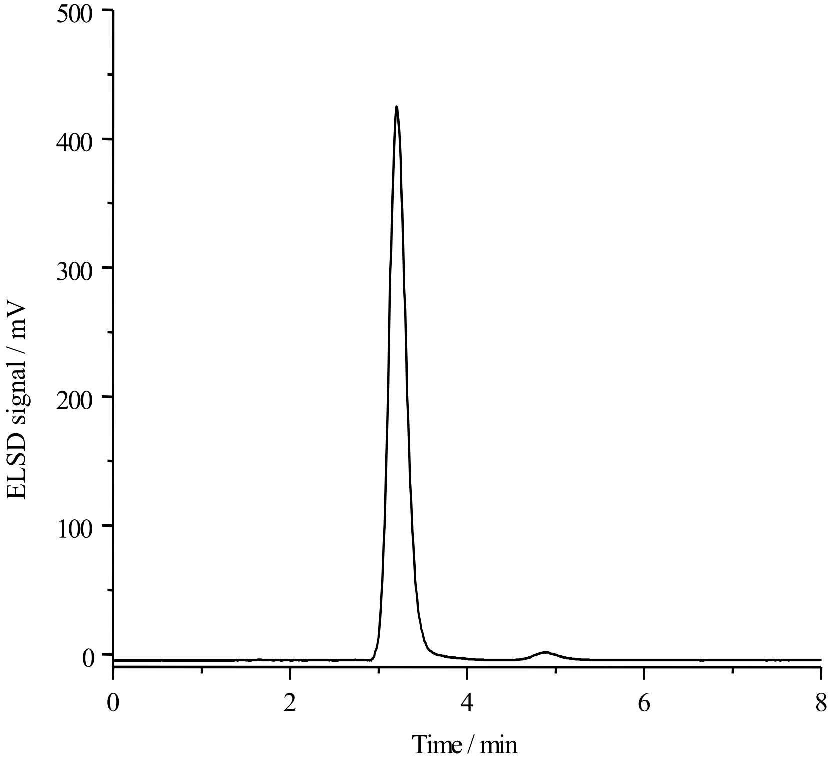

Figure 23. Chromatogram of intermediate compound (2). Purity > 98%. Conditions: EtOAc : MeOH = 70 : 30, 2.0 mL/min, 5 μm silica column.

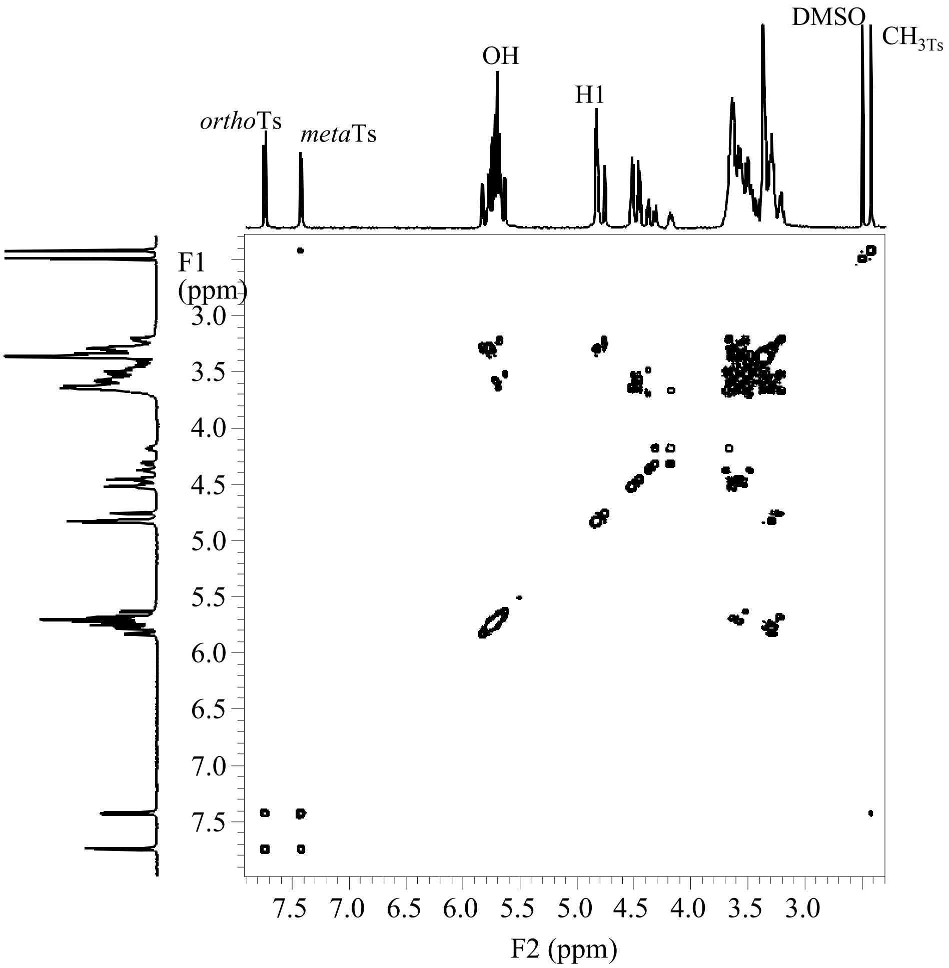

Figure 24. ^1H-^1H COSY of intermediate compound (2) in DMSO-d_6, using a 500 MHz NMR spectrometer.

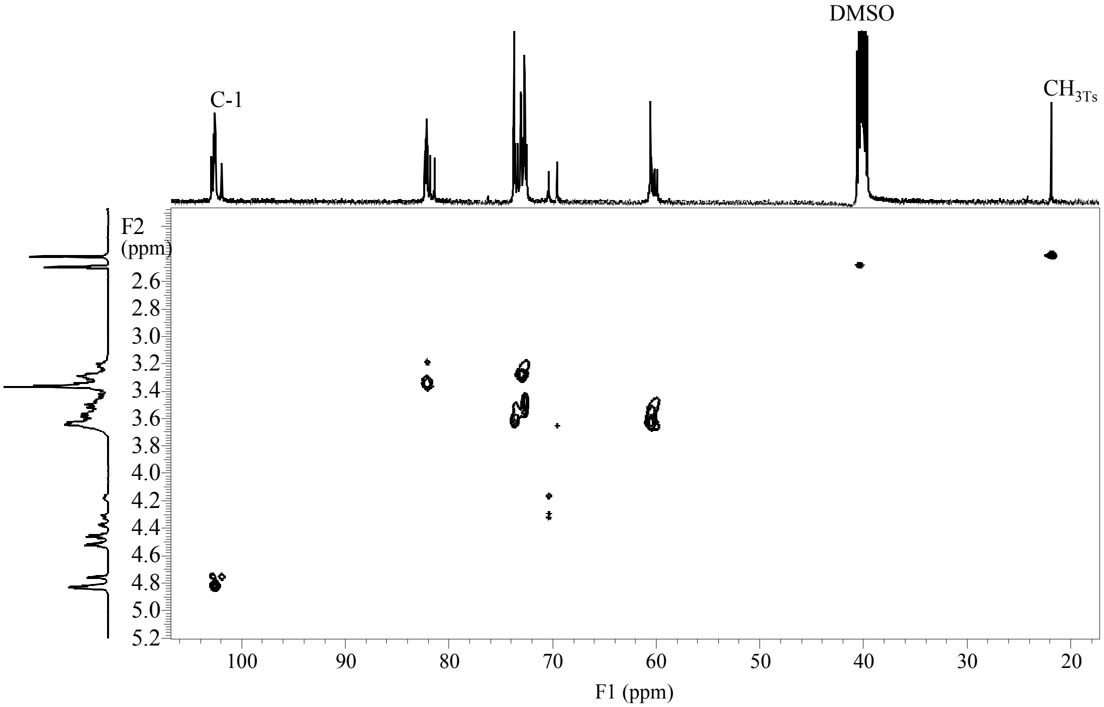

Figure 25. ^{1}H-^{13}C HMQC of intermediate compound (2) in DMSO-d_6, using a 500 MHz NMR spectrometer.

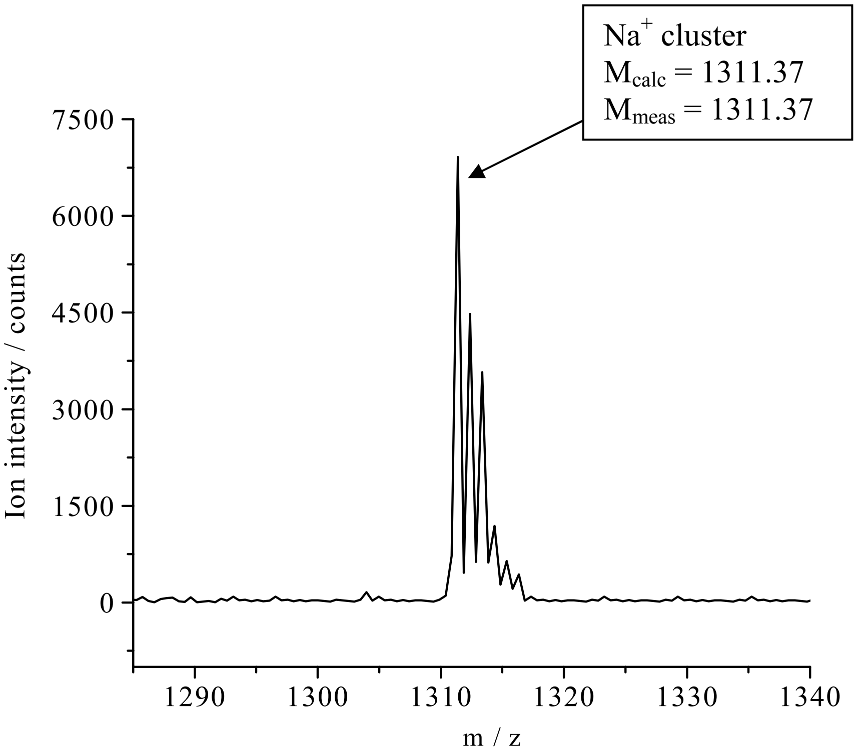

Figure 26. A portion of MALDI-TOF-MS spectrum of intermediate compound (2).

2.3.3 Mono(6-deoxy-6-pyridinium)-β-cyclodextrin (CDP)

Then, the mono(6-*O*-tosyl)-β-CD, intermediate (2), was used to synthesize a mono-quaternarized β-CD according to a modified procedure described in [94]. The modification involved adding dry pyridine (both reagent and solvent) to a reaction flask purged with nitrogen, followed by addition of intermediate compound (2). The flask was heated to 70 °C and stirred under a nitrogen blanket for 48 hours. Progress of the reaction was followed by direct UV-detection CE, using a 50 mM phosphoric acid buffer titrated with lithium hydroxide to pH 2.13 as BE, with the detector placed at the cathode. Next, excess pyridine was evaporated under reduced pressure, the residue was dissolved in deionized water, and the undissolved solids were filtered off. After concentration of the aqueous solution to about 60% of its original volume by evaporation, solid material was precipitated from the solution by slow addition of acetone. The precipitate was then collected by filtration, dissolved in a minimum volume of water, and reprecipitated with acetone. The procedure was repeated 3 times, the product was dried in a vacuum oven at room temperature, and analyzed by CE. The isomeric purity of the final product, mono(6-deoxy-6-pyridinium)-β-cyclodextrin (CDP), was determined by CE to be greater than 98% as shown in Figure 27.

The structure of CDP was verified by high-resolution ^{1}H and ^{13}C NMR spectroscopy. The peak assignments were determined from the 1-dimensional ^{1}H and ^{13}C NMR spectra, coupled with 2-dimensional ^{1}H-^{1}H COSY and ^{1}H-^{13}C HMQC NMR spectroscopy. ^{1}H NMR data in D_2O: δ 8.82 (doublet, 2 H, pyridine, J = 6.0 Hz); δ 8.51 (triplet, 1 H, pyridine, J = 8.0 Hz,); δ 8.00 (doublet of doublets, 2 H, pyridine, J = 6.0

Hz, J = 8.0 Hz); δ 7.53 (doublet, 2 H, tosylate, J = 8.0 Hz); δ 7.07 (doublet, 2 H, tosylate, J = 8.0 Hz); δ 5.06 (doublet, 1 H-1' of the monosubstituted glucopyranose unit, J = 7.5 Hz); δ 4.99 (doublet, 1 H-1, J = 3.5); δ 4.90 – 4.84 (multiplet, 4 H-1); δ 4.79 (doublet, 1 H-1, J = 3.5); δ 4.12 (triplet, 1 H, J = 9.0); δ 3.96 – 3.93 (multiplet 37 H); δ 3.26 (triplet, 1 H, J = 9.0); δ 2.73 (doublet, 1 H, J = 10); δ 2.35, 2.33 (doublet of doublets, 1 H, J = 4.0); δ 1.96 (singlet, CH_3, tosylate). ^{13}C NMR data in D_2O: δ 146.1 (C_{pyr}); δ 145.5 (C_{pyr}); δ 145.4 (C_{Ts}); δ 137.5 (C_{Ts}); δ 128.0 (C_{Ts}); δ 127.9 (C_{Ts}); δ 125.4 (C_{Ts}); δ 100.9 – 102.3 (multiplet, C-1); δ 83.6; δ 82.9; δ 81.4; δ 80.6; δ 73.4; δ 73.0; δ 72.3; δ 72.1; δ 71.9; δ 71.3; δ 70.2; δ 61.6; δ 60.8; δ 59.8; δ 58.7; δ 20.7 (CH_{3Ts}). ^1H - ^1H COSY NMR spectrum in Figure 28 shows all the proton contours that are related to the molecule.

The molecular mass of CDP was determined by high resolution MALDI-TOF-MS. A portion of the mass spectrum of CDP is shown in Figure 29. The measured m/z value of 1196.53 agrees well with the calculated value, 1196.41, for the monoisotopic (M) parent ion of CDP.

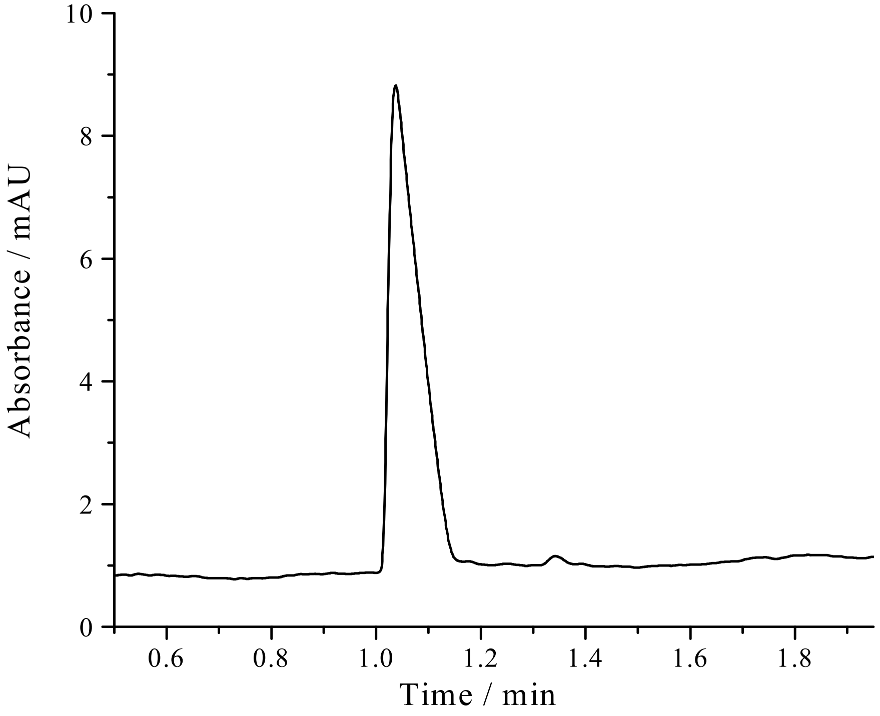

Figure 27. UV-detection electropherogram of CDP. Purity > 98%. Conditions: 50 mM phosphoric acid / LiOH, pH = 2.13, (+) to (-) polarity, Lt/Ld = 26.4 / 19.6 cm, 18 kV, 214 nm, T = 20 °C.

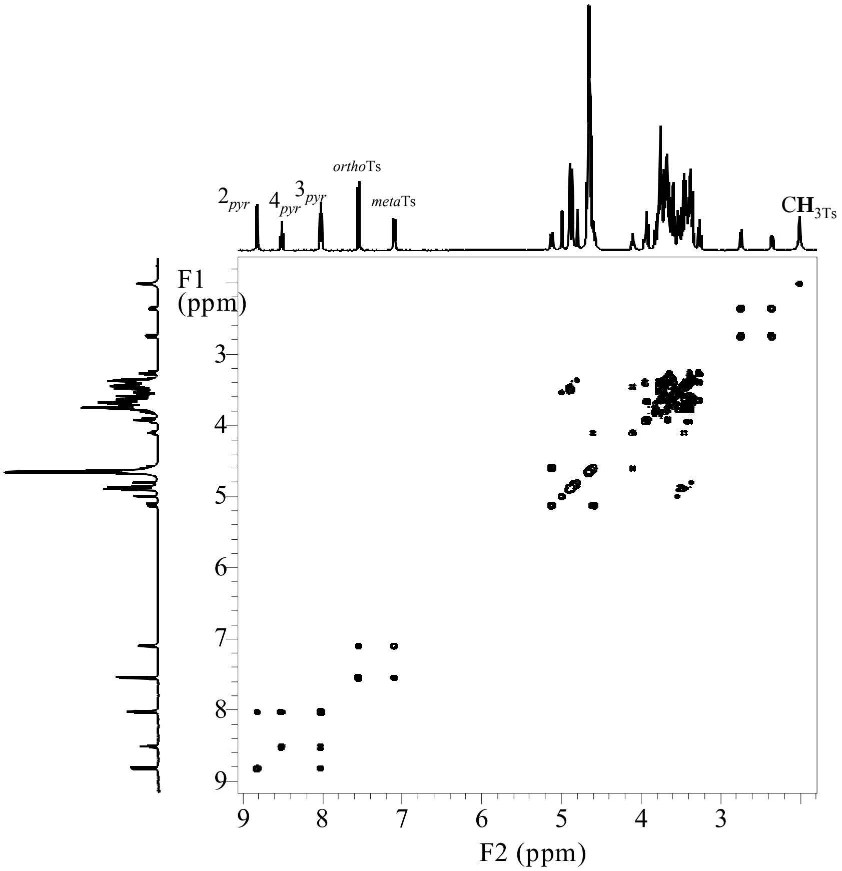

Figure 28. ^1H-^1H COSY of CDP in D_2O, using a 500 MHz NMR spectrometer.

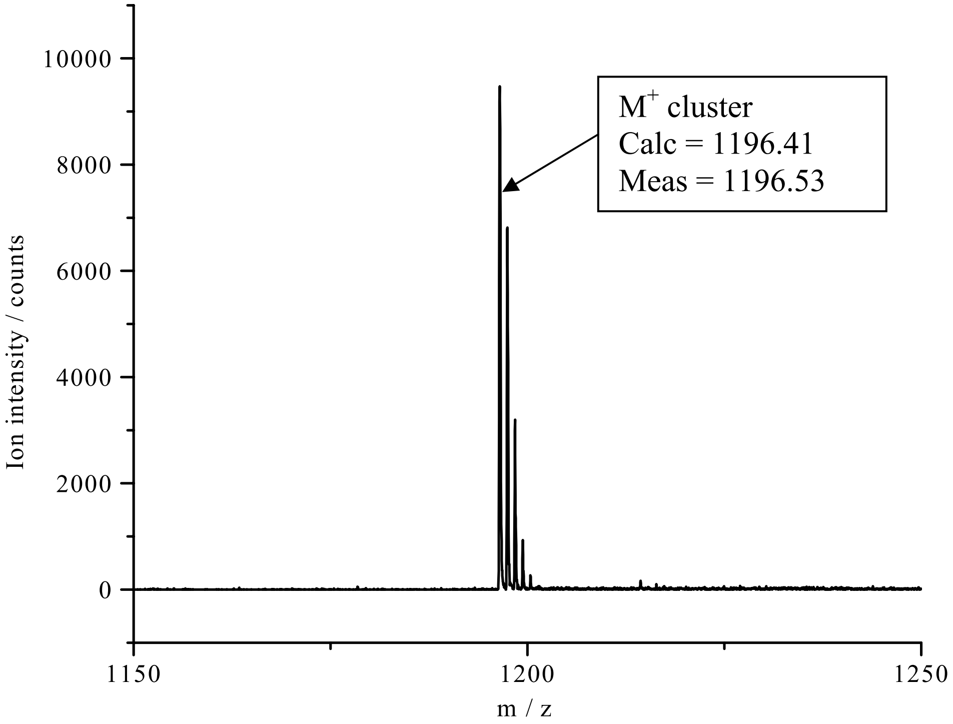

Figure 29. A portion of high resolution MALDI-TOF-MS spectrum of CDP. The measured m/z value of 1196.53 is in agreement with the value calculated for the monoisotopic parent ion.

2.3.4 Mono(6-deoxy-6-*N, N, N', N', N'*-pentamethylethylenediamino)- β-cyclodextrin

Mono(6-deoxy-6-*N*,*N*,*N*',*N*',*N*'-pentamethylethylenediamino)-β-cyclodextrin, intermediate (3), was synthesized based on the procedure used for the synthesis of CDP. Dry intermediate (2**)** was added to N,N', N'-trimethylethylenediamine in the reaction flask, heated to 60 °C under a blanket of dry nitrogen for 18 hours. Progress of the reaction was monitored by two complementary methods; (i) indirect UV-detection CE, using a 20 mM acetic acid solution titrated to pH 4.55 with 10 mM imidazole as the BE, and (ii) direct UV-detection CE, using 25 mM phosphoric acid titrated to pH 2.55 with lithium hydroxide as the BE to follow the disappearance of mono-tosylated β-CD. The second method was based on the results of previous experiments, which showed that unreacted neutral tosyl β-CD, in low pH phosphoric acid/LiOH buffer, complex with dihydrogen phosphate and became negatively charged. After quenching, the reaction mixture was evaporated to dryness under reduced pressure. The resulting solid was dissolved in a minimum volume of water, and precipitated by slow addition of ethanol. Further purification was performed by repeating the procedure 3 times. The product was dried in a vacuum oven at room temperature, and analyzed by CE. Figure 30 depicts the aqueous indirect UV-detection electropherogram of intermediate compound (3). The final isomeric purity of intermediate compound (3) is greater than 98%.

The structure of intermediate compound (3) was verified by high-resolution ^{1}H and ^{13}C NMR spectroscopy. The peak assignments were determined from the 1-dimensional ^{1}H and ^{13}C NMR spectra, coupled with 2-dimensional ^{1}H-^{1}H COSY and ^{1}H-

^{13}C HMQC NMR spectroscopy. ^{1}H NMR data in CD_3SOCD_3: δ 5.96 (doublet, 1 (O**H**), J = 6.5 Hz); δ 5.81 – 5.65 (multiplet, 14 (O**H**)); δ 4.87, 4.84, 4.80 (three sets of doublets, 7 H-1, J = 5 Hz); δ 4.60 – 4.39 (broad singlet, 5 (O**H**)); δ 3.76 – 3.52 (multiplet, 26 H); δ 3.43 – 3.25 (13 H); δ 3.18 (triplet, 1 H, J = 10 Hz); δ 2.71(doublet, 1 H, J = 15 Hz); δ 2.47 (quartet, 2 H, J = 5 Hz); δ 2.41 – 2.35 (multiplet, 1 H); δ 2.33 – 2.24 (multiplet, 1 H); δ 2.17 (singlet, (C$\mathbf{H_3}$)N); δ 2.09 (singlet, 2(C$\mathbf{H_3}$)N); ^{13}C NMR data in CD_3SOCD_3: 102.83 – 102.24 (multiplet, C-1); δ 45.98 (($\underline{\mathbf{C}}H_3)_2$N); δ 43.90 (($\underline{\mathbf{C}}H_3$)N); ^{1}H - ^{1}H COSY and ^{1}H - ^{13}C HETCOR NMR spectra in Figures 31 and 32 show only those proton and carbon contours that are related to the glucose unit.

High resolution MALDI-TOF-MS was used to determine the molecular mass of intermediate (3). A portion of the mass spectrum (the Na^+ and K^+ ion-adduct portion) of intermediate (3) is shown in Figure 33. The calculated molecular mass values for the H^+, Na^+ and K^+ ion-adducts of the parent molecule, 1219.48 and 1241.47, 1257.44, agree well with the values obtained using MALDI-TOF-MS, 1219.29 and 1241.47, 1257.27, indicating the existence of the target material, mono(6-deoxy-N,N,N’,N’,N’-6-pentamethylethylenediamine)-β-cyclodextrin.

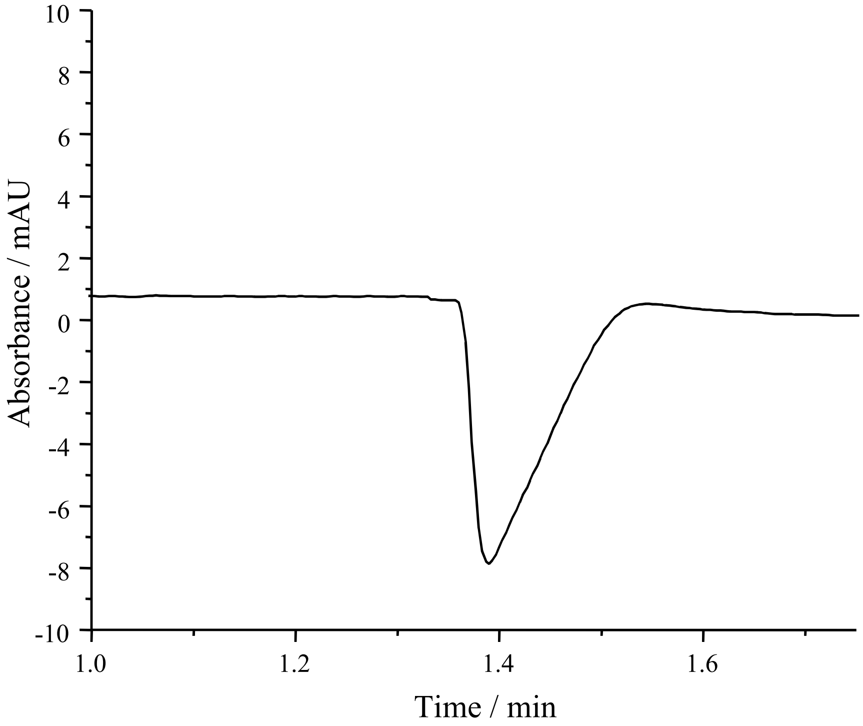

Figure 30. Indirect UV-detection electropherogram of intermediate compound (3). Purity > 98%. Conditions: 20 mM acetic acid / imidazole, pH = 4.6, (+) to (-) polarity, Lt/Ld = 26.4 / 19.6 cm, 18 kV, 214 nm, T = 20 °C.

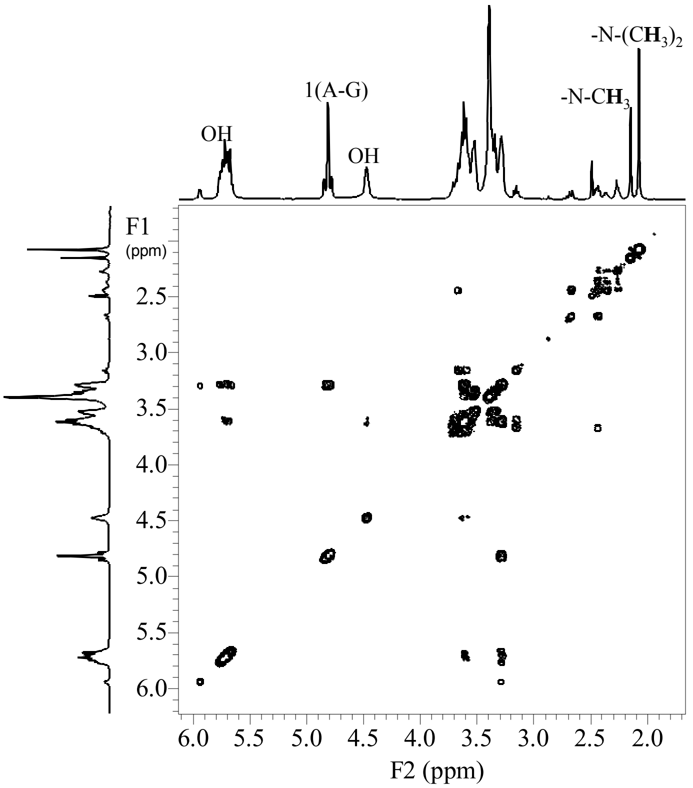

Figure 31. ^1H-^1H COSY of intermediate compound (3) in DMSO-d_6, using a 500 MHz NMR spectrometer.

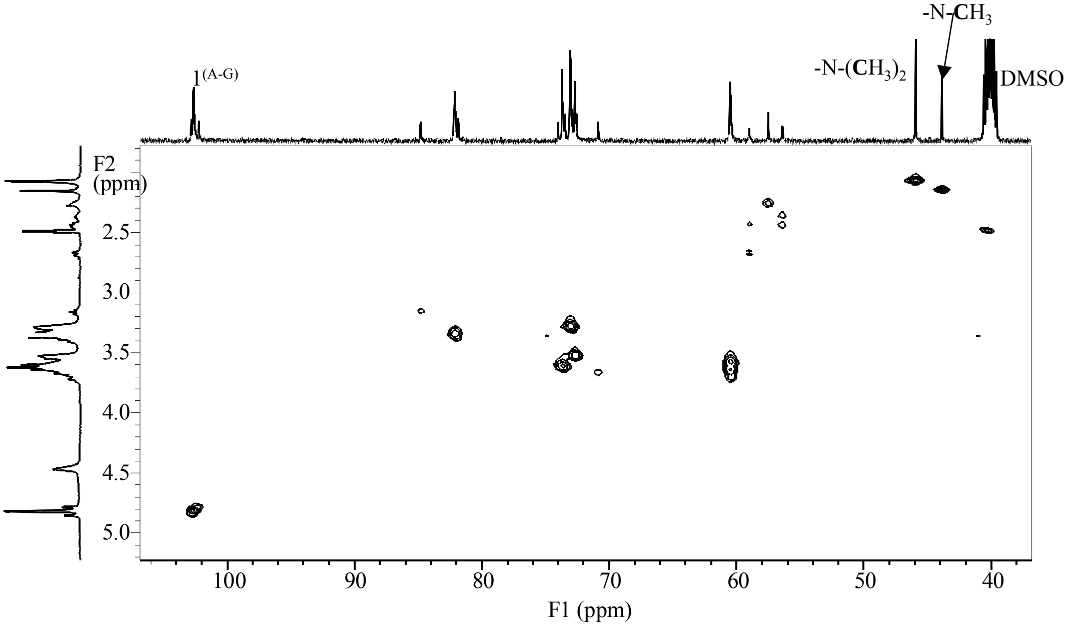

Figure 32. ^{1}H-^{13}C HMQC of intermediate compound (3) in DMSO-d_6, using a 500 MHz NMR spectrometer.

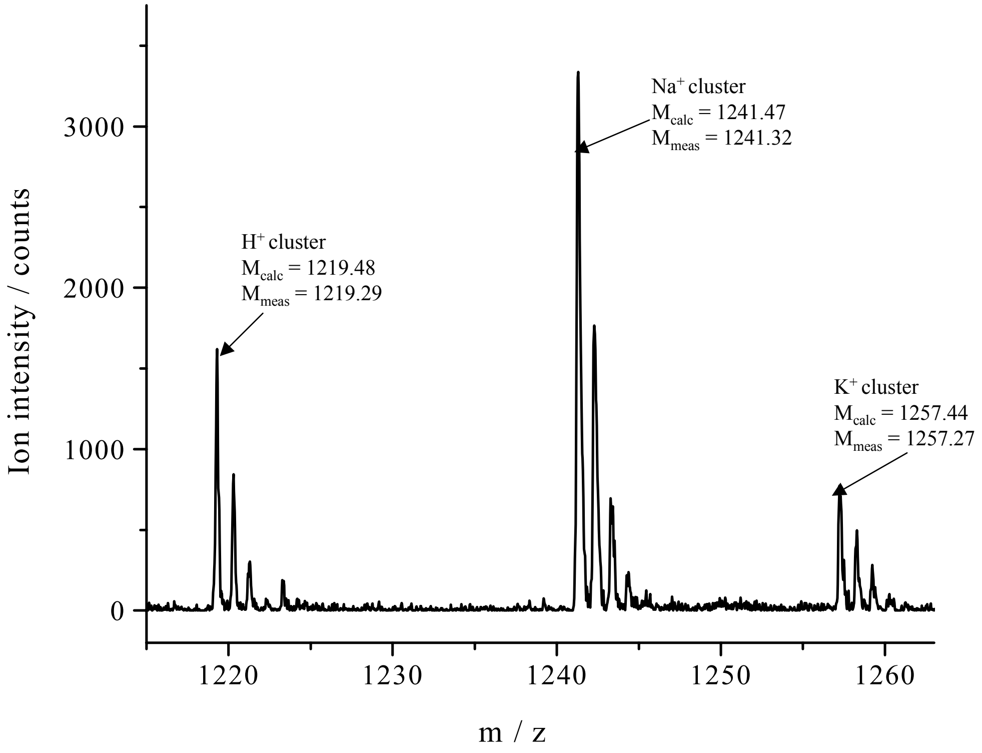

Figure 33. A portion of the high resolution MALDI-TOF-MS spectrum of intermediate (3). Measured m/z values are in agreement with those calculated for the monoisotopic proton, sodium, and potassium adducts.

2.3.5 Mono(6-deoxy-6-*N,N,N',N',N'*-pentamethylethylenediammonio)-β-cyclodextrin Iodide

Intermediate compound (4) was synthesized according to the common synthetic method for preparation of quaternary ammonium derivatives. Dry DMF was added into a three-neck reaction flask, and purged with dry nitrogen. Then, intermediate (3) was dissolved in DMF, followed by slow addition of methyl iodide. The flask was stirred under a blanket of nitrogen, heated to 40 °C, and refluxed. Progress of the reaction was monitored by indirect UV-detection CE, using a 20 mM acetic acid solution, titrated to pH 4.55 with 10 mM imidazole as the BE. The workup involved evaporation of the reaction solvent under reduced pressure, dissolving the residue in a minimum volume of deionized water, and precipitation with acetone. The solids were collected by suction filtration. This procedure was repeated three times to obtain pure intermediate (4**),** having iodide as the counter ion. CE analysis of the final product, after drying in a vacuum oven at room temperature, showed an isomeric purity of > 98% for the target, Figure 34.

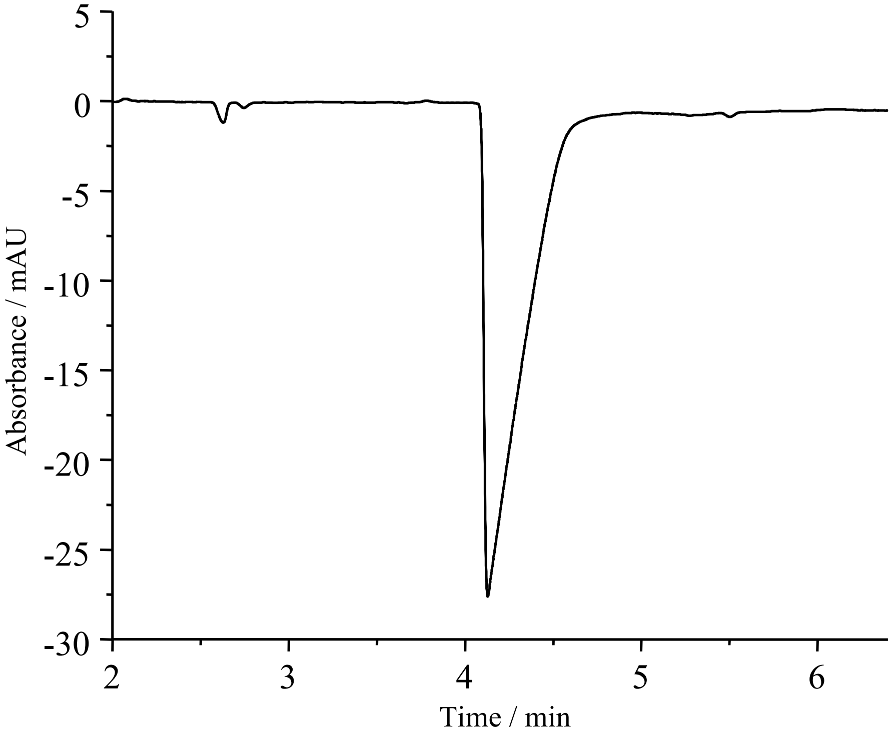

Figure 34. Indirect UV-detection electropherogram of intermediate compound (4). Purity > 98%. Conditions: 20 mM acetic acid / imidazole, pH = 4.6, (+) to (-) polarity, Lt/Ld = 26.4 / 19.6 cm, 18 kV, 214 nm, T = 20 °C.

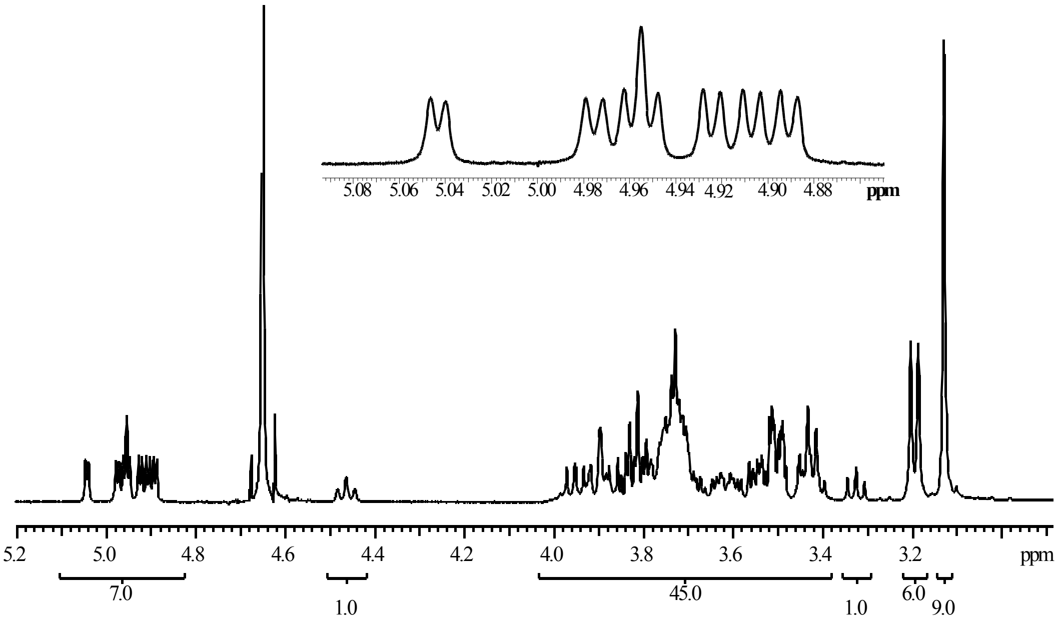

Figure 35. ^{1}H NMR spectrum of intermediate compound (4) in D_2O, obtained by using 500 MHz NMR spectrometer.

The structure of intermediate compound (4) was verified by high-resolution ^{1}H and ^{13}C NMR spectroscopy. The peak assignments were determined from the 1-dimensional ^{1}H and ^{13}C NMR spectra, coupled with 2-dimensional ^{1}H-^{1}H COSY and ^{1}H-^{13}C HMQC NMR spectroscopy. Figure 35 shows the full ^{1}H NMR spectrum of intermediate compound (4). ^{1}H NMR data in D_2O: δ 5.05 (doublet, 1 H-1, J = 5.0 Hz); δ 4.98 (doublet, 1 H-1, J = 5.0 Hz); δ 4.96 (triplet, 2 H-1, J = 3.5 Hz, J = 3.5 Hz); δ 4.93 (doublet, 1H-1, J = 4.0 Hz): δ 4.91 (doublet, 1 H-1, J = 4.0 Hz); δ 4.89 (doublet, 1 H-1, J = 4.0 Hz); δ 4.46 (triplet, 1 H-5, J = 10.0 Hz, J = 10.0 Hz); δ 4.01 – 3.39 (multiplet, 44 H); δ 3.33 (triplet, 1 H-4, J = 10 Hz, J = 10.0 Hz); δ 3.20, 3.19 (two sets of $(C\mathbf{H_3})N$); δ 3.13 (singlet, $3(C\mathbf{H_3})N$); ^{13}C NMR data in D_2O: δ 102.57 – 101.67 (C-1$^{(B-G)}$); δ 100.67 (C-1^{A}); δ 81.93 (C-4^{A}); δ 67.47 (C-5^{A}); δ 54.01 $3(\underline{\mathbf{C}}H_3)N$; δ 53.00, 52.64 $2(\underline{\mathbf{C}}H_3)N$. ^{1}H - ^{1}H COSY and ^{1}H - ^{13}C HMQC NMR spectra in Figures 36 and 37 show only those proton and carbon contours that are related to the glucose unit.

High resolution ESI-TOF-MS was used to determine the molecular mass of intermediate (4). Figure 38 shows a portion of the mass spectrum of the $(M\text{-}2I^{-})/z$ ion of intermediate compound (4). The calculated $(M\text{-}2I^{-})/z$ value, 624.25, agrees well with the measured one, 624.26, indicating that the desired product was prepared.

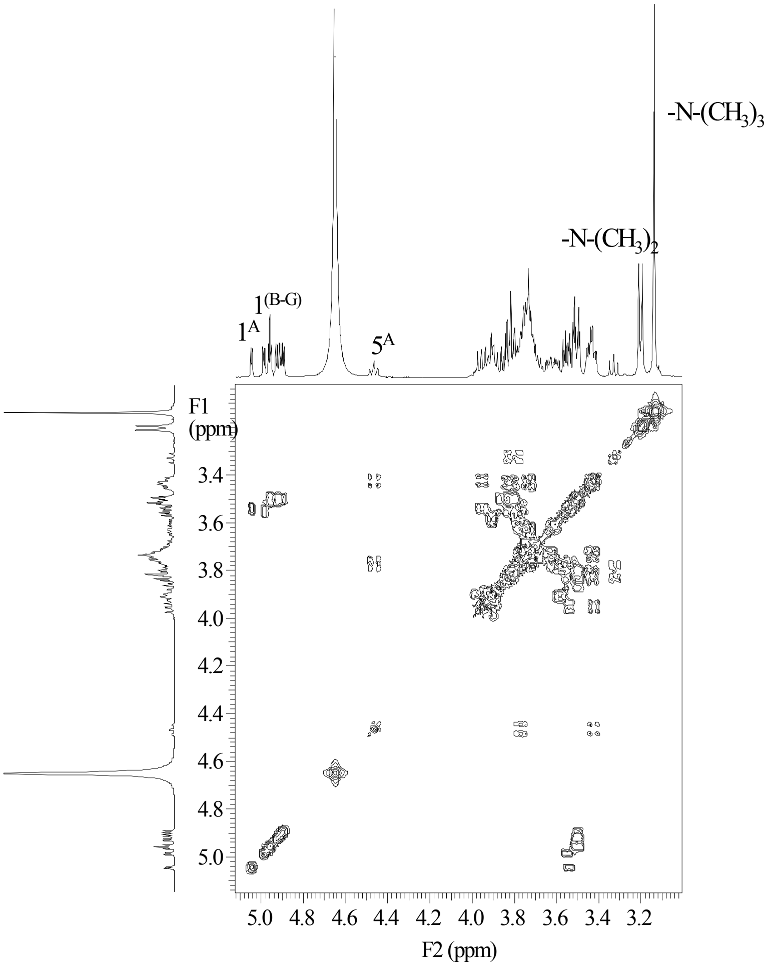

Figure 36. ^{1}H-^{1}H COSY of intermediate compound (4) in D_2O, using a 500 MHz NMR spectrometer.

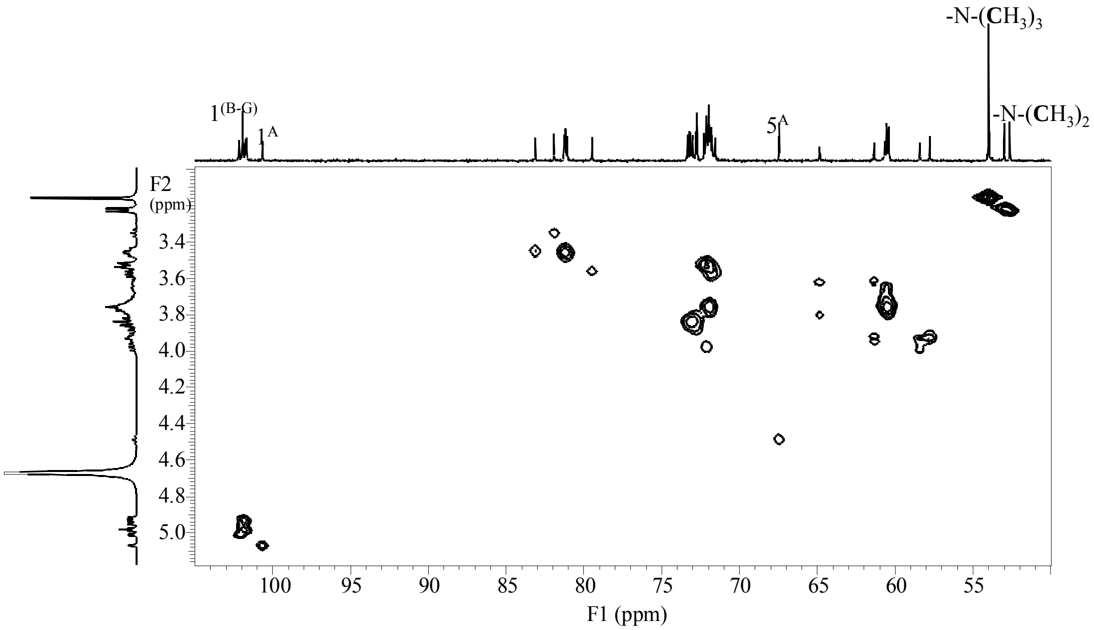

Figure 37. ^{1}H-^{13}C HMQC of intermediate compound (4) in D_2O, obtained by using a 500 MHz NMR spectrometer.

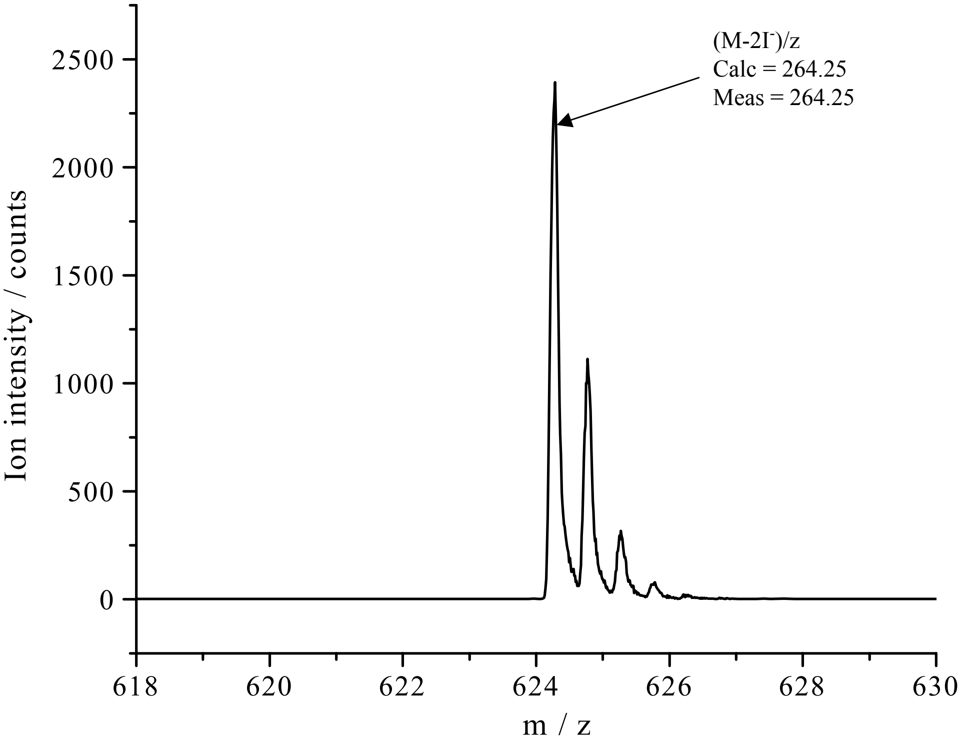

Figure 38. A portion of the high resolution ESI-TOF-MS spectrum of intermediate compound (4).

2.3.6 Mono(6-deoxy-6-*N,N,N',N',N'*-pentamethylethylenediammonio)-cyclomaltoheptaose Chloride (PEMEDA-BCD)

Finally, the iodide counter ion of intermediate (4) was exchanged with chloride, using a strong anion exchanger. Mono(6-deoxy *N,N,N',N',N'*-6-pentamethylethylenediammonio)-cyclomaltoheptaose iodide was dissolved in a minimum volume of water, and applied to a bed of strong anion exchanger (Amberlite IRA-400, OH form), and eluted with water. The collected, basic effluent was then titrated with HCl to a neutral pH. Evaporation of the solvent provided the pure final product as off-white crystals. The exchange of iodide by chloride was confirmed by direct UV-detection CE analysis of the final product, using a 25 mM phosphoric acid solution titrated to pH 2.55 with lithium hydroxide as the BE, and the detector placed at the anode.

High resolution MALDI-TOF-MS was used to determine the molecular mass of PEMEDA-BCD. Figure 39 shows a portion of the mass spectrum for PEMEDA-BCD after exchange of the counter ion. The calculated m/z value agrees well with the measured value confirming that the desired material, PEMEDA-BCD, was successfully made.

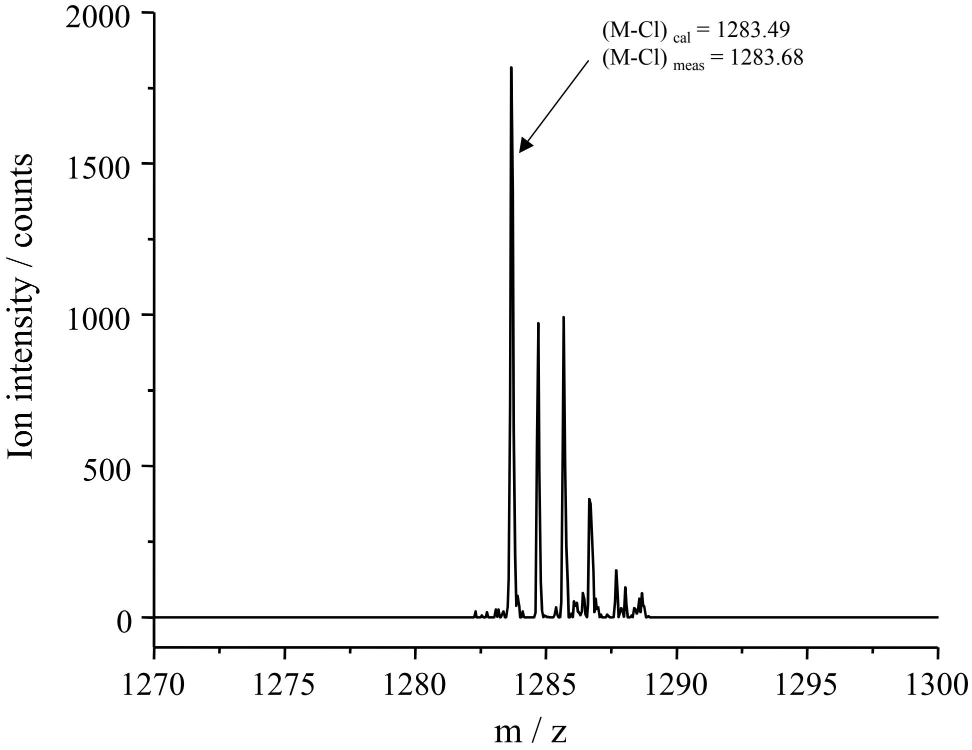

Figure 39. A portion of the high resolution MALDI-TOF-MS spectrum of PEMEDA-BCD.

2.4 Synthesis of Anionic Analytes

Ten anionic racemic analytes, 1-phenyl-1-*O*-sulfo-propane, 2-phenyl-1-*O*-sulfo-propane, 1-phenyl-2-*O*-sulfo-propane, 1-phenyl-1-*O*-sulfo-butane, 2-phenyl-1-*O*-sulfo-butane, 1-phenyl-2-*O*-sulfo-propane, 1-phenyl-1-*O*-sulfo-pentane, 1-phenyl-2-*O*-sulfo-pentane, 1-phenyl-1,2-di-*O*-sulfo-ethane, trans-2-phenyl-1-*O*-sulfo-cyclohexane, were synthesized by sulfating the corresponding alcohols with sulfur trioxide pyridine complex (SO_3-py) in DMF. All the sulfated analytes were prepared by the same procedure. Progress of the reaction was monitored by direct UV-detection CE, using a BE containing 20 mM boric acid titrated to pH 9.0 with LiOH. The workup procedure involved the evaporation of the excess solvent until a paste was obtained. The paste was dissolved in a small volume of deionized water, and titrated to pH 7 with a sodium hydroxide solution. The solution that resulted was added to an equal volume of acetone, excess sodium sulfate precipitated, and was filtered off. Then, the filtrate was evaporated to dryness at 40 °C to obtain the sodium salts of the sulfated analytes. Figure 40 depicts the CE separation of a representative of the anionic analytes.

High resolution ESI-TOF-MS was used to determine the molecular mass of the anionic analytes. Figures 41 to 45 show portions of the mass spectra of the (M-Na^+) ion of some of the anionic analytes. The calculated m/z values agree well with the measured ones confirming that the desired anionic analytes were successfully synthesized.

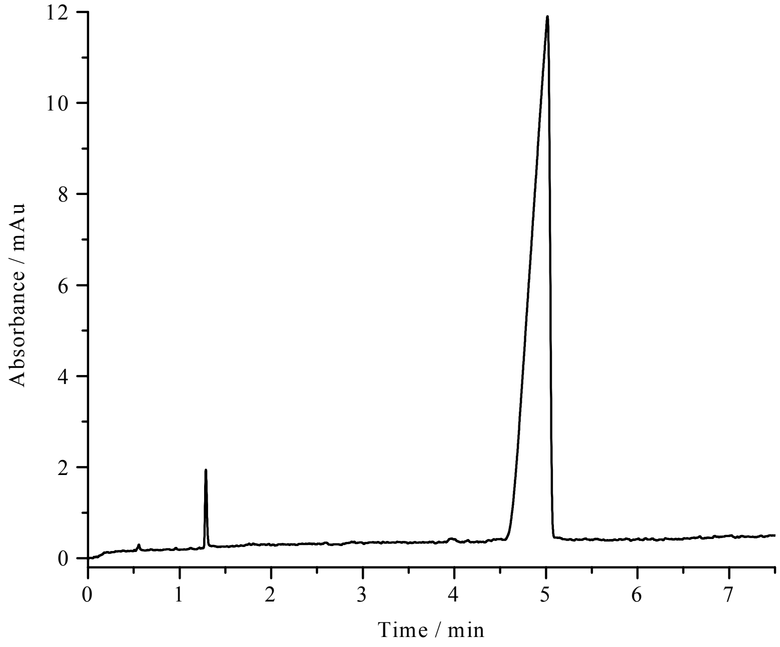

Figure 40. Direct UV-detection electropherogram of 1-phenyl-2-*O*-sulfo-propane. Purity > 99%. Conditions: 25 μm I. D. fused silica capillary, 20 mM boric acid / LiOH pH = 9.0, 18 kV (+) to (-) polarity, 214 nm.

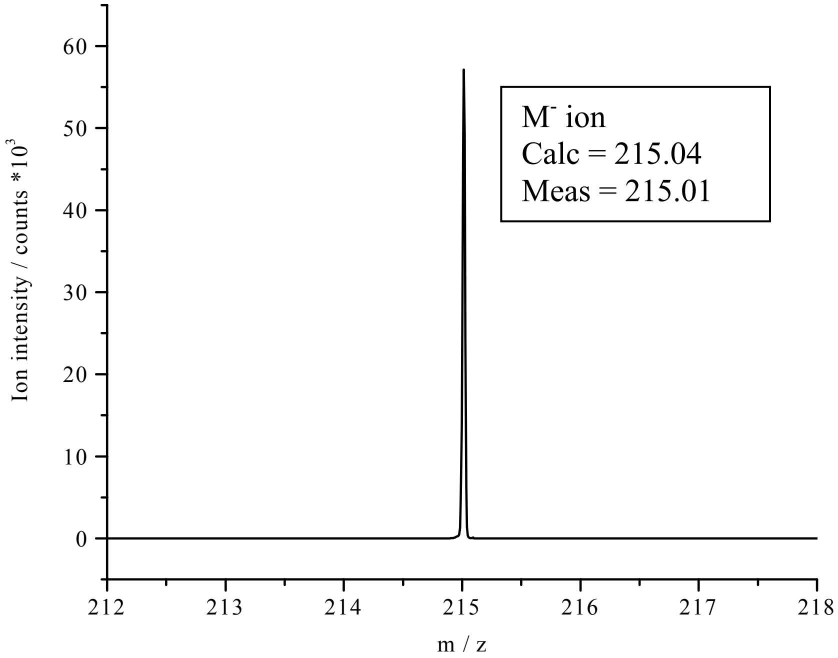

Figure 41. A portion of the high resolution ESI-TOF-MS spectrum of 1-phenyl-2-*O*-sulfo-propane. The measured m/z value of 215.01 agrees with 215.04 calculated for the monoisotopic ion.

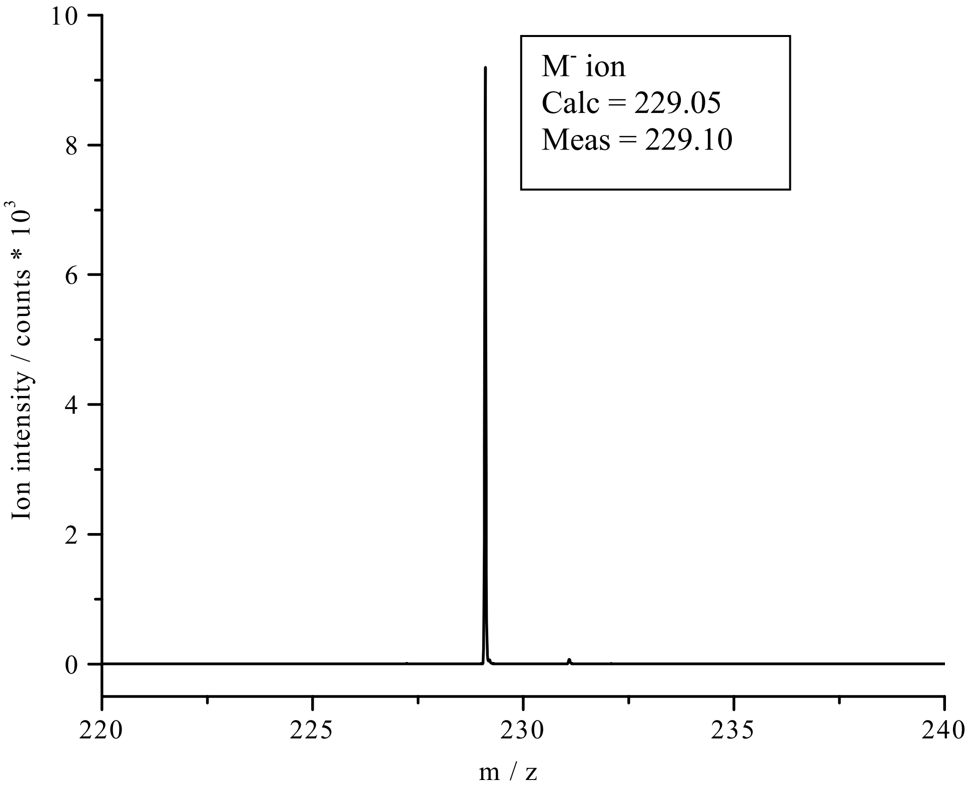

Figure 42. A portion of the high resolution ESI-TOF-MS spectrum of 1-phenyl-2-*O*-sulfo-butane. The measured m/z value of 229.10 agrees with the 229.05 value calculated for the monoisotopic ion.

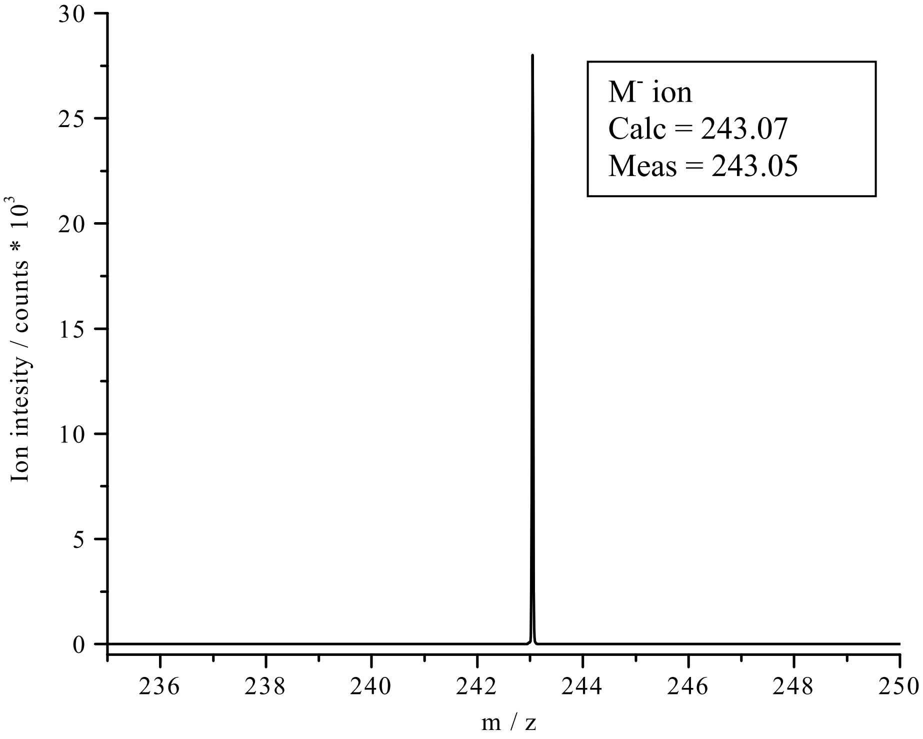

Figure 43. A portion of the high resolution ESI-TOF-MS spectrum of 1-phenyl-2-*O*-sulfo-pentane. The measured m/z value of 243.04 agrees with the 243.07 value calculated for the monoisotopic ion.

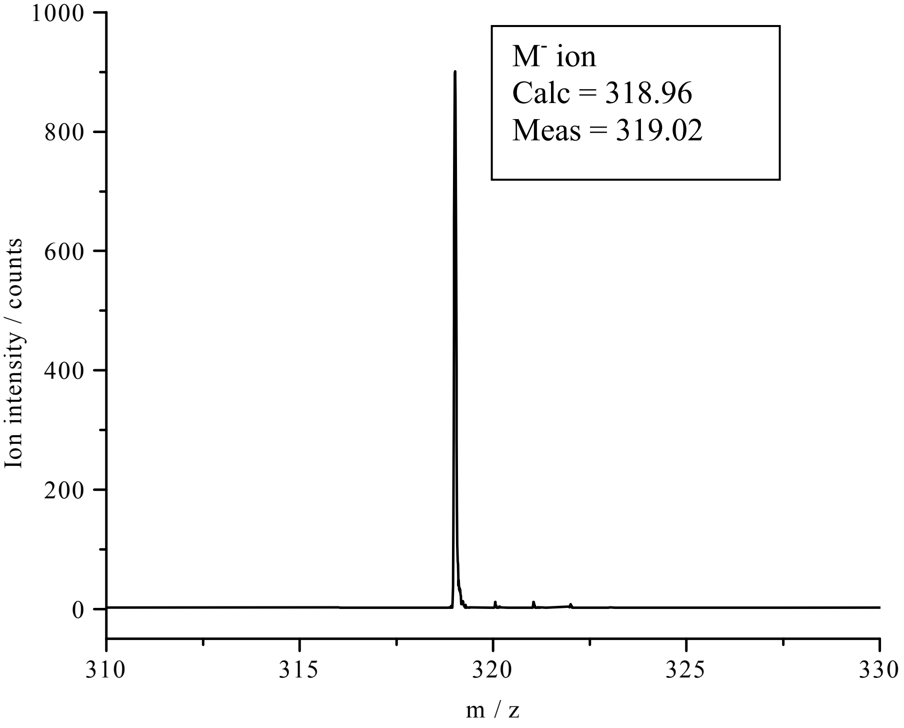

Figure 44. A portion of the high resolution ESI-TOF-MS spectrum of 1-phenyl-1,2-di-*O*-sulfo-ethane monosodium salt . The measured m/z value of 319.02 agrees with the 318.96 value calculated for the monoisotopic monoanion.

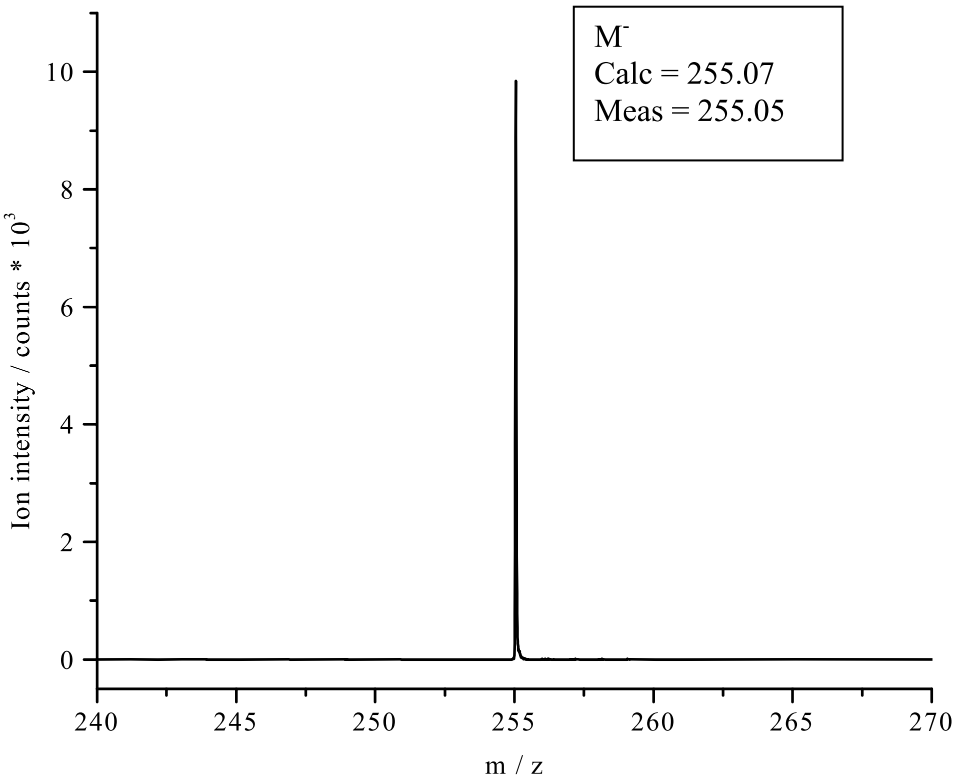

Figure 45. A portion of the high resolution ESI-TOF-MS spectrum of trans-2-phenyl-1-*O*-sulfo-cyclohexane. The measured m/z value of 255.05 agrees with the 255.07 value calculated for the monoisotopic ion.

2.5 Summary of Synthesis Methods

The chloride salts of heptakis(6-deoxy-6-morpholinio)-cyclomaltoheptaose and the tosylate salts of mono(6-deoxy-6-*N,N,N',N',N'*-pentamethylethylenediammonio)-cyclomaltoheptaose, and mono(6-deoxy-6-pyridinium)-cyclomaltoheptaose have been synthesized at a large scale. The key to successful synthesis of these products lies in the selectivity of the first synthetic step of each scheme. Although these procedures have been reported in the literature, the modifications reported here have permitted large quantities to be made at high purity, which facilitated the synthesis of the final products. Subsequent procedures for the final products have not been previously reported in the literature. The choice of reagents for the synthesis was very crucial. For example, complete amination of the CD on the primary face could only be done with morpholine. Ten anionic analytes have also been synthesized using known procedures. These analytes are permanently charged, and will serve as probes for the evaluation of the newly synthesized cationic chiral resolving agents.

The purity of each intermediate and the final products was determined by HPLC, direct UV-detection and indirect UV-detection CE. The structural identity of each CD derivative was confirmed by 1D ^{1}H NMR and ^{13}C NMR, 2D NMR and MALDI-TOF-MS. HMBCD and PEMEDA-BCD are single-isomer, cationic CDs with purities greater than 98%, and have been thoroughly characterized for use as chiral resolving agents in capillary electrophoresis.

CHAPTER III

SEPARATION OF ENANTIOMERS

Charged cyclodextrins derivatives (CCDs) have frequently been used as chiral selectors in CE [95]. Chiral recognition with cyclodexrtrin (CD) analogues typically results from an inclusion of a hydrophobic portion of the analyte into the CD cavity as well as interactions with the hydroxy groups at the rims of the cavity [96]. In addition to these intermolecular interactions, CCDs also take advantage of ion-pairing interactions to stabilize the inclusion complex. HMBCD and PEMEDA-BCD are positively charged β-CDs differing in the number of charges and substituents on the CD skeleton. According to the CHARM model [49], when strong electrolyte resolving agents, such as HMBCD and PEMEDA-BCD are used for the CE resolution of enantiomers, only two stock BEs, one with a low pH and another with a high pH are required to find the conditions that lead to the highest enantioselectivities. Previous work done with single-isomer sulfated CDs shows that good resolution and favorable β values are obtained in low pH BEs where most of the weak base analytes are protonated. Although HMBCD and PEMEDA-BCD are designed for the separation of anionic analytes, separation studies with nonionic and cationic analytes were also performed in this work.

3.1 Separations with HMBCD

Two groups of analytes were used for the study of enantiomer separations with HMBCD; the new, sulfated, permanently charged anionic analytes, and a set of weak acid analytes, both in high pH BEs. In addition to hydrophobic, hydrogen bonding, and weak van der Waals interactions, there are also electrostatic interactions which stabilize the complexes formed by the negatively charged anions and the multiply, positively charged, highly water soluble heptakis(6-deoxy-6-morpholinio)-cyclomaltoheptaose chloride (HMBCD).

3.1.1 Materials

All the analytes were obtained from Sigma (St. Louis, MO), except for the sulfated analytes, which were synthesized and characterized in our laboratory as described in the previous chapter. Methanesulfonic acid, ethanolamine, and dimethylsulfoxide were purchased from Aldrich Chemical Company (Milwaukee, WI). HMBCD was synthesized and analytically characterized in our laboratory as described in Chapter II. Deionized water from a Milli-Q unit (Millipore, Milford, MA) was used to prepare all the solutions that were used in the experiments. The high pH stock buffer was prepared by titration of a 25 mM ethanolamine solution to pH 9.3 with methanesulfonic acid. The chiral resolving agent-containing BEs were prepared immediately prior to use by weighing out the required amounts of the chloride salt of HMBCD into 25 ml volumetric flasks and bringing the volumes to mark with the stock BE solution.

3.1.2 CE Conditions

All enantiomer separations were performed on a P/ACE 2010 capillary electrophoresis instrument using a 25 μm i.d., bare fused silica capillary (Polymicro Technologies, Phoenix, AZ, USA) with a total length (L_t) of 26.4 cm, injector to detector length of 19.6 cm (L_d). A window for UV detection was prepared by removing a section of the polyimide coating with a flame, and then the capillary was wiped clean with a methanol-soaked Kimwipe. All separations were obtained at 9-18 kV applied potential, positive to negative or negative to positive electrode polarity, at 214 nm detection wavelength, and 20 ^{o}C cartridge coolant temperature. Between runs, the capillary was flushed with deionized water for 4 min, followed by the running buffer for 2 min. The analytes were either pressure injected by 2 psi nitrogen for 1 s or electrokinetically injected by 10 kV for 5 s. All solutions used were passed through a 0.45μm pore size disc filter prior to use.

3.1.3 Methods

Dimethylsulfoxide (DMSO), which has been reported to have zero effective mobility with charged CDs [97], was selected as the electroosmotic flow mobility marker for HMBCD as well. Its suitability as mobility marker was experimentally verified according to the procedure reported in the literature [98]. To determine the suitability of DMSO as neutral marker, the capillary was filled with HMBCD-free BE (NHBE). Then a band of the 50 mM HMBCD-containing BE (HBE) was injected into the capillary, followed by a narrow band of DMSO, and a second band of HBE which sandwiched the DMSO band. The injection sequence was repeated with NHBE replacing the HBE bands. Then all bands were pressure mobilized past the detector with the injection end of the capillary still immersed into the NHBE vial. This first mobilization allowed the recording of the first UV trace. As soon as the second NHBE band moved past the detector, the pressure was released from the inlet. Next the entire band train was pushed back into the first portion of the capillary, before the detector, by application of pressure at the outlet end of the capillary. Next, the separation potential was applied for a short migration time. If the sandwiched-DMSO in HBE complexed with the chiral selector, the DMSO-chiral selector complex will migrate with the combined bulk flow velocity and its own electrophoretic velocity. But, the sandwiched-DMSO in NHBE will migrate only with the bulk flow velocity. In the last step, another narrow band of DMSO was injected, and all bands were pressure-mobilized past the detector by applying pressure to the inlet vial with the NHBE, and the second detector trace was then recorded. Figure 46 shows two superimposed UV detector traces of DMSO during the first and second pressure mobilization steps. The first pass shows the DMSO position inside the HBE band before electrophoresis. HBE band is bounded on both sides by NHBE bands. The second detector trace was obtained after a short electrophoresis step, and mobilization of all bands past the detector by nitrogen pressure. The position of DMSO in the HBE before and after electrophoresis, with respect to its position in the NHBE bands, is identical. Because of the identical migration of DMSO in both the HBE and NHBE, it was concluded that DMSO does not complex with 50 mM HMBCD (or less). The broadening of the band and the DMSO peak in the second pass is attributed to additional laminar movement caused by the mobilization pressure and by electrophoresis.

Since DMSO has zero effective mobility in all HMBCD BEs used in this work, it can be used as neutral marker to calculate the electroosmotic flow (EOF) mobilities. DMSO was co-injected with each sample to obtain effective mobilities, μ^{eff}, of the enantiomers from the observed mobilities, μ^{obs}, as:

$$\mu_1^{eff} = \mu_1^{obs} - \mu^{eof} \tag{10}$$

The peak resolution values Rs, were calculated using the following Equation:

$$Rs = \frac{2(t_2 - t_1)}{1.70(w_1^h + w_2^h)} \tag{11}$$

where, subscript 2 refers to the enantiomer which has a lower effective mobility in the lowest HMBCD BE that was used, t_1 and t_2 are the observed migration times of the enantiomers and w^h_1 and w^h_2 are the peak widths at half heights of the respective enantiomer peaks. According to the resolution equation (equation 9) [49], the higher the applied potential, the higher the Rs value that can be obtained. However, Joule heating limits the potential that can be applied. In order to determine the highest potentials where Ohm's plots were still linear, the true electrophoretic currents were measured as a function of the applied potential value over the 0 to 50 mM HMBCD concentration range in 5 mM increments. All effective mobility values of the analytes reported in this dissertation were measured in the linear region of Ohm's plots. A

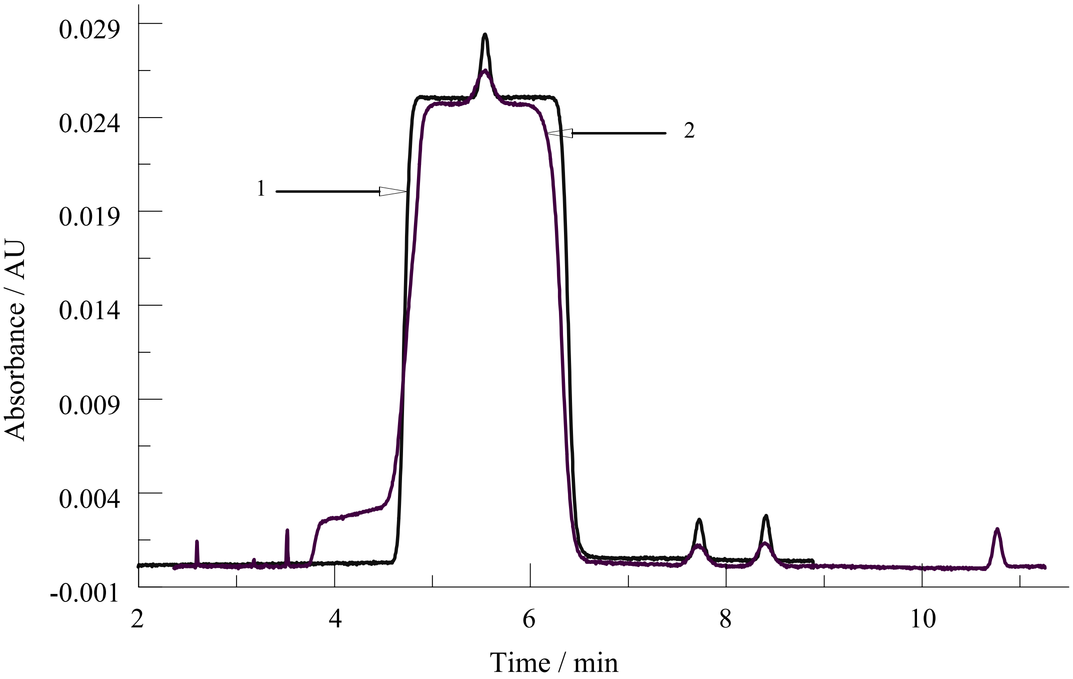

Figure 46. UV-detector traces of DMSO. Before electrophoresis, Trace 1, and after electrophoresis, Trace 2.

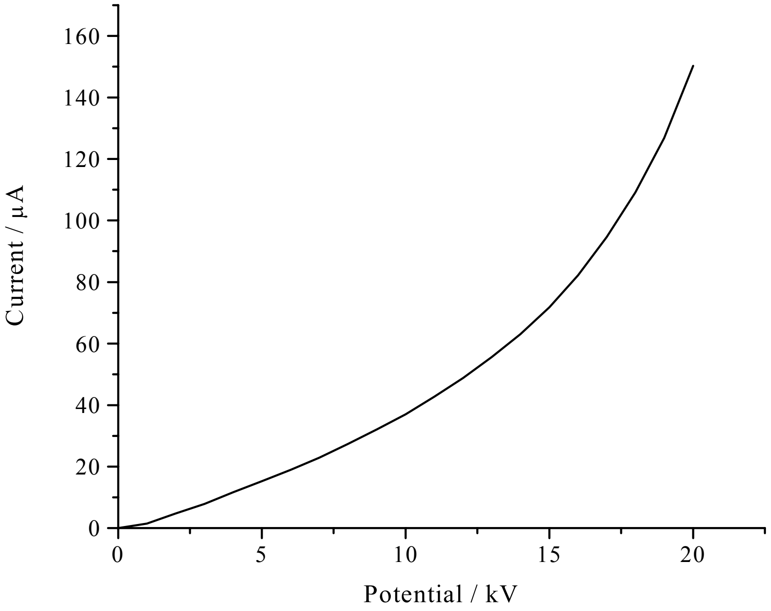

Figure 47. Ohm’s plot obtained with a 50 mM HMBCD BE.

typical Ohm's plot obtained with a 50 mM HMBCD BE is shown in Figure 47. The viscosity values of the 0-50 mM HMBCD BEs were measured using the P/ACE 2010 unit as a viscometer [44]. The viscosity of the solution increased by about 20 % over the HMBCD concentration range studied.

3.1.4 Results and Discussion

The separation behavior of a series of strong anions, weak acid, and neutral analytes (Figure 48) were studied with BEs that contained various concentrations of HMBCD. Shown in Tables 1 and 2 are the effective mobilities of the less mobile enantiomers, μ^{eff}, the separation selectivities, α, the measured peak resolution values, Rs, the corresponding dimensionless, normalized EOF mobility values, β, and the injector-to-detector potential drop values, U, for the strong anions and weak acid analytes respectively. An entry of N/A indicates that a value could not be calculated due to overlap with either a non-comigrating system peak or the neutral marker peak. The applied potential decreased with increasing HMBCD concentration, ranging from 15 kV in the 5 mM HMBCD-containing BE to 9 kV in the 50 mM HMBCD-containing BE. The mobilities of the anodic EOF (μ_{EOF}) were between -(3 to 35) $\times 10^{-5}$ cm^2/Vs over the 5 to 50 mM HMBCD concentration range, indicating that HMBCD absorbed on the walls of the capillary. Under these conditions, the free, uncomplexed, negatively charged analytes migrate in the direction of the EOF, while the analyte-HMBCD complexes migrate in the opposite direction.

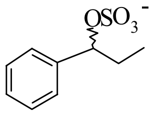

S01: 1-Phenyl-1-*O*-sulfo-propane

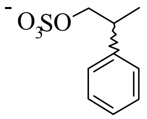

S02: 2-Phenyl-1-*O*-sulfo-propane

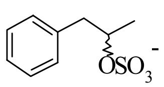

S03: 1-Phenyl-2-*O*-sulfo-propane

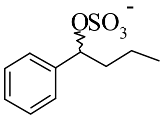

S04: 1-Phenyl-1-*O*-sulfo-butane

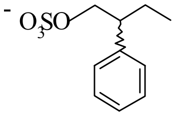

S05: 2-Phenyl-1-*O*-sulfo-butane

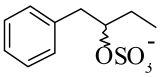

S06: 1-Phenyl-2-*O*-sulfo-butane

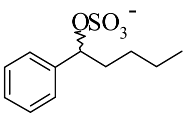

S07: 1-Phenyl-1-*O*-sulfo-pentane

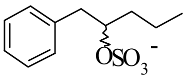

S08: 1-Phenyl-2-*O*-sulfo-pentane

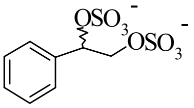

S09: 1-Phenyl-1,2-di-*O*-sulfo-ethane

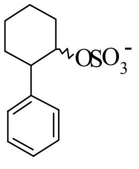

S10: trans-2-Phenyl-1-*O*-sulfo-cyclohexane

Figure 48. Names and structures of the strong electrolytes (all sodium salts), weak base, weak acid, neutral, and ampholytic analytes.

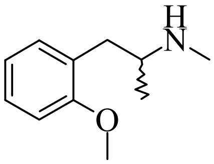

B01: Methoxyphenamine

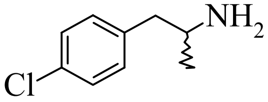

B02: 4-Chloroamphetamine

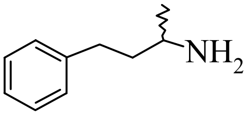

B03: 3-amino-1-phenylbutane

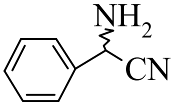

B04: Phenylglycinonitrile

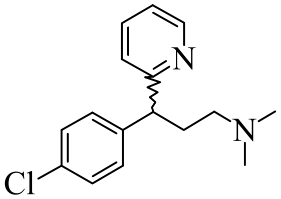

B05: Chlorpheniramine

Figure 48. Continued.

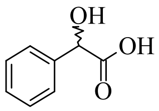

A01: 2-Hydroxy-2-phenylacetic acid

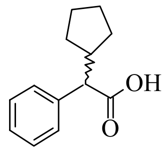

A02: 2-Cyclopentyl-2-phenylacetic acid

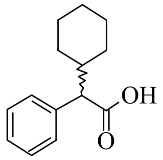

A03: 2-Cyclohexyl-2-phenylacetic acid

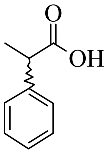

A04: 2-Phenylpropionic acid

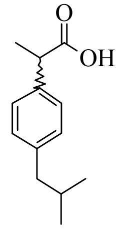

A05: 2-(4-sec-Butyl-phenyl)propionic acid

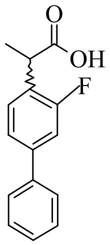

A06: Flurbiprofen

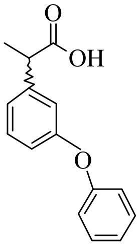

A07: Fenoprofen

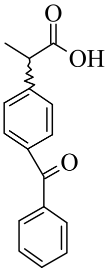

A08: Ketoprofen

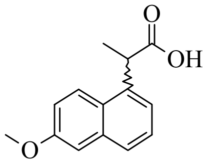

A09: Naproxen

Figure 48. Continued.

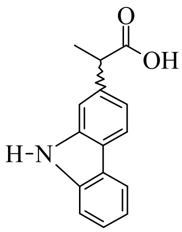

A10: Carprofen

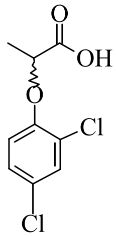

A11: 2-(2,4-Dichlorophenoxy)-propionic acid

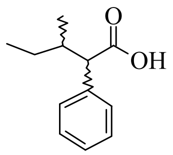

A12: 2-Phenyl-3-methylvaleric acid

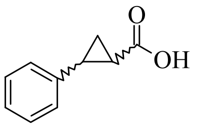

A13: trans-2-Phenyl-1-cyclopropane carboxylic acid

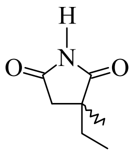

A14: Ethosuximide

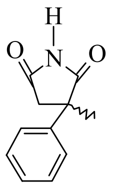

A15: 2-Methyl-2-phenylsuccinimide

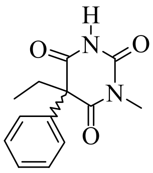

A16: Mephobarbital

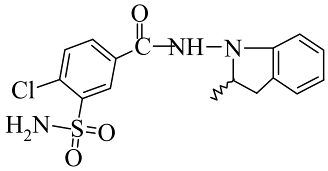

A17: Indapamide

Figure 48. Continued.

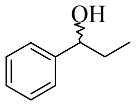

N01: 1-Phenylpropanol

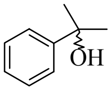

N02: 2-Phenyl-2-propanol

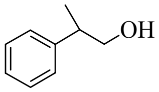

N03: 2-Phenyl-1-propanol

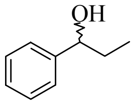

N04: 1-Phenybutanol

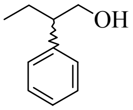

N05: 2-Phenylbutanol

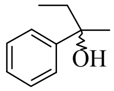

N06: 2-Phenyl-2-butanol

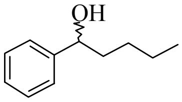

N07: 1-Phenylpentanol

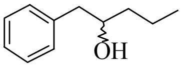

N08: 1-Phenyl-2-pentanol

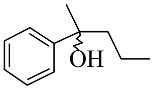

N09: 2-Phenyl-2-pentanol

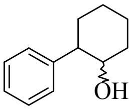

N10: trans-2-Phenyl-1-cyclohexanol

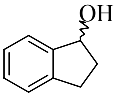

N11: 1-Indanol

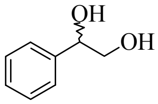

N12: Styrene glycol

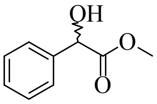

N13: Methylmandelate

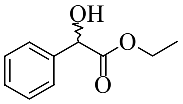

N14: Ethylmandelate

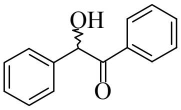

N15: Benzoin

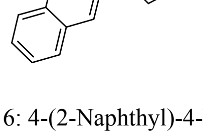

N16: 4-(2-Naphthyl)-4-butyrolactone

Figure 48. Continued.

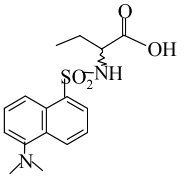

Z01: Dansyl-1-amino-n-butyric acid

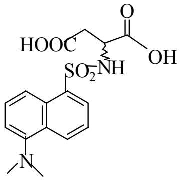

Z02: Dansyl-aspartic acid

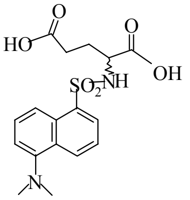

Z03: Dansyl-glutamic acid

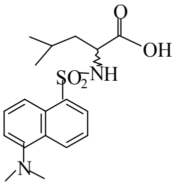

Z04: Dansyl-leucine

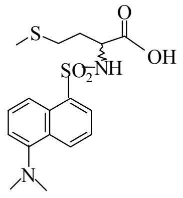

Z05: Dansyl-methionine

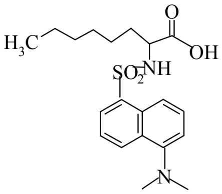

Dansyl-caprylic acid

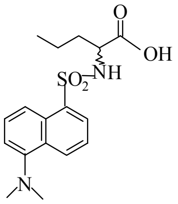

Z07: Dansyl-norvaline

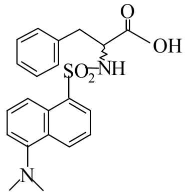

Z08: Dansyl-phenylalanine

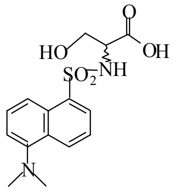

Z09: Dansyl-serine

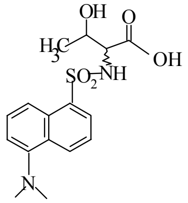

Z10: Dansyl-threonine

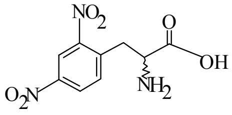

Z11: Dinitrophenyl-alanine

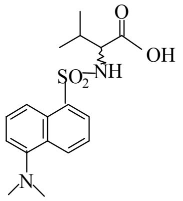

Z12: Dansyl-valine

Figure 48. Continued.

Table 1.

Separation data for the strong electrolyte analytes as a function of HMBCD concentration in pH = 9.3 BE. μ in (10^{-5} cm^2 V^{-1}s^{-1}) units.

HMBCD (mM)	0			5				10	
U (kV)				-15				-12	
Analyte	μ	μ	α	β	Rs	μ	α	β	Rs
S01	-31.7	-6.87	1.00	4.3	0.0	-5.32	1.18	5.2	<0.6
S02	-29.6	-2.64	1.61	20.5	1.2	-1.11	4.34	22.6	0.9
S03	-25.3	-7.73	1.25	3.8	1.4	-5.66	1.24	4.9	1.5
S04	-25.9	-7.82	1.00	3.8	0.0	-4.49	1.00	6.1	0.0
S05	-23.8	-9.58	1.00	3.1	0.0	-7.95	1.00	3.6	0.0
S06	-22.5	-10.1	1.00	2.9	0.0	-8.40	1.00	3.2	0.0
S07	-22.5	-6.39	1.00	4.7	0.0	-4.00	1.00	6.8	0.0
S09	-53.0	-21.2	1.00	1.6	0.0	-17.5	1.00	1.7	0.0
S10	-28.2	-8.08	1.00	3.7	0.0	-5.23	1.00	5.2	0.0

Table 1. Continued

HMBCD (mM)	0			20				30	
U (kV)				-9				-9	
Analyte	μ	μ	α	β	Rs	μ	α	β	Rs
S01	-31.7	-3.85	1.14	5.9	1.5	-2.99	1.20	7.2	1.5
S02	-29.6	1.25	0.59	-17	1.3	1.27	0.73	-16	1.3
S03	-25.3	-5.17	1.13	4.3	1.3	-4.35	1.15	4.9	1.5
S04	-25.9	-3.03	1.00	7.5	0.0	-2.26	1.00	9.7	0.0
S05	-23.8	-6.88	1.00	3.2	0.0	-6.28	1.00	3.6	0.0
S06	-22.5	-6.03	1.00	3.7	0.0	-5.50	1.00	4.0	0.0
S07	-22.5	-2.07	1.00	11.1	0.0	-1.84	1.00	12	0.0
S09	-53.0	-15.7	1.00	1.4	0.0	-13.6	1.00	1.6	0.0
S10	-28.2	-3.47	1.00	6.5	0.0	-2.73	1.00	8.5	0.0

Table 1. Continued

HMBCD (mM)	0			50	
U (kV)				-7	
Analyte	μ	μ	α	β	Rs
S01	-31.7	-1.86	1.21	8.9	1.2
S02	-29.6	1.32	0.75	-13	1.6
S03	-25.3	-2.35	1.24	7.1	1.7
S04	-25.9	-1.21	1.36	14	0.9
S05	-23.8	-3.73	1.00	4.5	0.0
S06	-22.5	-3.72	1.00	4.4	0.0
S07	-22.5	-1.09	1.00	15	0.0
S09	-53.0	-11.5	1.000	1.4	0.0
S10	-28.2	-1.3	1.32	13	1.2

Table 2.

Separation data for weak acid analytes as a function of HMBCD concentration in pH = 9.3 BE. μ in (10^{-5} cm^{2} V^{-1}s^{-1}) units.

HMBCD (mM)	0	5				10			
U (kV)		-15				-12			
Analyte	μ	μ	α	β	Rs	μ	α	β	Rs
A01	-35.4	-18.6	1.00	1.7	0.0	-15.3	1.00	1.8	0.0
A08	-22.7	-12.6	1.00	2.4	0.0	-10.9	1.00	2.6	0.0
A09	-24.1	-11.9	1.00	2.7	0.0	-8.28	1.00	3.5	0.0
A10	-21.9	-3.88	1.00	8.0	0.0	-4.43	1.00	65	0.0
A14	-22.1	-5.15	1.00	6.2	0.0	-3.77	1.00	7.6	0.0
A16	-27.5	-13.6	1.00	2.3	0.0	-12.3	1.00	2.3	0.0
A17	-7.9	-2.62	1.00	8.7	0.0	-1.06	1.00	27	0.0

Table 2. Continued

HMBCD(mM)	0	20				30			
U (kV)		-9				-9			
Analyte	μ	μ	α	β	Rs	μ	α	β	Rs
A01	-35.4	-14.7	1.00	1.7	0.0	-14.6	1.00	1.6	0.0
A08	-22.7	-9.53	1.00	2.6	0.0	-9.49	1.00	2.4	0.0
A09	-24.1	-6.95	1.00	3.5	0.0	-6.50	1.00	3.6	0.0
A10	-21.9	2.23	1.00	-11	0.0	4.24	1.00	-5.4	0.0
A14	-22.1	-3.75	1.00	6.6	0.0	-4.69	1.00	4.6	0.0
A16	-27.5	-11.2	1.00	-2.2	0.0	-10.8	1.00	1.9	0.0
A17	-7.9	1.34	1.00	-18	0.0	4.65	1.00	-47	0.0

3.1.4.1 Separation of the Enantiomers of Strong Electrolyte Analytes with HMBCD

The enantiomers of 3 of the 10 anionic compounds tested were separated within the concentration range studied. The anionic effective mobilities of the enantiomers of these analytes decreased rapidly as the concentration of HMBCD was increased from 0 to 10 mM, thereafter, the mobilities remained approximately constant, reaching -3×10^{-5} cm^2/Vs as the concentration of HMBCD was increased to 50 mM for the weakly complexing analytes. For the strongly complexing anionic analytes, the effective anionic mobilities decreased, crossed the zero mobility line, became cationic, and reached 5×10^{-5} cm^2/Vs at 50 mM as the concentration of HMBCD was increased. Typical effective mobility curves are shown in the top left panel of Figure 49 for four analytes. The mobilities reflect the increasing degree of complexation of the anionic analyte with increasing HMBCD concentration and the mobility-reducing effects of both the higher ionic strength and the higher viscosity that came with the increased concentration of HMBCD. The corresponding separation selectivities for the weakly complexing enantiomers decreased slightly to a minimum and then increased slowly as the concentration of HMBCD was increased (Figure 49, top right panel), in agreement with the predictions of the CHARM model [49]. For the strongly binding analytes, separation selectivity first increased as the mobilities approached the point where they crossed the zero line, then became less than unity as the concentration of HMBCD was increased further (Figure 49, bottom right panel).

The size and structure of the anionic analytes can have a significant effect on the extent of enantiorecognition by HMBCD. Differences in the number of carbon atoms in

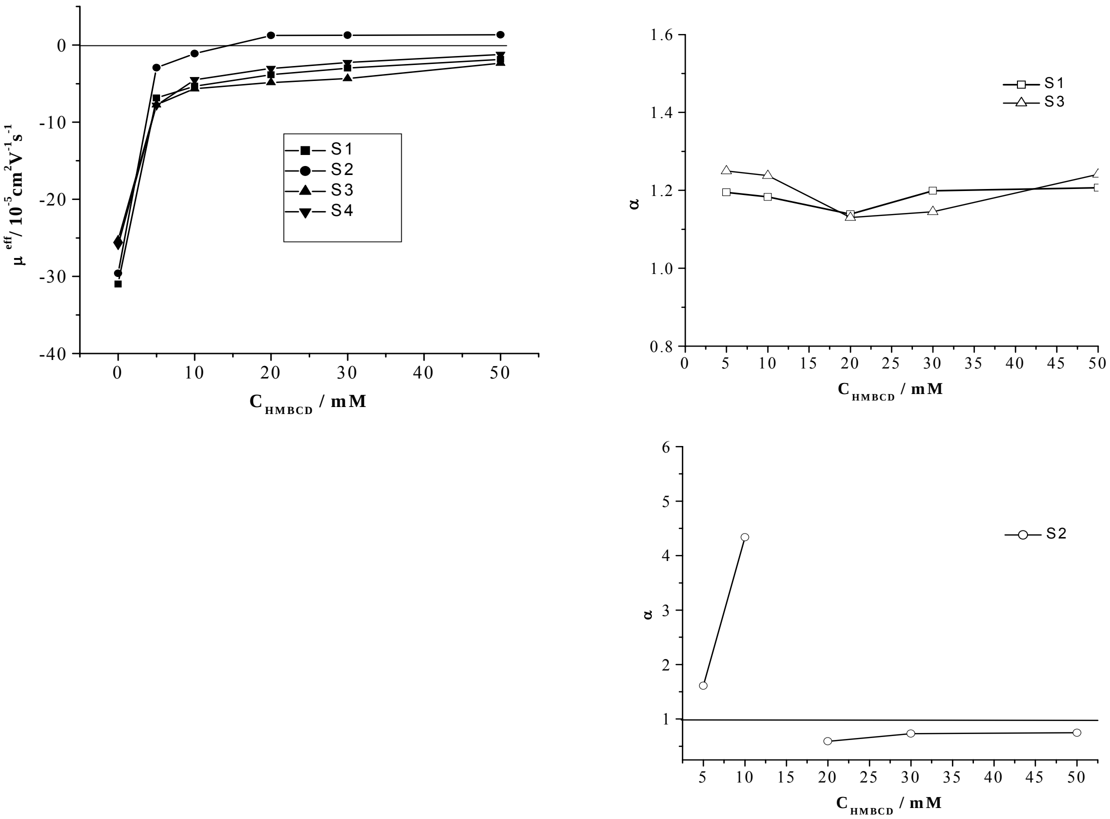

Figure 49. Typical effective mobilities and separation selectivities for the enantiomers of selected strong electrolytes with HMBCD in pH = 9.3 BEs. Top left panel: effective mobilities. Top right panel: separation selectivites for S1 and S3. Bottom right panel selectivity for S2.

the hydrophobic chain that contains the chiral center can affect the separation selectivity significantly. For example, the enantiomers of 1-phenyl-1-*O*-sulfo-propane (S01), 2-phenyl-1-*O*-sulfo-propane (S02), 1-phenyl-2-*O*-sulfo-propane (S03), all having three carbon atoms in the alkyl chain were separated with HMBCD BEs. However, the enantiomers of the different isomers of phenylsulfobutane and of phenylsulfopentane, with longer alkyl chains could not be resolved under the same conditions. The position of the charge on the analyte relative to the aromatic ring also played a part in the chiral recognition process. For example, the enantiomers of phenylsulfopropane isomers, S01, S02 and S03 were separated in the HMBCD BEs.However, comparison of their separation selectivities and effective mobilities showed that the enantiomers of S02, having the charge and chiral center closer to the aromatic ring, complexed more strongly, and had higher separation selectivity values than the other two.

3.1.4.2 Separation of the Enantiomers of Weak Acids with HMBCD

Table 2 lists the effective mobilities of the less mobile enantiomers, μ (the average of three measurements, typical RSD values less than 3%), the separation selectivities, α, the peak resolution values, Rs, the normalized EOF mobility values, β, and the injector-to-detector potential drop values, U (in kV), obtained in the separation of ten weak acid analytes studied in the concentration ranged 5 mM to 30 mM HMBCD at pH 9.3. All weak acid analytes were fully dissociated in this BE. The anionic effective mobilities of the enantiomers of these analytes, like those of the strong electrolytes, decreased rapidly between 0 and 10 mM concentration of HMBCD. As the concentration of HMBCD increased further, the effective mobilities only increased minimally and reached -3×10^{-5} cm^2/Vs at the highest concentration used (see Figure 50). The effective mobilities of the enantiomers of two weak acid analytes, ketoprofen and carprofen, decreased much faster than for the rest of the other weak acid analytes. They crossed the zero mobility line, and became cationic at 10 mM concentration of HMBCD. This behavior is indicative of stronger interactions between the multiply charged HMBCD and the molecules of ketoprofen and carprofen than those of the other weak acid analytes. The slow changes in the anionic effective mobilities above the 10 mM HMBCD concentration could be attributed to the combined effects of increased ionic strength and viscosity that were brought about by the increased HMBCD concentration [44].

Despite the strong interactions of some of the weak acid analytes with HMBCD, no separation was observed for enantiomers of the weak acid analytes studied. Even the enantiomers of ketoprofen and carprofen, whose effective mobilities crossed the zero mobility line, could no be separated over the entire concentration range of HMBCD studied. It is instructive to see that the separation behavior of the anions of both the strong and weak acids show that analyte structure had a similar effect on the complexation process for both groups of analytes. Except for mandelic acid, all weak acid analytes were much larger than the phenylsulfopropanes, which were resolved with HMBCD. Therefore, it could be argued that in the case of weak acid analytes, size may have hindered inclusion complexation with HMBCD, because the effective cavity size of HMBCD is diminished by the morpholinium substituent groups.

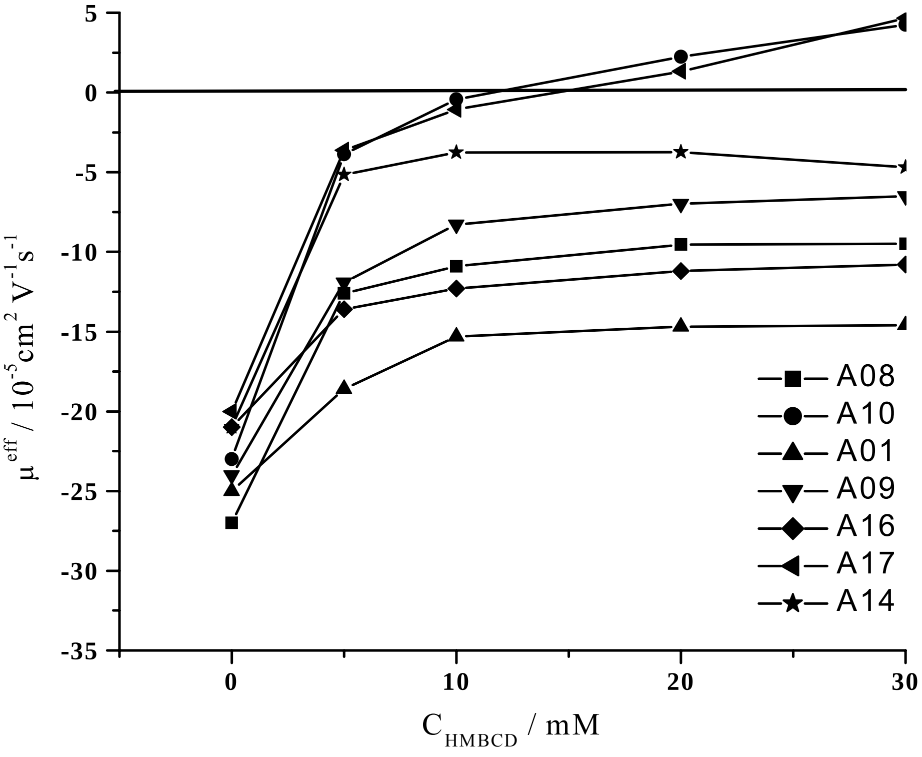

Figure 50. Effective mobilities of the enantiomers of weak acid analytes in pH = 9.3 BE with HMBCD.

3.2 Separations with PEMEDA-BCD

According to the CHARM model [49], the higher the effective charge (z^{eff}) of the charged cyclodextrin (CCD), the higher the peak resolution with all other conditions being equal. The minimum number of effective charges a CCD may have is 1. Therefore, assuming a 1:1 stiochiometry for complexation between a monoanionic chiral analyte, and a CCD with $z^{eff} = 1$, the net charge of the resulting analyte-CD complex is zero. In such a situation, the analyte-CD complex will migrate with the electroosmotic flow. But under the same analytical conditions, complexation between the monoanionic analyte and a dicationic cyclodextrin will result in an analyte-CD complex with a net charge of one, i.e., the complex will migrate cationically. PEMEDA-BCD has two quaternary ammonium groups linked to one of the glucose units of CD, giving it the properties of a strong electrolyte.

3.2.1 Materials

Some of the analytes were obtained as described earlier in this chapter. Phosphoric acid, hydrochloric acid, methanesulfonic acid, ethanolamine, lithium hydroxide, benzyltrimethylammonium bromide and *p*-toluenesulfonic acid were purchased from Aldrich Chemical Company (Milwaukee, WI). Mono(6-deoxy-6-*N,N,N′,N′,N′*-pentamethylethylenediammonio)-cyclomaltoheptaose chloride (PEMEDA-BCD) was synthesized and analytically characterized in our laboratory as described in Chapter II.

3.2.2 Capillary Electrophoretic Methods

CE measurements were carried out with a P/ACE 2050 and a P/ACE 2100 instrument, the UV detectors were set to 214 nm. 27 μm i.d., untreated fused-silica capillaries (Polymicro Technologies, Phoenix, AZ, USA) with a total length of 26.4 cm and injector-to-detector length of 19.6 cm were used. The aqueous stock buffers were prepared by titrating a 25 mM solution of phosphoric acid in Milli-Q water (Millipore, Milford, MA, USA) to pH 2.54 with lithium hydroxide for the low pH BEs, and by titrating a 25 mM solution of ethanolamine to pH 9.30 with methanesulfonic acid for the high pH BEs. The stock buffers were used to prepare, daily, the 0-50 mM PEMEDA-BCD BEs for the CE separations. All solutions were filtered prior to use through a 0.45 μm Nalgene nylon membrane filter (VWR, South Plainfield, NJ, USA). The analytes were dissolved in the BEs and co-injected for 1 s by 1 psi nitrogen along with the EOF marker, DMSO or the external cationic mobility marker, benzyltrimethylammonium bromide, or the external anionic mobility marker, *p*-toluenesulfonic acid, from a solution approximately 0.5 mM in both the analyte and the respective marker. In situations where coinjection of the mobility marker was not feasible, the mobility marker was injected electrokinetically, separately, from the opposite end of the capillary. The effective mobilities of the external mobility markers, benzyltrimethylammonium bromide and *p*-toluenesulfonic acid in the various PEMEDA-BCD-containing BEs were determined using the three-band pressure-mediated CE (PreMCE) method [99]. The suitability of DMSO as a neutral marker for this study was experimentally determined as described earlier in this chapter. Figure 51 shows two superimposed UV detector traces of DMSO during the first and second pressure mobilization steps. Since the migration of DMSO in both the 50 mM PEMEDA-BCD BE and the chiral resolving agent free BE are identical, it was concluded that DMSO does not complex with PEMEDA-BCD at concentrations of 50 mM or less. Electrophoretic currents were measured in the 5, 10, 20, 30, 40, and 50 mM PEMEDA-BCD BEs to find the highest applied potentials for the effective mobility measurements that were still within the linear region of the respective Ohm's plots. To establish that PEMEDA-BCD was stable for enantiomer separations by CE, a portion of a 50 mM PEMEDA-BCD BE was stored in the refrigerator and then analyzed at intervals, using indirect UV detection CE. After 90 days, no signs of degradation were observed as depicted by the electropherograms shown in Figure 52. PEMEDA-BCD was used for the CE separation of the enantiomers of 10 strong electrolyte analytes, 17 weak acids, 12 zwitterionic, and 16 nonionic compounds (mostly pharmaceuticals) in both low and high pH media. These compounds are part of our standard CD evaluation kit, except for the 10 strong electrolytes. The structures of the analytes are shown in Figure 46. The effective mobilities of the enantiomers, $\mu^{eff}{}_1$ and $\mu^{eff}{}_2$, were calculated from μ_{EOF} and the observed mobility values, $\mu^{obs}{}_1$ and $\mu^{obs}{}_2$; using equation 10. Separation selectivities, α, were calculated as $\alpha = \mu^{eff}{}_1 / \mu^{eff}{}_2$; the normalized electroosmotic flow mobility values, β, as $\beta = \mu_{EOF} / \mu^{eff}{}_2$. (Subscript assignment followed the arbitrary, but consistent convention introduced in Ref. 49: for a combination of monoanionic analytes and a multiply, positively charged resolving agent this convention results in separation selectivities that vary between +1 and + infinity as long as both enantiomers migrate anionically, it results in separation selectivities that vary between – infinity and 0 as long as one enantiomer migrates cationically and the other migrates anionically, and it results in separation

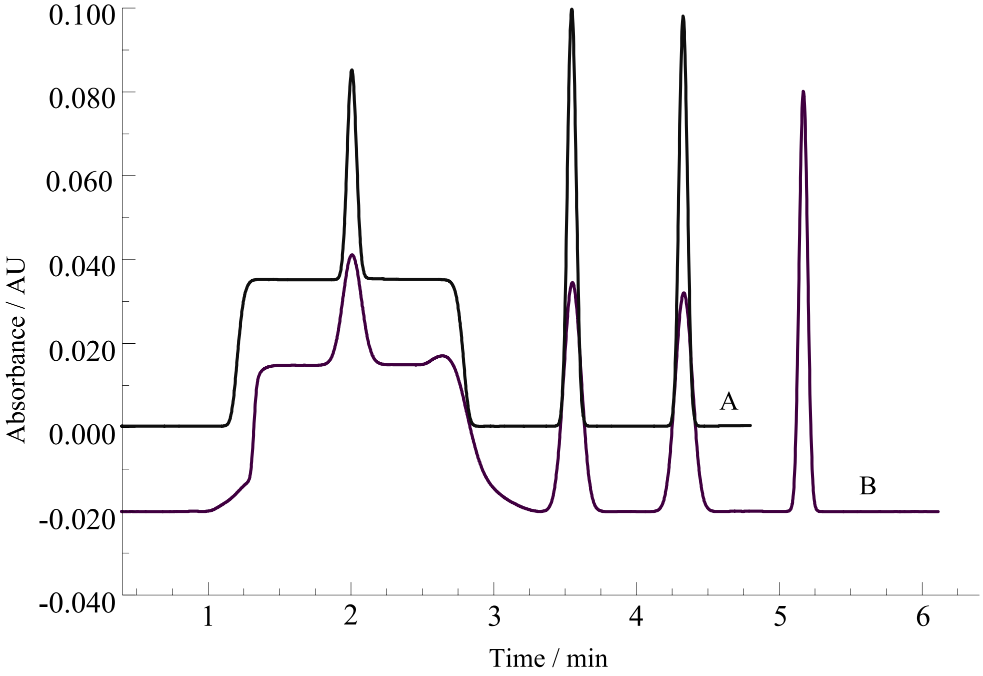

Figure 51. UV detector traces of DMSO. PEMEDA-BCD-free BE before electrophoresis (trace A), and 50 mM PEMEDA-BCD-containing BE after electrophoresis (trace B).

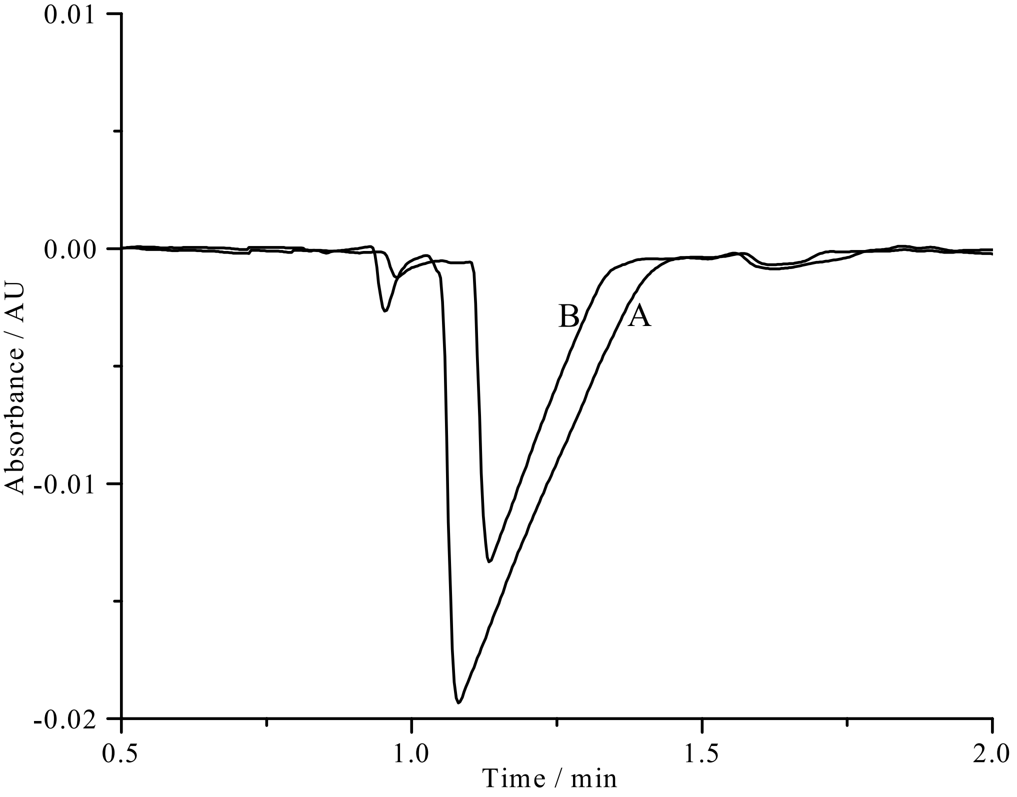

Figure 52. Indirect UV-detection electropherograms of a 50 mM PEMEDA-BCD solution. (A) fresh solution; (B) after 90 days.

selectivities that vary between 0 and +1 once both enantiomers migrate cationically). Peak resolution was calculated using the peak width at half height method, equation 11.

3.2.3 Results and Discussion

The next seven tables list the effective mobilities of the less mobile enantiomers, μ (the average of three measurements, typical RSD values less than 3%), the separation selectivities, α, the peak resolution values, Rs, the normalized EOF mobility values, β, and the injector-to-detector potential drop values, U (in kV), obtained in the PEMEDA-BCD BEs. When effective mobility data could not be calculated because of an overlap with a non-comigrating system peak, the neutral marker peak or the ionic mobility marker peak, an entry of N/A is used in the tables. Over the 1 to 20 mM PEMEDA-BCD concentration range, the μ_{EOF} values were in the (-4) $\times 10^{-5}$ $cm^2V^{-1}s^{-1}$ to (7) $\times 10^{-5}$ $cm^2V^{-1}s^{-1}$ range for the acidic aqueous PEMEDA-BCD-containing BEs and in the (-2)$\times 10^{-5}$ $cm^2V^{-1}s^{-1}$ to (10) $\times 10^{-5}$ $cm^2V^{-1}s^{-1}$ range for the basic aqueous PEMEDA-BCD-containing BEs. In both cases, the negative μ_{EOF} values indicate that the walls of the capillary were partially covered by PEMEDA-BCD.

3.2.3.1 Separation of the Enantiomers of Strong Electrolyte Analytes with PEMEDA-BCD in Low pH BEs

Table 3 shows the results obtained for the *O*-sulfo test analytes. Since the charge of the *O*-sulfo test analytes does not change as the pH of the BE is increased from 2.54 to 9.30, detailed studies were only carried out in the acidic BEs by varying the concentration of PEMEDA-BCD in the 1 to 20 mM range. In the absence of PEMEDA-BCD, the newly synthesized monoanionic analytes (S1-S8, S10) have effective mobilities in the –(15 to 30) x 10^{-5} $cm^2V^{-1}s^{-1}$ range, while the effective mobility of the dianionic analyte, S9 is about twice as high, –53 x 10^{-5} $cm^2V^{-1}s^{-1}$, as expected. In the absence of PEMEDA-BCD, for the same substitution pattern, the effective mobilities decreased as the length of the alkyl chain of the *O*-sulfo-alkanes was increased (compare S01, S04 and S07 for the 1-phenyl-1-*O*-sulfo-alkanes; S02 and S05 for the 2-phenyl-1-*O*-sulfo-alkanes, and S03, S06 and S08 for the 1-phenyl-2-*O*-sulfo-alkanes). The mobility decrease per methylene unit was about 2-to-3 times higher for the 1-*O*-sulfo derivatives than for the 2-*O*-sulfo derivatives (compare the S01, S04 and S07 series, and the S02 and S05 series with the S03, S06 and S08 series). In the absence of PEMEDA-BCD, for the same alkyl chain length, the effective mobilities decreased as the substitution pattern went from 1-phenyl-1-*O*-sulfo-alkanes to 2-phenyl-1-*O*-sulfo-alkanes to 1-phenyl-2-*O*-sulfo-alkanes (compare S01, S02 and S03 for the propane derivatives, S04, S05 and S06 for the butane derivatives, and S07 and S08 for the pentane derivatives), indicating an increase in the hydrated ion radii of the

Table 3.

Separation data for strong electrolyte analytes as a function of PEMEDA-BCD concentration in pH = 2.5 BE. μ in (10^{-5} cm^{2} V^{-1}s^{-1}) units.+

PEMEDA- BCD (mM)	0	2				5			
U (kV)		-15				15			
Analyte	μ	μ	α	β	Rs	μ	α	β	Rs
S01	-31.7	-23.4	1.04	-0.8	1.1	-0.26	1.24	-26	1.1
S02	-29.6	-14.5	1.00	-0.2	0.0	6.46	1.00	0.6	0.0
S03	-25.3	1.57*	0.74	2.4	1.5	4.99	0.92	0.5	1.2
S04	-25.9	-12.9	1.05	-0.6	3.2	0.45	0.84	9.3	1.3
S05	-23.8	-15.0	1.00	-0.4	0.0	4.28	1.00	0.9	0.0
S06	-22.5	1.49*	0.75	1.5	1.7	4.63	0.89	0.5	1.9
S07	-22.5	-16.6	1.17	-0.4	0.8	0.85	0.83	0.0	1.1
S08	-19.4	-13.4	1.06	-1.2	1.4	4.69	0.84	0.8	0.9
S09	-53.0	-44.2	1.01	-0.5	0.2	-26.7	1.01	-0.2	<0.6
S10	-28.2	-13.2	1.05	-0.4	1.2	0.26	0.81	17.5	3.2

* 18 kV

Table 3. Continued

PEMEDA- BCD (mM)	0	10				20			
U (kV)		9				9			
Analyte	μ	μ	α	β	Rs	μ	α	β	Rs
S01	-31.7	3.64	0.90	0.0	3.5	4.10	0.92	-0.2	2.9
S02	-29.6	8.09	1.00	0.0	0.0	8.95	1.00	-0.4	0.0
S03	-25.3	5.58	0.95	0.0	1.5	5.64	0.97	-0.3	1.5
S04	-25.9	3.00	0.88	-0.4	5.2	4.08	0.91	-0.5	5.2
S05	-23.8	6.48	1.00	0.0	0.0	7.29	1.00	-0.4	0.0
S06	-22.5	5.19	1.00	0.0	0.0	5.14	1.00	-0.3	0.0
S07	-22.5	4.63	0.94	0.0	0.8	4.98	0.93	-0.4	0.6
S08	-19.4	7.00	0.97	-0.2	1.7	8.07	0.98	-0.3	1.1
S09	-53.0	-12.4	1.04	0.2	<0.6	-9.82	1.03	0.4	0.6
S10	-28.2	3.40	0.88	0.0	2.2	4.74	0.96	-0.2	1.3

O-sulfo ions. The increase was smaller for the 2-phenyl-, larger for the 2-*O*-sulfo pattern.

Once PEMEDA-BCD was added to the BE, the anionic effective mobilities decreased as the PEMEDA-BCD concentration was increased, they became cationic (except for S9, which is a dianion) and increased further without reaching the limiting mobilities by 20 mM, the highest PEMEDA-BCD concentration tested here. This behavior indicates that PEMEDA-BCD interacts with the 1-phenyl-1-*O*-sulfo-alkanes less strongly than with the 2-phenyl-1-*O*-sulfo-alkanes and the 1-phenyl-2-*O*-sulfo-alkanes (compare the mobilities for the S01, S04 and S07 series with those of the S02 and S05 series, and the S03, S06 and S08 series). It is remarkable that the enantiomers of 2-phenyl-1-*O*-sulfo-propane (S02) and 2-phenyl-1-*O*-sulfo-butane (S05) were not resolved in the entire 0 to 20 mM PEMEDA-BCD concentration range, despite the fact that the β values were quite favorable. While one could speculatively invoke differences in the inclusion patterns, the true explanation will have to come from detailed NMR spectroscopic studies. Fortunately, since PEMEDA-BCD recently became available in adequate quantities, such studies are now possible. Overall, the effective mobility and separation selectivity patterns observed for S1 to S10 follow the predictions of the CHARM model [49] corrected for the ionic strength effects [44]. As typical examples, the mobility and separation selectivity curves of S01, S04 and S08 are shown in Figure 53. Separation selectivities are the best in the vicinity of the PEMEDA-BCD concentration where the effective mobilities change from anionic to cationic values.

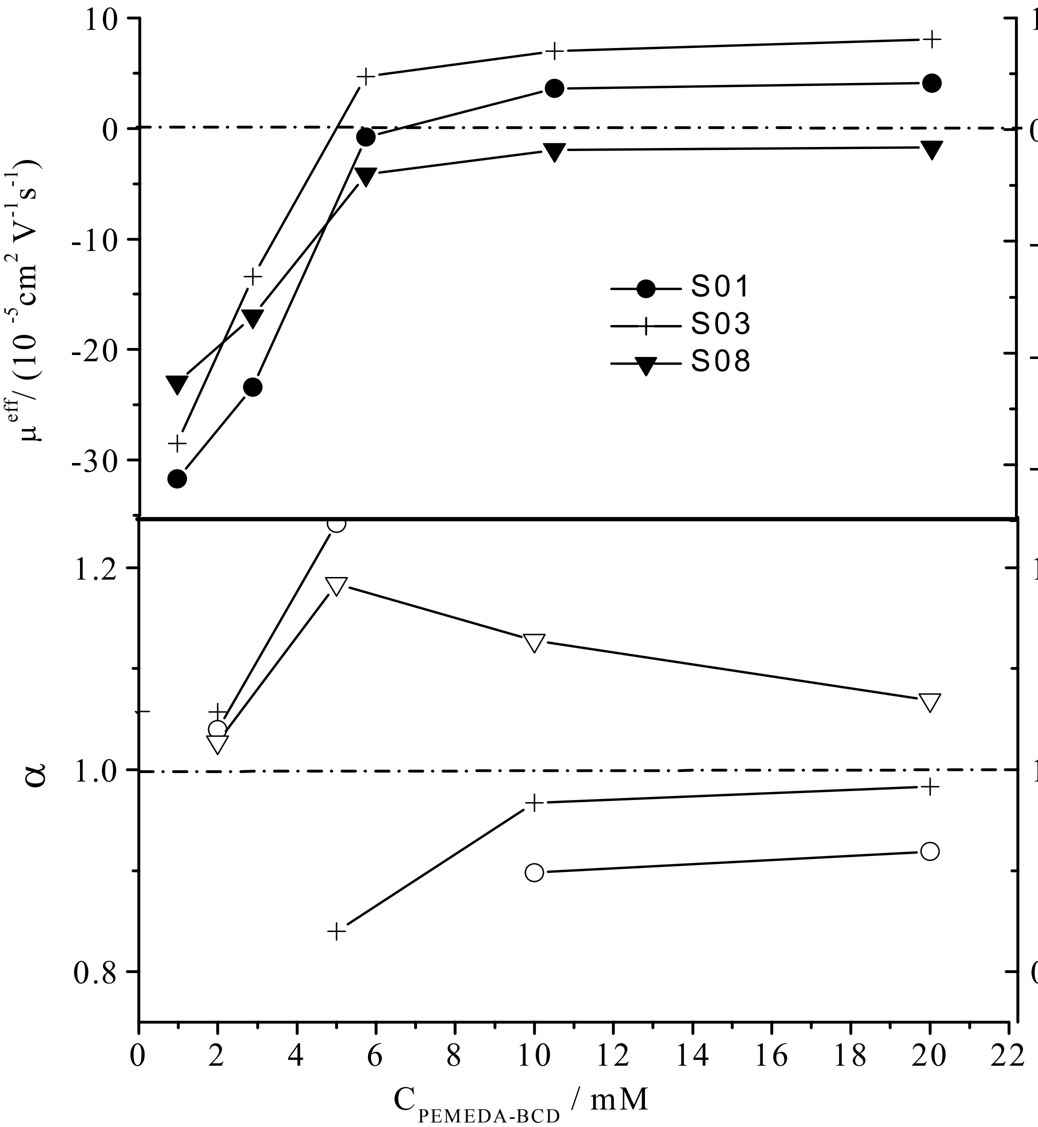

Figure 53. Effective mobilities (top portion) and separation selectivities (bottom portion) for the enantiomers of the strong electrolyte analytes. pH = 2.5 PEMEDA-BCD BE.

Table 4.

Separation data for weak acid analytes as a function of PEMEDA-BCD concentration in pH = 2.5 BE. μ in (10^{-5} cm^2 V^{-1}s^{-1}) units.

PEMEDA-BCD (mM)	0	1				2			
U (kV)		12				12			
Analyte	μ	μ	α	β	Rs	μ	α	β	Rs
A01	-3.17	-1.70	1.00	-1.9	0.0	-1.17	1.00	-3.6	0.0
A02	0.0	13.2	1.00	0.4	0.0	14.2	1.00	0.3	0.0
A03	0.0	6.82	1.00	0.3	0.0	14.7	1.00	0.6	0.0
A04	0.0	3.48	1.00	1.5	0.0	6.70	1.00	0.6	0.0
A05	0.0	13.4	1.00	0.5	0.0	14.2	1.00	0.3	0.0
A07	0.0	10.5	1.00	0.4	0.0	12.0	1.00	0.4	0.0
A09	0.0	10.8	1.04	0.6	1.5	12.5	1.03	0.3	1.2
A12	0.0	10.2	1.03	0.7	0.6	12.6	1.04	0.3	1.0
A13	0.0	5.58	1.00	1.2	0.0	8.68	1.00	0.4	0.0
A14	0.0	0.69	1.00	5.6	0.0	1.2	1.00	3.3	0.0
A15	0.0	5.38	1.07	1.0	<0.6	7.29	1.06	3.7	<0.6
A16	0.0	5.42	1.16	4.5	2.8	7.64	1.14	4.1	3.7
A17	0.0	0.86	1.23	8.2	0.9	1.59	1.22	3.4	1.9

Table 4. Continued

PEMEDA-BCD (mM)	0			3				5	
U (kV)				12				12	
Analyte	μ	μ	α	β	Rs	μ	α	β	Rs
A01	-3.17	-0.19	1.00	-17	0.0	0.53	1.13	5.5	<0.6
A02	0.0	16.1	1.00	0.2	0.0	15.2	1.00	0.3	0.0
A03	0.0	16.3	1.00	0.2	0.0	17.5	1.00	-0.2	0.0
A04	0.0	8.75	1.00	0.5	0.0	9.70	1.00	0.4	0.0
A05	0.0	16.4	1.00	0.3	0.0	13.8	1.00	-0.2	0.0
A07	0.0	14.0	1.00	0.3	0.0	13.8	1.00	-0.2	0.0
A09	0.0	13.1	1.02	0.2	1.0	13.5	1.02	-0.2	0.8
A12	0.0	13.6	0.04	0.2	1.8	13.9	1.08	0.2	0.9
A13	0.0	10.7	1.00	0.4	0.0	12.3	1.02	0.3	0.0
A14	0.0	1.62	1.00	2.6	0.0	2.18	1.00	1.2	0.0
A15	0.0	8.21	1.06	0.5	0.6	10.3	1.05	0.4	0.7
A16	0.0	9.36	1.11	4.0	3.7	10.8	1.09	0.4	2.5
A17	0.0	2.35	1.20	4.5	2.8	3.44	1.20	1.2	3.4

Table 4. Continued

PEMEDA-BCD (mM)	0	10				20			
U (kV)		12				9			
Analyte	μ	μ	α	β	Rs	μ	α	β	Rs
A01	-3.17	1.79	1.12	1.3	0.8	1.90	1.09	0.8	1.3
A02	0.0	14.5	1.00	-0.5	0.0	12.8	1.00	-0.3	0.0
A03	0.0	15.3	1.00	-0.6	0.0	13.0	1.00	-0.1	0.0
A04	0.0	13.0	1.00	-0.3	0.0	12.0	1.00	-0.3	0.0
A05	0.0	13.0	1.00	0.1	0.0	11.8	1.00	-0.2	0.0
A07	0.0	13.6	1.00	0.1	0.0	12.2	1.00	-0.1	0.0
A09	0.0	15.0	1.01	-0.5	0.8	12.5	1.00	-0.2	0.0
A12	0.0	13.6	1.00	0.2	0.0	13.0	1.00	-0.3	0.0
A13	0.0	13.5	1.00	0.1	0.0	12.6	1.00	-0.3	0.0
A14	0.0	4.00	1.00	0.2	0.0	4.89	1.00	0.3	0.0
A15	0.0	12.2	1.02	0.1	0.8	11.7	1.01	-0.1	0.5
A16	0.0	11.9	1.04	0.1	2.4	11.6	1.03	-0.2	1.7
A17	0.0	6.00	1.15	0.2	5.8	7.90	1.14	-0.2	6.6

3.2.3.2 Separation of the Enantiomers of the Weak Acid Analytes with PEMEDA-BCD in Low pH BEs

In the low pH BEs, where all weak acids are nondissociated (except mandelic acid, A01), the effective mobilities became cationic even at low PEMEDA-BCD concentrations and passed the expected shallow mobility maxima, except ethosuximide (A14) and indapamide (A17) whose effective mobilities remained about one half of what was observed for the other weak acid analytes, indicating a much weaker interaction with PEMEDA-BCD. For all the analytes, their effective mobilities ranged from a low of $3\text{x}10^{-5}$ $\text{cm}^2\text{V}^{-1}\text{s}^{-1}$ in 1 mM PEMEDA-BCD to a limiting high value of $13\text{x}10^{-5}$ $\text{cm}^2\text{V}^{-1}\text{s}^{-1}$ in the 20 mM PEMEDA-BCD BEs. Typical examples of the effective mobility curves are shown in Figure 54, top panel. Despite the strong interaction of most of the analytes with PEMEDA-BCD, enantioseparation was achieved only for five of the seventeen weak acids studied, even though the β values were quite reasonable (see Table 4).

Thus, in agreement with the dictums of the CHARM model [49], both low and high pH BEs need to be explored for the separation of the enantiomers of weak acid analytes, though the separation selectivity values are typically better when the effective mobilities of the analytes can go from anionic to cationic in the high pH BEs. As typical examples, separation selectivity curves for representatives of the weak acid analytes are shown in Figure 54, bottom panel, for the low pH BEs.

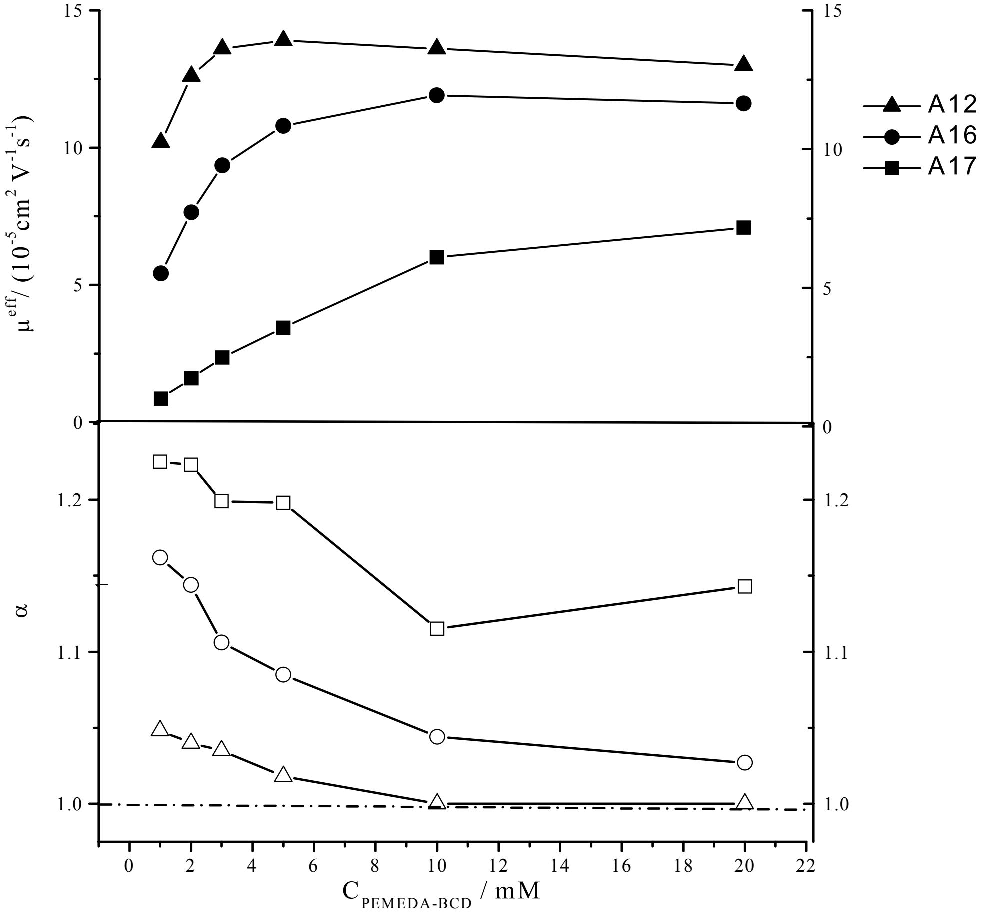

Figure 54. Typical effective mobility and separation selectivity curves for the enantiomers of weak acid analytes with PEMEDA-BCD in pH = 2.5 BEs.

3.2.3.3 Separation of the Enantiomers of Nonionic Analytes with PEMEDA-BCD in Low pH BEs

For the nonionic analytes, the effective cationic mobilities increased as the concentration of PEMEDA-BCD was increased, but remained low for the weakly complexing enantiomers, and only reaching a value of 13×10^{-5} cm^2/Vs for the more strongly complexing enantiomers in 20 mM PEMEDA-BCD BEs as shown in Table 5. Typical effective mobility curves are shown in the top panel of Figure 55, for the strongly and weakly complexing analytes.

The enantiomers of eight of the sixteen nonionic compounds tested in the low pH PEMEDA-BCD BEs were separated. It is interesting to see that only the analytes with the hydroxy group attached directly to the chiral carbon atom and one bond away from the aromatic ring were separated, indicating the influence of the aromatic ring on the inclusion complexation between the analytes and the PEMEDA-BCD. The corresponding separation selectivities increased to a maximum (at very low PEMEDA-BCD concentrations for the more strongly complexing enantiomers) and then decreased slowly as the concentration of PEMEDA-BCD was increased (Figure 55, bottom panel), in agreement with the predictions of the CHARM model [49].

Table 5.

Separation data for neutral analytes as a function of PEMEDA-BCD concentration in pH = 2.5 BE. μ in (10^{-5} cm^{2} V^{-1}s^{-1}) units.

PEMEDA-BCD (mM)	0	1				2			
U (kV)		15				10			
Analyte	μ	μ	α	β	Rs	μ	α	β	Rs
N01	0.0	1.98	1.00	4.2	0.0	3.24	1.08	1.6	0.7
N02	0.0	3.32	1.00	1.8	0.0	5.77	1.00	0.8	0.0
N03	0.0	2.29	1.00	2.7	0.0	4.28	1.00	1.3	0.0
N04	0.0	3.21	1.10	2.9	<0.6	5.05	1.08	0.7	1.1
N05	0.0	4.75	1.00	1.3	0.0	7.03	1.00	0.5	0.0
N06	0.0	5.08	1.00	1.7	0.0	7.58	1.13	0.6	<0.6
N07	0.0	3.94	1.00	1.9	0.0	6.17	1.02	0.6	<0.6
N08	0.0	3.64	1.00	2.2	0.0	6.07	1.03	0.5	4.0
N09	0.0	5.47	1.00	1.4	0.0	6.20	1.00	0.6	0.0
N10	0.0	6.06	1.00	1.4	0.0	8.45	1.00	0.6	0.0
N11	0.0	0.96	1.00	6.2	0.0	1.65	1.00	3.3	0.0
N12	0.0	0.18	1.00	12.9	0.0	0.82	1.00	4.0	0.0
N13	0.0	0.66	1.00	8.4	0.0	1.21	1.12	3.1	1.1
N14	0.0	0.30	1.00	18.3	0.0	1.31	1.13	2.9	0.8
N15	0.0	6.00	1.20	1.2	4.4	7.91	1.15	0.5	4.4
N16	0.0	1.83	1.00	4.7	0.0	3.47	1.04	1.0	<0.6

Table 5. Continued

PEMEDA-BCD (mM)	0	3				5			
U (kV)		10				10			
Analyte	μ	μ	α	β	Rs	μ	α	β	Rs
N01	0.0	5.15	1.07	0.9	0.7	7.07	1.04	0.5	1.3
N02	0.0	7.82	1.00	0.4	0.0	9.80	1.00	0.3	0.0
N03	0.0	6.58	1.00	0.8	0.0	8.75	1.00	0.6	0.0
N04	0.0	7.01	1.08	0.4	0.9	8.76	1.06	0.4	0.8
N05	0.0	9.23	1.00	0.5	0.0	11.2	1.00	0.3	0.0
N06	0.0	9.94	1.02	0.3	<0.6	11.4	1.02	0.3	<0.6
N07	0.0	8.46	1.02	0.4	<0.6	10.4	1.01	0.3	<0.6
N08	0.0	7.19	1.11	0.6	<0.6	9.77	1.02	0.4	<0.6
N09	0.0	8.61	1.00	0.3	0.0	11.4	1.00	0.3	0.0
N10	0.0	10.8	1.00	0.4	0.0	12.0	1.00	0.3	0.0
N11	0.0	2.37	1.00	1.8	0.0	3.20	1.00	1.1	0.0
N12	0.0	1.42	1.00	3.0	0.0	2.29	1.04	1.3	<0.6
N13	0.0	1.95	1.10	2.4	0.9	2.76	1.10	1.3	0.8
N14	0.0	2.28	1.11	1.5	1.4	3.05	1.11	1.2	1.3
N15	0.0	10.1	1.12	0.5	4.3	11.5	1.09	0.3	3.6
N16	0.0	5.27	1.04	0.5	<0.6	6.87	1.03	0.5	<0.6

Table 5. Continued

PEMEDA-BCD (mM)	0	10				20			
U (kV)		9				9			
Analyte	μ	μ	α	β	Rs	μ	α	β	Rs
N01	0.0	9.26	1.04	0.1	0.9	9.63	1.03	-0.4	1.2
N02	0.0	11.7	1.00	0.1	0.0	12.2	1.00	-0.3	0.0
N03	0.0	9.50	1.00	0.1	0.0	10.3	1.00	-0.3	0.0
N04	0.0	11.5	1.03	-0.1	1.5	12.1	1.02	-0.4	1.1
N05	0.0	12.5	1.00	0.1	0.0	13.2	1.00	0.3	0.0
N06	0.0	12.4	1.00	0.1	0.0	12.8	1.00	-0.3	0.0
N07	0.0	11.4	1.01	0.1	0.6	11.9	1.00	-0.3	0.0
N08	0.0	11.8	1.01	0.1	0.6	12.3	1.00	0.3	0.0
N09	0.0	12.9	1.00	0.1	0.0	12.5	1.00	-0.3	0.0
N10	0.0	12.8	1.00	0.1	0.0	13.1	1.00	-0.3	0.0
N11	0.0	6.07	1.01	-0.2	0.6	7.31	1.01	-0.6	0.6
N12	0.0	3.97	1.23	0.3	0.9	4.93	1.05	-0.6	0.6
N13	0.0	4.88	1.08	0.1	1.5	6.40	1.07	-0.6	1.1
N14	0.0	5.33	1.08	0.1	2.2	7.85	1.07	-0.5	7.3
N15	0.0	12.3	1.05	0.1	2.6	12.7	1.03	-0.3	1.9
N16	0.0	8.90	1.02	0.2	0.6	10.3	1.01	-0.3	<0.6

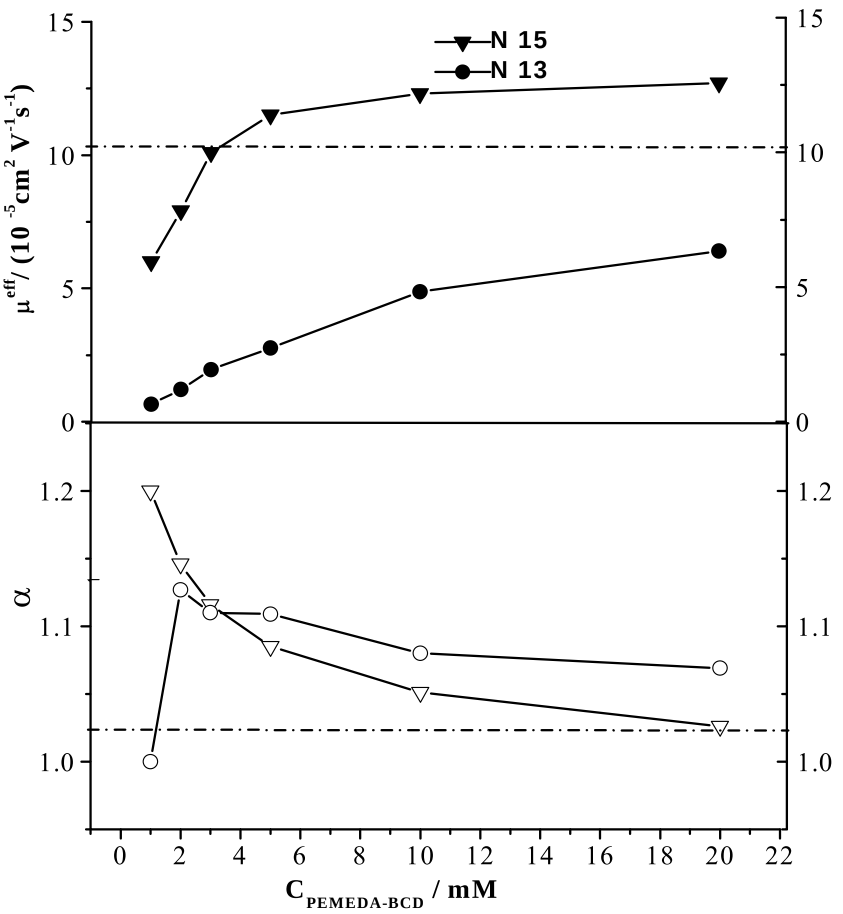

Figure 55. Effective mobility and separation selectivity curves for the enantiomers of nonionic analytes with PEMEDA-BCD in pH =2.5 BEs.

3.2.3.4 Separation of the Enantiomers of Weak Base Analytes with PEMEDA-BCD in Low pH BEs

Although PEMEDA-BCD was designed for the separation of anionic analytes, an attempt was made to separate the enantiomers of cationic analytes as well. A set of five basic test analytes was studied in low pH BEs containing various concentrations of PEMEDA-BCD. The results obtained are shown in Table 6. The effective mobilities, in the absence of PEMEDA-BCD, ranged from 21×10^{-5} cm^2/Vs to 30×10^{-5} cm^2/Vs, as expected, because at pH 2.5 all weak base analytes were protonated. Because the analytes were positively charged, they migrated in the same direction as PEMEDA-BCD, toward the cathode, and complexation was not favored due to ionic repulsion between the positively charged analytes and the positively charged chiral resolving agent. Upon addition of the chiral resolving agent into the BE, the cationic effective mobilities of the enantiomers of the five basic analytes decreased by an average of three mobility units as the concentration of PEMEDA-BCD was increased. The observed decrease in mobility could be due to the effects of increased ionic strength and viscosity. For example, the cationic mobility of methoxyphenamine (B01), dropped from 20.7 mobility unit in a BE with no chiral resolving agent to 19.0 mobility units in a 20 mM PEMEDA-BCD BE, indicating the absence of complexation between the basic analyte and the cationic chiral resolving agent. Consequently, no separation of the enantiomers was obtained for this class of analytes with PEMEDA-BCD.

Typical electropherograms for the enantiomers of strong electrolytes, weak acids, and neutral analytes obtained with PEMEDA-BCD in the low pH BE are depicted in

Figures 56 and 57. The numbers and letters beside the peaks correspond to those used to identify the analytes (see Figure 46), while the values in parenthesis indicate the concentrations of PEMEDA-BCD used to obtain the separations. Good resolutions were observed for the strong electrolytes, as well as the nonionic analytes in the low pH BE.

Table 6.

Separation data for weak base analytes as a function of PEMEDA-BCD concentration in pH = 2.5 BE. μ in (10^{-5} cm^2 V^{-1}s^{-1}) units.

PEMEDA-BCD (mM)	0			1				2	
U (kV)				18				18	
Analyte	μ	μ	α	β	Rs	μ	α	β	Rs
B01	20.7	21.1	1.00	0.3	0.0	21.2	1.00	0.2	0.0
B02	29.7	30.1	1.00	0.2	0.0	30.1	1.00	0.2	0.0
B03	23.2	24.3	1.00	0.5	0.0	24.1	1.00	0.2	0.0
B04	22.0	22.5	1.00	0.3	0.0	22.6	1.00	0.2	0.0
B05	22.2	22.8	1.00	0.3	0.0	22.6	1.00	0.2	0.0

Table 6. Continued

PEMEDA-BCD (mM)	0			5				10	
U (kV)				15				12	
Analyte	μ	μ	α	β	Rs	μ	α	β	Rs
B01	20.7	20.1	1.00	0.1	0.0	20.3	1.00	0.0	0.0
B02	29.7	28.8	1.00	0.1	0.0	26.5	1.00	0.0	0.0
B03	23.2	23.4	1.00	0.1	0.0	21.6	1.00	0.0	0.0
B04	22.0	21.3	1.00	0.1	0.0	21.1	1.00	0.0	0.0
B05	22.2	22.0	1.00	0.1	0.0	20.8	1.00	0.0	0.0

Table 6. Continued

PEMEDA-BCD (mM)	0			20	
U (kV)				12	
Analyte	μ	μ	α	β	Rs
B01	20.7	19.0	1.00	-0.1	0.0
B02	29.7	24.6	1.00	-0.1	0.0
B03	23.2	19.5	1.00	-0.2	0.0
B04	22.0	18.9	1.00	-0.1	0.0
B05	22.2	18.7	1.00	-0.1	0.0

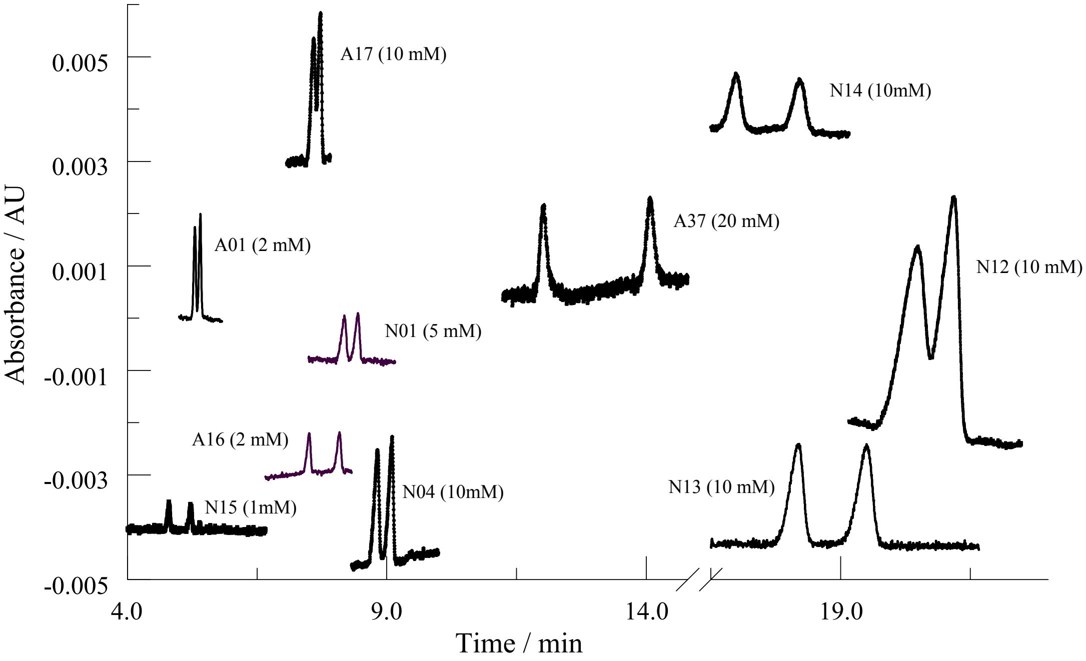

Figure 56. Typical electropherograms for the enantiomers of the weak acid and neutral analytes with PEMEDA-BCD in pH = 2.5 BEs.

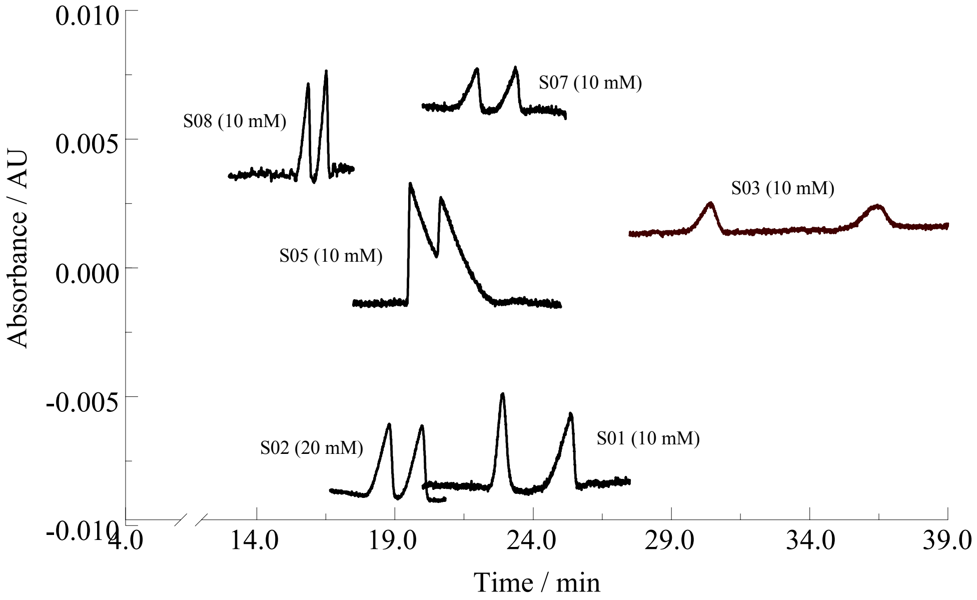

Figure 57. Typical electropherograms for the enantiomers of strong electrolytes with PEMEDA-BCD in pH = 2.5 BEs.

3.2.3.5 Separation of the Enantiomers of Weak Acid Analytes with PEMEDA-BCD in High pH BEs

Since PEMEDA-BCD showed excellent enantiorecognition for both strong electrolytes and nonionic analytes in the low pH BE, there was good reason to extend the studies to high pH where all the weak acids will be deprotonated, which might lead to favorable conditions for chiral resolution. Table 7 shows the results obtained for the weak acid test analytes in the high pH PEMEDA-BCD BEs. It is well known [49] that separation selectivities for weak electrolyte analytes can be different in their dissociated and nondissociated forms (i.e., the separations can be desionoselective, ionoselective and duoselective [49]). Therefore, the weak acid analytes were tested both in the pH = 2.54 BEs (Table 4), where they were nondissociated (except mandelic acid, A01), and in the pH = 9.30 BEs, where they were fully dissociated (except indapamide, A17). In the high pH BE, in the absence of PEMEDA-BCD, the effective mobilities of the weak acid analytes varied in the - (22 to 35) x 10^{-5} cm^2 $V^{-1}s^{-1}$ range, which is reasonable in light of their structure and charge.

For the group of the 2-phenylacetic acid derivatives (A01 to A03), the effective mobilities remained highly anionic for the hydrophylic 2-hydroxy derivative (A01), even at a PEMEDA-BCD concentration of 20 mM, while the effective mobilities of the 2-cyclopentyl (A02) and 2-cyclohexyl (A03) derivatives became cationic even with such a low PEMEDA-BCD concentration as 3 mM. At a high enough PEMEDA –BCD concentration (above 5 mM), the effective mobilities of A02 and A03 became close to each other, and slightly decreased with increasing PEMEDA-BCD concentration, due

Table 7.

Separation data for weak acid analytes as a function of PEMEDA-BCD concentration in pH = 9.3 BE. μ in $(10^{-5}\ \mathrm{cm}^2\ \mathrm{V}^{-1}\mathrm{s}^{-1})$ units.

PEMEDA-BCD (mM)	0	1				3			
U (kV)		18				15			
Analyte	μ	μ	α	β	Rs	μ	α	β	Rs
A01	-35.4	-32.1	1.00	-0.2	0.0	-27.9	1.02	-0.1	<0.6
A02	-24.2	-3.14	1.20	-2.6	1.3	1.86	0.88	2.3	1.6
A03	-23.2	1.84	0.56	8.0	1.5	5.71	0.94	0.7	1.0
A04	-28.6	-28.4	1.00	-0.4	0.0	-22.6	1.03	-0.2	1.2
A05	-23.4	6.37	1.00	0.8	0.0	9.21	0.94	0.4	1.0
A06	-23.4	5.41	0.98	1.1	0.6	8.48	1.00	0.4	0.0
A07	-23.2	2.19	0.91	2.5	1.5	5.76	0.98	0.9	<0.6
A08	-22.7	-3.32	1.10	-1.9	1.5	1.04	0.85	3.5	1.1
A09	-24.1	-2.86	1.11	-2.1	1.3	1.40	0.86	2.9	0.9
A10	-21.9	-1.92	1.09	-4.4	<0.6	4.94	0.97	0.8	<0.6
A11	-30.0	-21.1	1.01	-0.3	<0.6	-13.9	1.05	-0.2	1.5
A12	-27.5	-16.1	1.05	-0.5	1.0	-5.89	1.16	-0.6	4.7
	-27.5	-14.3	1.04	-0.5	0.7	N/A	N/A	N/A	N/A
A13	-27.6	-18.8	1.05	-0.4	1.6	-4.42	1.16	-0.5	4.8
A16	-27.5	-20.1	1.02	-0.4	1.3	-13.1	1.06	-0.2	1.7
A17	-7.9	-4.46	1.04	-1.8	1.8	-2.93	1.16	-0.8	3.8

Table 7. Continued

PEMEDA-BCD (mM)	0	5				10			
U (kV)		15				12			
Analyte	μ	μ	α	β	Rs	μ	α	β	Rs
A01	-35.4	-25.1	1.03	-0.1	1.1	-18.1	1.05	0.1	1.4
A02	-24.2	4.21	0.95	0.4	1.1	4.00	0.97	0.5	0.8
A03	-23.2	6.54	0.95	0.3	1.1	5.56	0.98	0.3	0.9
A04	-28.6	-14.8	1.05	-0.2	1.6	-13.4	1.08	0.2	1.1
A05	-23.4	9.10	0.99	0.3	<0.6	8.79	1.00	0.2	0.0
A06	-23.4	8.80	1.00	0.23	0.0	7.62	1.00	0.3	0.0
A07	-23.2	6.78	1.00	0.4	<0.6	5.71	1.00	0.3	0.0
A08	-22.7	3.06	0.94	0.7	1.1	3.68	0.97	0.5	0.8
A09	-24.1	3.97	0.96	0.4	0.9	3.93	0.98	0.5	0.7
A10	-21.9	6.31	0.99	0.2	0.7	5.50	1.00	0.3	0.0
A11	-30.0	-10.5	1.05	-0.1	2.2	-5.79	1.08	0.4	3.2
A12	-27.5	N/A	N/A	N/A	N/A	2.12	0.90	1.2	1.9
	-27.5	N/A	N/A	N/A	N/A	1.15	0.77	2.2	3.4
A13	-27.6	N/A	N/A	N/A	N/A	0.81	0.65	3.1	4.1
A16	-27.5	-9.45	1.08	-0.2	3.6	3.75	0.81	0.7	1.30
A17	-7.9	N/A	N/A	N/A	N/A	6.83	0.47	4.5	6.9

Table 7. Continued

PEMEDA-BCD (mM)	0			20	
U (kV)				10	
Analyte	μ	μ	α	β	Rs
A01	-35.4	-17.6	1.06	-0.1	2.0
A02	-24.2	N/A	N/A	N/A	N/A
A03	-23.2	N/A	N/A	N/A	N/A
A04	-23.2	N/A	N/A	N/A	N/A
A05	-23.4	N/A	N/A	N/A	N/A
A06	-23.4	N/A	N/A	N/A	N/A
A07	-23.2	N/A	N/A	N/A	N/A
A08	-22.7	N/A	N/A	N/A	N/A
A09	-24.1	N/A	N/A	N/A	N/A
A10	-21.9	N/A	N/A	N/A	N/A
A11	N/A	N/A	N/A	N/A	N/A
A12	-27.5	2.46	0.96	0.3	1.4
	-27.5	1.89	0.91	0.4	2.9
A13	-27.6	1.59	0.87	0.5	3.1
A16	-27.5	4.00	0.84	0.2	4.5
A17	-7.9	8.95	0.75	0.3	9.7

to the increased ionic strength and viscosity of the BE. This migration behavior suggests that hydrophobic interactions are important for A02 and A03, and are stronger for the 2-cyclohexyl derivative (A03) than for the 2-cyclopentyl derivative (A02).

For the profens (A04 to A10), 2-phenylpropionic acid (A04) showed a surprisingly weak interaction with PEMEDA-BCD: its effective mobility went from -28 mobility units at 0 mM PEMEDA-BCD to only -13 mobility units at 10 mM PEMEDA-BCD, while ibuprofen (A05) and flurbiprofen (A06) went from an initial value of about -23 mobility units at 0 mM PEMEDA-BCD to about 7 mobility units at 10 mM PEMEDA-BCD. Though the other profens (fenoprofen, A07, ketoprofen, A08, naproxene, A09 and carprofen, A10) interacted a little less strongly with PEMEDA-BCD than ibuprofen and flurbiprofen, their effective mobilities also became cationic by 10 mM PEMEDA-BCD. For all the profens that eventually migrated cationically, the cationic effective mobilities passed a shallow maximum as the PEMEDA-BCD concentration was increased, again as a result of the increased ionic strength and increased viscosity of the BEs. The rest of the weak acid analytes studied (A11 through A17) have more varied structural features and cannot be as readily categorized as the 2-phenylacetic acid and 2-phenylpropionic acid derivatives. For some of them, such as A11, the effective mobilities remained anionic in the entire PEMEDA-BCD concentration range, for others, such as A16, the interactions between the analyte and PEMEDA-BCD were as strong as for the profens.

As far as separation selectivity and peak resolution go, both α and Rs are at their best values in the vicinity of the PEMEDA-BCD concentration where the anionic effective mobility becomes cationic. This is in agreement with the predictions of the CHARM model [49], corrected for ionic strength effects [44]. Typical examples of the effective mobility curves and separation selectivities are shown in Figure 58 (the top and bottom panels, respectively) for the strongly, moderately, and weakly binding enantiomers.

Typical electropherograms for the enantiomers of the weak acid, obtained with PEMEDA-BCD in pH 9.3 BE are shown in Figure 59. The values on the left column in the figures represent the concentration of PEMEDA-BCD for the electropherograms in that row, the numbers and the letters beside the peaks correspond to those used in Figure 46 to identify the analytes. The anantiomers of all the weak acids were resolved in the high pH BE with PEMEDA-BCD.

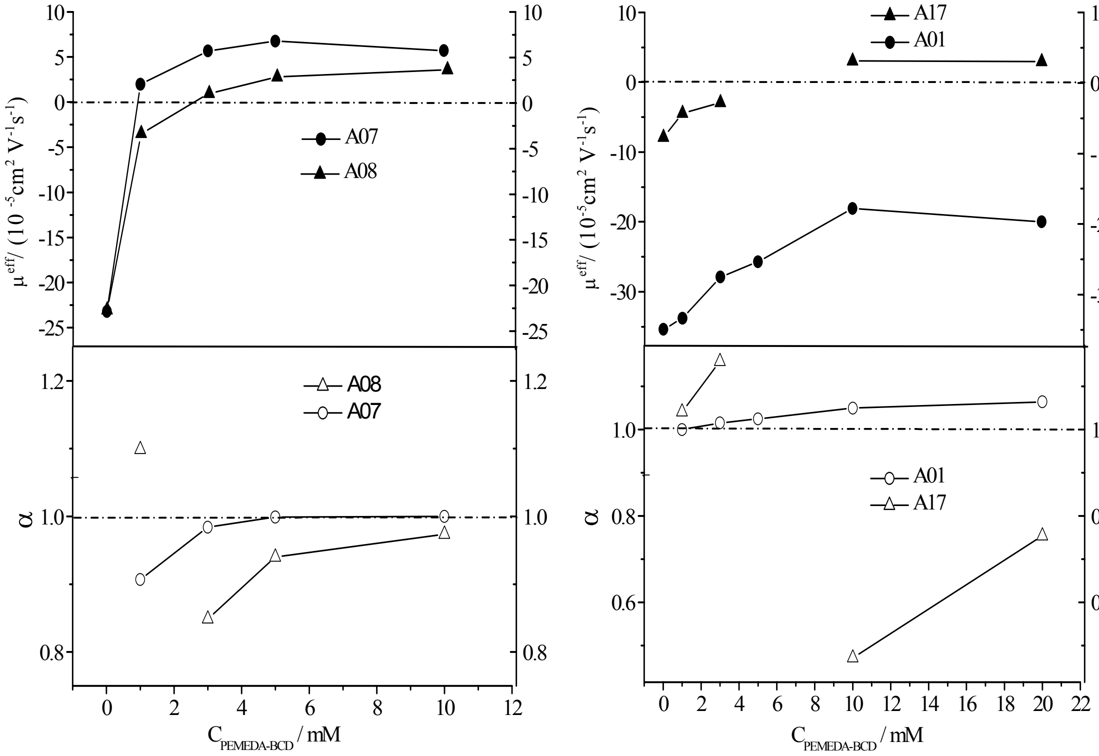

Figure 58. Effective mobilities and separation selectivities for the enantiomers of weak acids with PEMEDA-BCD in pH = 9.3 BEs. Left: strongly binding analytes (effective mobility: top panel and separation selectivity: bottom panel). Right: moderately binding and weakly binding analytes (effective mobility: top panel and separation selectivity: bottom panel).

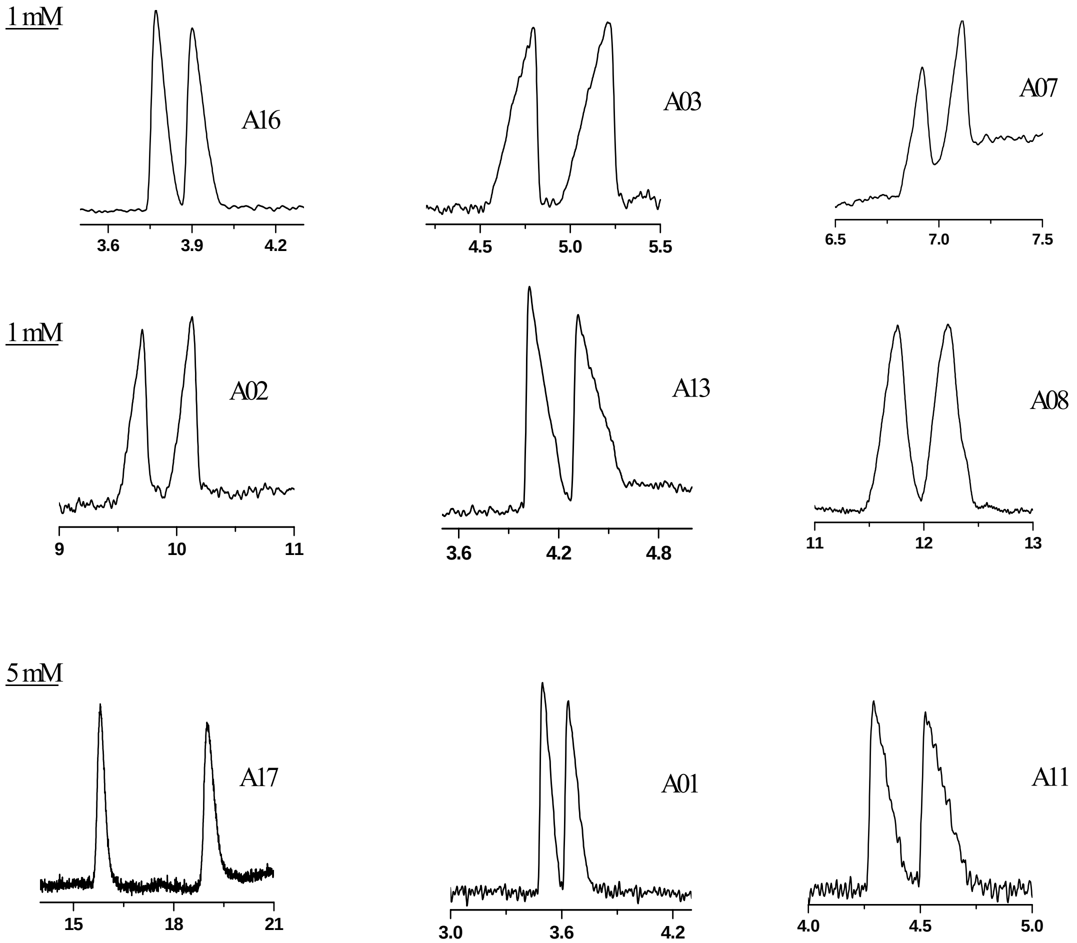

Figure 59. Typical electropherograms for the enantiomers of weak acid analytes with PEMEDA-BCD in pH = 9.3 BEs.

3.2.3.6 Separation of the Enantiomers of Ampholytic Analytes with PEMEDA-BCD in High pH BEs

A series of ampholytic analytes whose ionization states depend on the pH of the BE was studied using PEMEDA-BCD. At pH 9.3, all ampholytic analytes were deprotonated, anionic, allowing for increased ionic interactions between them and the chiral resolving agent. Table 8 shows the results obtained for the twelve dansylated ampholytic test analytes studied with PEMEDA-BCD. Initially, in the BEs without PEMEDA-BCD, all enantiomers of this group of analytes had anionic effective mobilities ranging from –17.3 mobility unit for DNS-caprylic acid to –34.0 mobility units for DNS-glutamic acid. This agrees with data already reported for this group of analytes in their fully deprotonated forms [76]. Following the addition of PEMEDA-BCD into the BE, the anionic effective mobilities of the analytes decreased. Similarly to what was observed for the weak acid analytes, the anionic effective mobilities continued to decrease with an increase in the PEMEDA-BCD concentration, crossed the zero mobility line, became cationic, and reached 9.3 x 10^{-5} $cm^2 V^{-1}s^{-1}$, except for DNS-aspartic acid and DNS-glutamic acid, which have two negative charges in the high pH BEs. As the concentration of PEMEDA-BCD was increased, the mole fraction of the analyte-charged CD complex also increased. This, in turn, increased the cationic effective mobility of the analyte-charged CD complex. However, for the doubly negatively charged analytes, the increase in mole fraction did not translate to an equal increase in the positive effective charge because the PEMEDA-BCD has only

Table 8.

Separation data for ampholytic analytes as a function of PEMEDA-BCD concentration in pH = 9.3 BE. μ in (10^{-5} cm^2 V^{-1}s^{-1}) units.

PEMEDA-BCD (mM)	0			1				3	
U (kV)				18				15	
Analyte	μ	μ	α	β	Rs	μ	α	β	Rs
Z01	-18.6	-14.2	1.03	-0.5	1.3	-5.74	1.10	-0.4	2.7
Z02	-23.0	-14.2	1.02	-0.5	1.0	-6.48	1.05	-0.5	2.2
Z03	-24.0	-15.7	1.01	-0.6	<0.6	-9.96	1.01	-0.4	0.6
Z04	-28.4	-16.7	1.07	-0.4	5.3	-11.4	1.22	-0.3	12.5
Z05	-25.3	-17.9	1.00	-0.5	0.0	-10.9	1.00	-0.2	0.0
Z06	-33.7	-25.0	1.03	-0.3	0.9	-13.7	1.06	-0.2	1.5
Z07	-17.3	-12.7	1.03	-0.6	1.6	N/A	N/A	N/A	N/A
Z08	-23.4	-15.7	1.02	-0.5	0.8	-8.01	1.07	-0.3	1.5
Z09	-23.2	-16.0	1.02	-0.5	1.3	-8.31	1.04	-0.3	1.4
Z10	-34.0	-26.4	1.01	-0.4	<0.6	-15.2	1.03	-0.2	1.8
Z11	-24.8	-16.0	1.01	-0.5	0.8	-7.81	1.04	-0.2	0.9
Z12	-18.2	-14.6	1.02	-0.5	0.6	-7.53	1.04	-0.4	0.9

Table 8. Continued

PEMEDA-BCD (mM)	0			5				10	
U (kV)				15				12	
Analyte	μ	μ	α	β	Rs	μ	α	β	Rs
Z01	-18.6	N/A	N/A	N/A	N/A	2.29	0.95	2.4	1.1
Z02	-23.0	N/A	N/A	N/A	N/A	8.78	0.97	0.6	1.2
Z03	-24.0	-6.34	1.02	-0.3	1.5	-2.15	1.14	-2.1	2.1
Z04	-28.4	-8.94	1.33	-0.2	12.8	N/A	N/A	N/A	N/A
Z05	-25.3	-5.16	1.00	-0.1	0.0	N/A	N/A	N/A	N/A
Z06	-33.7	-10.8	1.07	-0.3	2.4	-9.22	1.04	-0.6	1.3
Z07	-17.3	N/A	N/A	N/A	N/A	2.92	0.75	2.3	3.7
Z08	-23.4	-5.37	1.12	-0.3	2.8	-1.64	1.34	-2.3	2.1
Z09	-23.2	-5.51	1.08	-0.4	2.5	-1.01	1.41	-3.7	2.1
Z10	-34.0	-12.2	1.03	-0.2	1.3	-10.3	1.04	-0.5	1.4
Z11	-24.8	-6.56	1.06	-0.3	2.2	-2.04	1.24	-2.0	3.2
Z12	-18.2	N/A	N/A	N/A	N/A	-0.11	2.64	-14.3	1.4

Table 8. Continued

PEMEDA-BCD (mM)	0			20	
U (kV)				12	
Analyte	μ	μ	α	β	Rs
Z01	-18.6	2.09	0.95	0.6	1.2
Z02	-23.0	6.63	0.81	0.2	10.3
Z03	-24.0	N/A	N/A	N/A	N/A
Z04	-28.4	N/A	N/A	N/A	N/A
Z05	-25.3	N/A	N/A	N/A	N/A
Z06	-33.7	-7.41	1.05	-0.6	2.8
Z07	-17.3	5.16	0.91	0.1	3.4
Z08	-23.4	N/A	N/A	N/A	N/A
Z09	-23.2	0.39	0.91	3.2	0.6
Z10	-34.0	-8.57	1.03	-0.5	1.3
Z11	-24.8	N/A	N/A	N/A	N/A
Z12	-18.2	1.54	0.95	0.3	1.3

two positive charges. Thus, DNS-aspartic acid and DNS-glutamic acid could not migrate cationically irrespectively of the concentration of PEMEDA-BCD used. Structural differences also affected the degree of complexation between the analytes and the chiral resolving agent. For example, dinitrophenylalanine, the only ampholytic analyte without the dansyl group showed the weakest complexation with PEMEDA-BCD. However, it is interesting to see that DNS-phenylalanine, having an unsubstituted aromatic ring close to the chiral center showed the strongest complexation with PEMEDA-BCD among all the ampholytic analytes, indicating the role of the unsubstituted aromatic ring in the inclusion complexation [83,100]. In general, the enantiomers of the twelve ampholytic analytes can be classified into three groups: (1) strongly complexed enantiomers whose effective mobilities became cationic in the 0 mM to 10 mM PEMEDA-BCD concentration range, (2) moderately strongly binding analytes whose effective anionic mobilities became cationic in the 10 mM to 20 mM PEMEDA-BCD concentration range, and (3) weakly binding analytes whose effective mobilities remained anionic all through the PEMEDA-BCD concentration range studied. Figure 60, top panel, shows typical effective mobility plots for the enantiomers of each class of ampholytic analytes.

The corresponding separation selectivities show trends similar to what were observed before, the maximum values occur at the region where the effective mobilities cross the zero mobility line (Figure 60, bottom panel), except for DNS-aspartic acid and DNS-glutamic acid.The enantiomers of all twelve ampholytic analytes were resolved in the pH 9.3 PEMEDA-BCD BE, except for the enantiomers of DNS-methionine. DNS-valine showed the highest separation selectivity values, and as expected, the doubly charged DNS-glutamic acid exhibited the lowest separation selectivity values in the PEMEDA-BCD BE.

Typical electropherograms for the enantiomers of the ampholytic analytes obtained by using PEMEDA-BCD, pH 9.3, BEs are shown in Figure 61. The values on the left column in the figure represent the concentration of PEMEDA-BCD for the electropherograms in that row, the numbers and the letters beside the peaks correspond to those used in Figure 46 to identify the analytes. Excellent resolution was obtained for several of these analytes. The anantiomers of eleven of the twelve ampholytic analytes were resolved in the high pH BE with PEMEDA-BCD.

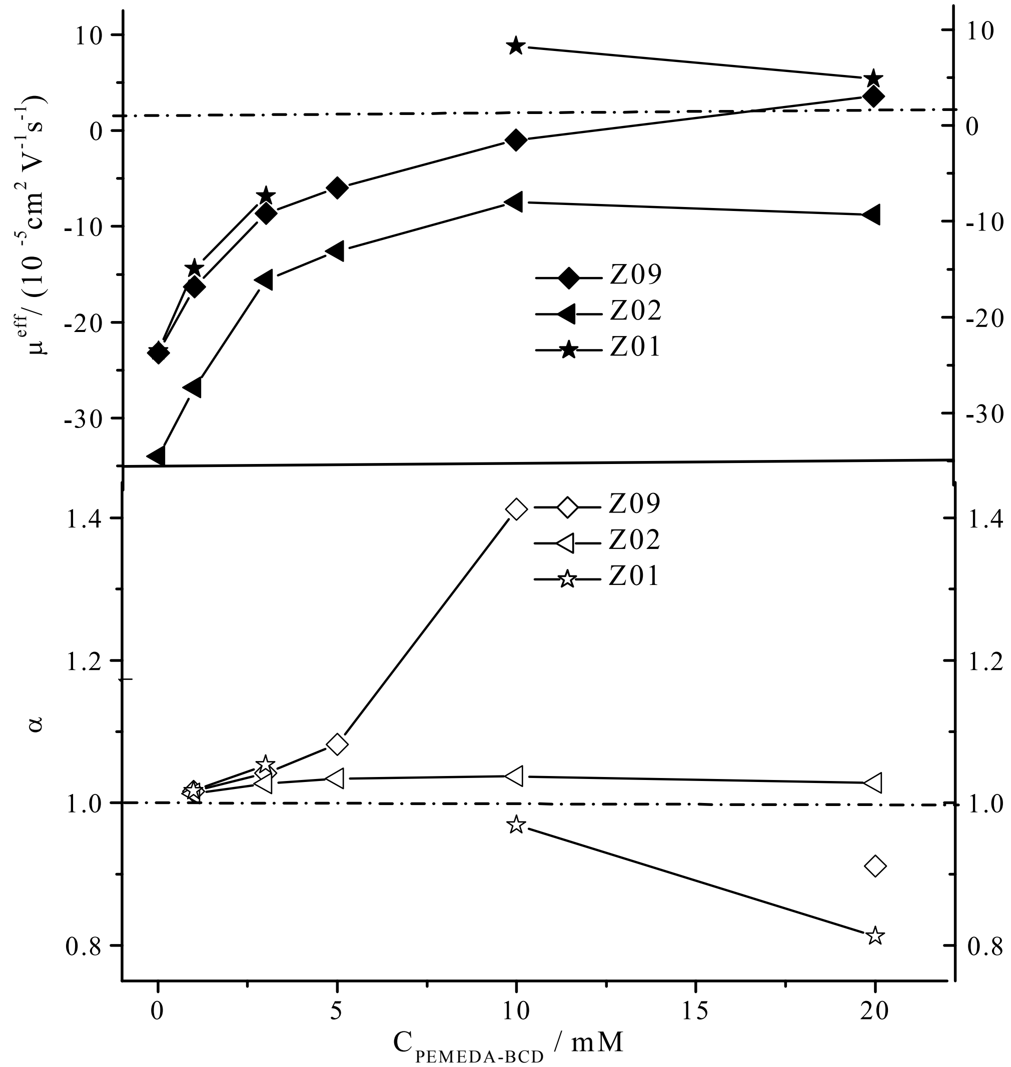

Figure 60. Effective mobility and separation selectivity curves for the enantiomers of the ampholytic analytes with PEMEDA –BCD in pH 9.3 BEs.

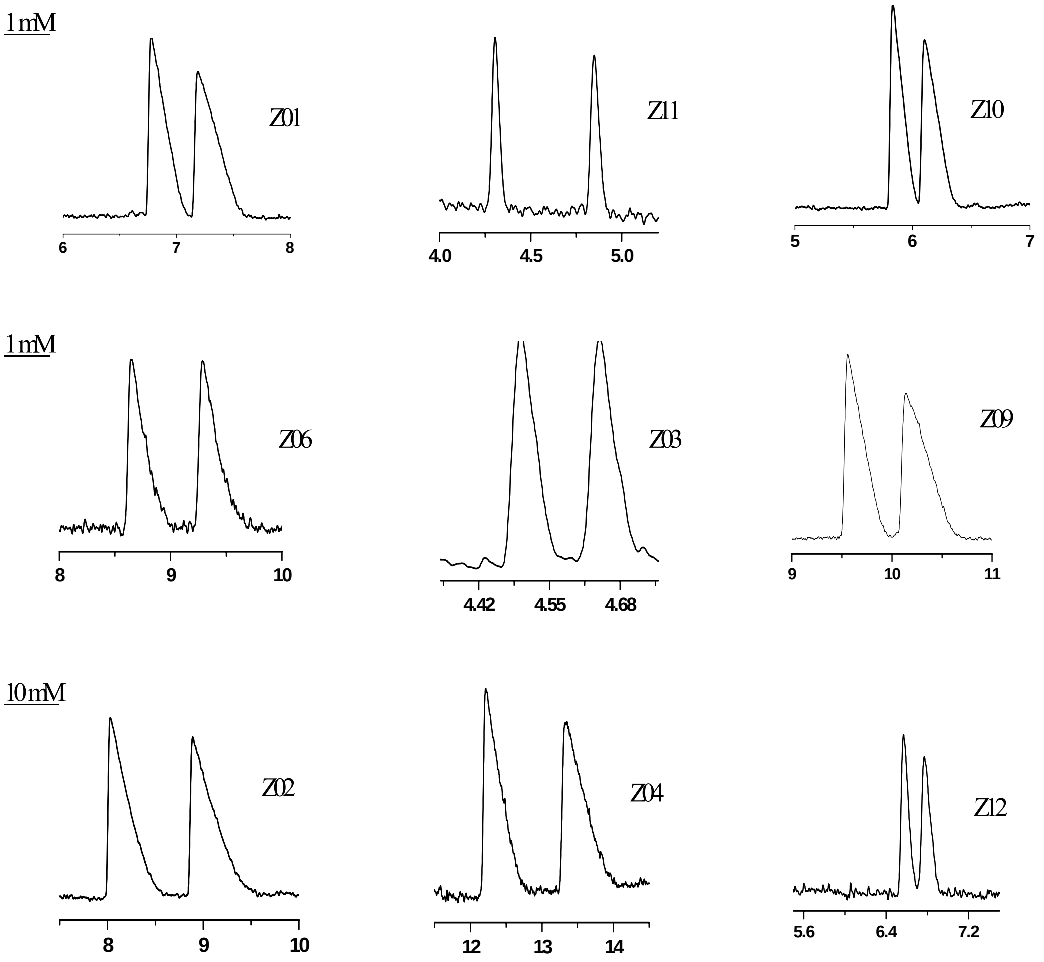

Figure 61. Typical electropherograms for the enantiomers of ampholytic analytes with PEMEDA-BCD in pH = 9.3 BEs.

3.2.3.7 Separation of the Enantiomers of Nonionic Analytes with PEMEDA-BCD in High pH BEs

Table 9 shows the values obtained for the separation of the enantiomers of nine nonionic analytes with PMEDA-BCD in high BE. At 1 mM PEMEDA-BCD concentration, all analytes migrated cationically due to complexation with the chiral resolving agent. Two distinctive types of separations were observed for this group of analytes: (1) weakly binding analytes whose cationic effective mobilities varied in the range (0.5 to 4.5) x 10^{-5} $cm^2 V^{-1}s^{-1}$, and (2) strongly binding analytes with effective mobilities starting at about 5 x 10^{-5} $cm^2 V^{-1}s^{-1}$ in 1 mM to 10 x 10^{-5} $cm^2 V^{-1}s^{-1}$ in 20 mM PEMEDA-BCD concentration BEs. Figure 62, top panel, shows representative mobility curves for each type of separation.

The separation selectivities for the enantiomers of the strongly binding analytes shown in Figure 62, bottom panel, decreased with an increase in the concentration of PEMEDA-BCD, in agreement with the predictions of the CHARM model [49]. The separation selectivities for the enantiomers of the weakly binding analytes increased initially, then decreased slowly to a shallow minimum as the concentration of PEMEDA-BCD was increased in the BE. High separation selectivities and favorable beta values, resulted in separation of the enantiomers of several nonionic analytes studied in the pH 9.3 PEMEDA-BCD BEs.

Typical electropherograms for the neutral analytes obtained by using PEMEDA-BCD, pH 9.3, BEs are shown in Figure 63. The values on the left column in

Table 9.

Separation data for nonionic analytes as a function of PEMEDA-BCD concentration in pH = 9.3 BE. μ in (10^{-5} cm^2 $V^{-1}s^{-1}$) units.

PEMEDA-BCD (mM)	0	1				3			
U (kV)				18				15	
Analyte	μ	μ	α	β	Rs	μ	α	β	Rs
N01	0	1.73	1.21	3.2	1.4	4.24	1.09	0.6	1.1
N04	0	2.51	1.24	2.0	1.3	5.75	1.10	0.6	1.2
N07	0	3.41	1.03	2.1	1.6	6.78	1.05	0.4	1.3
N08	0	3.04	1.19	1.9	1.8	6.33	1.14	0.5	2.5
N12	0	0.37	1.00	20.3	0.0	1.30	1.04	1.9	0.6
N13	0	0.51	1.00	14.2	0.0	1.27	1.12	2.0	1.7
N14	0	0.69	1.07	10.4	<0.6	1.56	1.13	1.6	1.8
N15	0	3.99	1.22	1.9	4.6	7.82	1.12	0.3	5.8
N16	0	6.08	1.05	0.9	2.0	9.02	1.05	0.3	2.8

Table 9. Continued

PEMEDA-BCD (mM)	0			5				10	
U (kV)				15				12	
Analyte	μ	μ	α	β	Rs	μ	α	β	Rs
N01	0	5.34	1.06	0.4	1.1	7.00	1.04	0.3	1.6
N04	0	6.43	1.07	0.3	1.6	7.33	1.05	0.5	0.8
N07	0	7.79	1.03	0.3	0.8	8.62	1.01	0.2	0.6
N08	0	7.12	1.09	0.3	2.3	7.57	1.05	0.5	1.3
N12	0	1.46	1.08	1.4	0.8	1.77	1.09	1.1	1.3
N13	0	1.57	1.17	14	2.1	2.02	1.15	0.9	2.5
N14	0	1.98	1.18	1.0	2.7	2.99	1.14	0.6	2.6
N15	0	8.57	1.09	0.3	4.4	9.49	1.05	0.1	2.6
N16	0	9.67	1.02	0.2	1.2	9.80	1.01	0.4	0.6

Table 9. Continued

PEMEDA-BCD (mM)	0			20	
U (kV)				10	
Analyte	μ	μ	α	β	Rs
N01	0	7.82	1.03	0.0	1.5
N04	0	7.60	1.03	0.4	1.2
N07	0	8.77	1.01	0.2	2.2
N08	0	7.66	1.02	0.4	3.0
N12	0	1.83	1.12	2.1	1.0
N13	0	2.34	1.13	1.4	1.8
N14	0	4.15	1.09	0.1	4.3
N15	0	9.70	1.03	0.0	2.0
N16	0	9.91	1.01	0.4	1.0

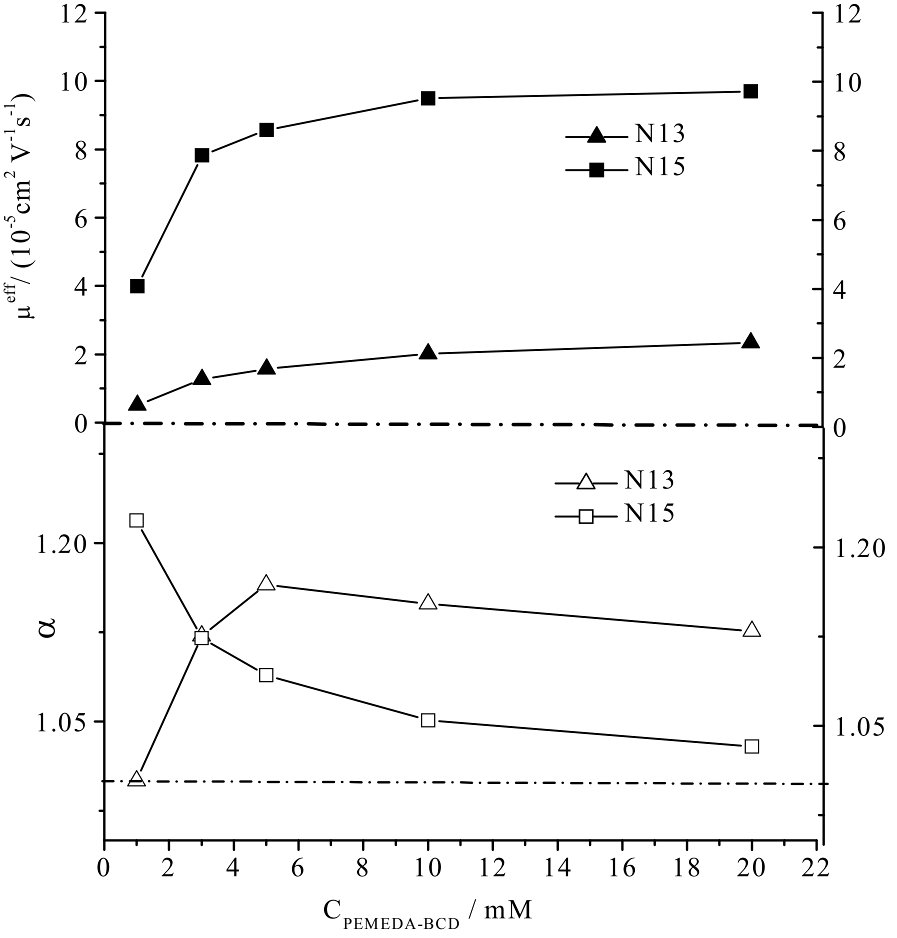

Figure 62. Effective mobility and separation selectivity curves for the enantiomers of nonionic analytes with PEMEDA-BCD in pH 9.3 BEs.

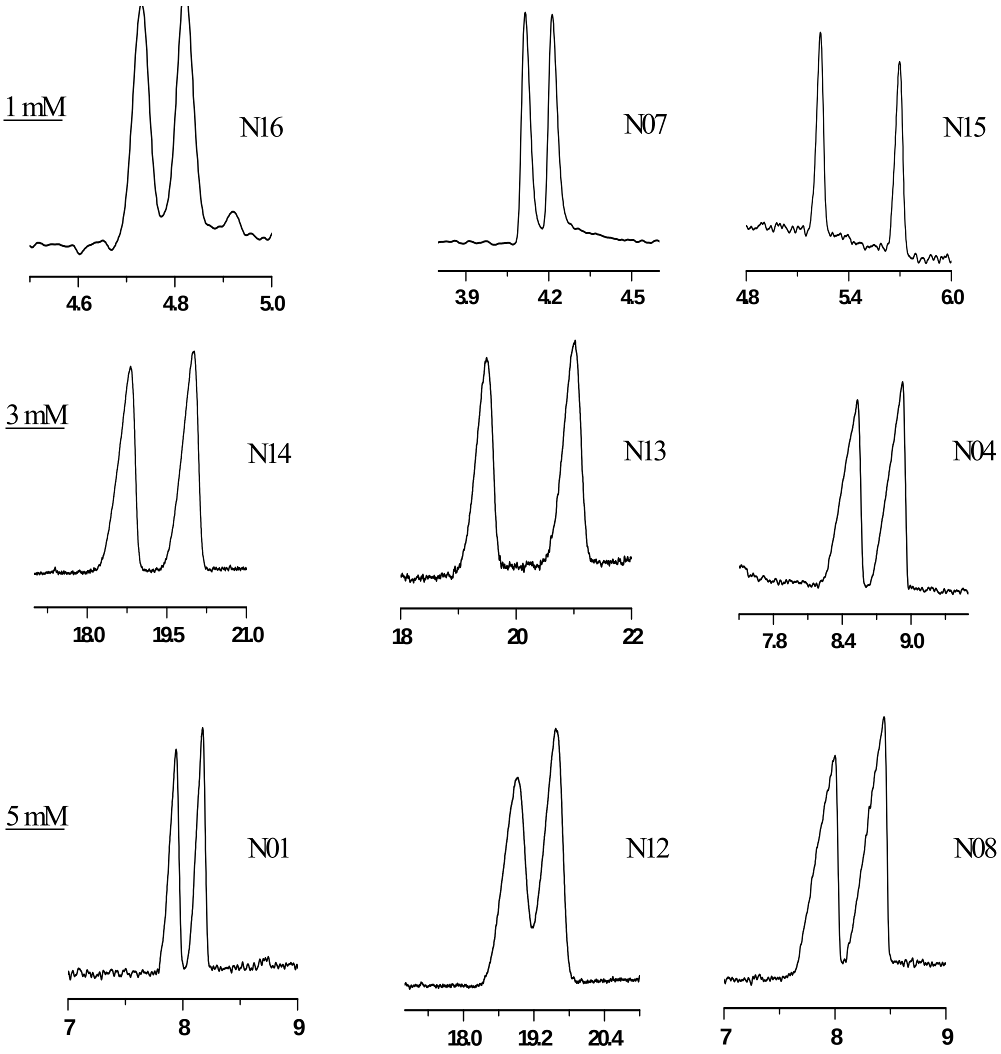

Figure 63. Typical electropherograms for the enantiomers of nonionic analytes with PEMEDA-BCD in pH = 9.3 BEs.

the figure represent the concentration of PEMEDA-BCD for the electropherograms in that row, the numbers and the letters beside the peaks correspond to those used in Figure 46 to identify the analytes. Over 85% of the neutral analytes were resolved in the high pH BE with PEMEDA-BCD.

3.2.4 Comparison of Separation of Enantiomers with HMBCD and PEMEDA-BCD BEs

In principle, with all things being equal, the higher the number of charges on the chiral resolving agent, the higher the peak resolution [49]. The major difference between HMBCD and PEMEDA-BCD is the number of charges they carry: the former has seven positive charges at the C-6 positions, while the later has one C-6 position substituted with a doubly positively charged group. Undoubtedly, the region around the cavity of CD is more crowded on HMBCD than on PEMEDA-BCD, which might lead to different interactions between the analytes and the chiral resolving agents. Figure 64 (top panel) shows the mobility plots obtained with HMBCD and PEMEDA-BCD for two anionic analytes (isomers of the newly synthesized phenylsulfopropane). It is interesting to see that their effective mobility trends are similar in shape, indicating similar complexation mechanism, with rapid decrease of the anionic effective mobility, reaching the limiting values as the concentration was increased. However, in the 5 mM PEMEDA-BCD BE, the anionic effective mobilities have already crossed the zero mobility line, and became cationic to level off at 20 mM PEMEDA-BCD concentration. For the HMBCD BE, the effective mobilities of the anionic analytes remained anionic all through concentration range studied, indicating that the binding constants for the analytes with HMBCD are lower as a result of unfavorable steric influence on the inclusion of the analytes into the CD cavity.

The enantiomers of both analytes were resolved with each of the two chiral resolving agents, HMBCD and PEMEDA-BCD. The corresponding separation selectivity plots (Figure 64, bottom section) show that separation selectivity increased to a maximum at the region where the anionic effective mobilities crossed the zero mobility line for the PEMEDA-BCD system, but for the HMBCD system, selectivity dropped to a minimum, then increased slightly at higher CD concentrations. According to Wren [101] the optimum concentration of the chiral selector for a pair of enantiomers is related to the stability constants, K, of the diastereomeric complexes by the equation:

$$C = \frac{1}{\sqrt{K_1 K_2}} \tag{12}$$

Since low concentrations of PEMEDA-BCD were sufficient to obtain separation of the enantiomers of the anions, the stability constants of the diastereomeric complexes of PEMEDA-BCD with the anionic analytes could be said to be high compared to the stability constants of diastereomeric complexes of HMBCD.

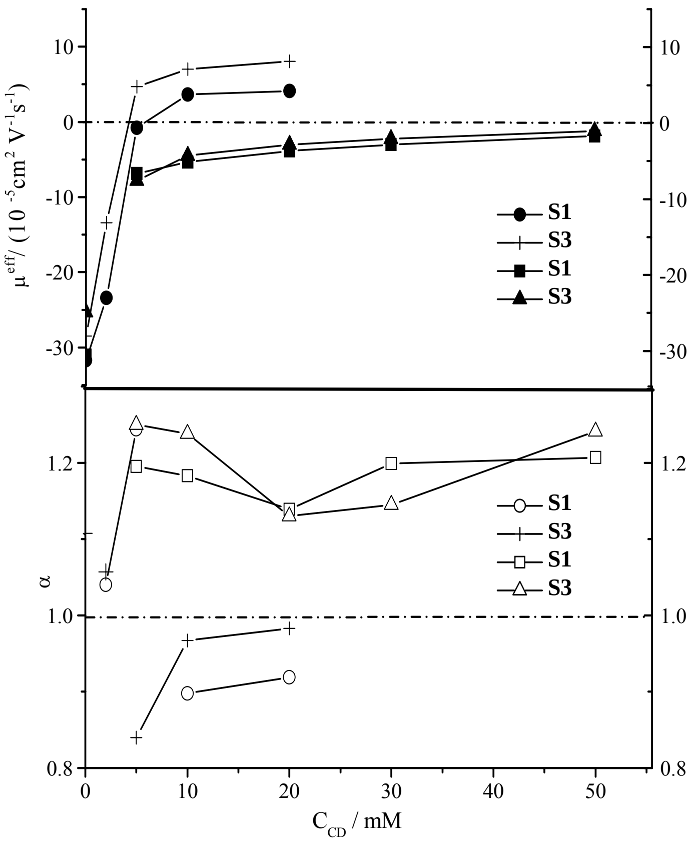

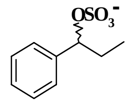

S1: 1-Phenyl-1-O-sulfo-propane

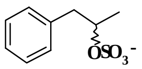

S3: 1-Phenyl-2-O-sulfo-propane

Figure 64. Comparison of separation of enantiomers with HMBCD (block and triangle) and PEMEDA-BCD (circle and cross) BEs.

CHAPTER IV

CONCLUSIONS

Permanently charged anionic single isomers of cyclodextrins (CD), in addition to resolving a broad array of chiral compounds, are important in the understanding of the interactions between the chiral selector and the analyte as well as simplifying optimization of enantiomer separations. Only small number of anionic chiral compounds were however resolved with these anionic cyclodextrins at high CD concentrations. This limitation has made the understanding of the separation behavior of the anionic compounds difficult. The need for a permanently charged cationic chiral resolving agent has led to the synthesis of two new products, heptakis(6-deoxy-6-morpholinio)-β-cyclodextrin chloride (HMBCD) and mono(6-deoxy-6-*N,N,N′,N′,N′*-pentamethylethylenediammonio)-β-cyclodextrin chloride (PEMEDA-BCD), in the family of charged single isomer cyclodextrins. Apart from their potential for enantioresolution of both neutral chiral analytes and anionic chiral analytes, introduction of positive charges on the β-CD enhances the solubility of β-CDs in aqueous media. The single-isomer cationic β-CDs can provide a very reproducible separation system.

HMBCD, PEMEDA-BCD, have been synthesized at a large scale by using direct substitution without the usual protection group technique at positions C-2 and C-3 of the CD. The key to successful synthesis of these products lies in the selective substitution of the hydroxyl groups at C-6 positions of the native β-CD with good leaving groups. The purity of each synthetic intermediate and of the final product was determined by either HPLC-ELSD or indirect UV-detection capillary electrophoresis. The chemical and structural identity of each single-isomer intermediate and final product was verified by 1D ^{1}H, ^{13}C, 2D COSY and HMQC NMR spectroscopy and also by high resolution MALDI-TOF MS and ESI-TOF MS. These complementary methods proved that HMBCD and PEMEDA-BCD are pure and have the characteristics of the targeted products.

A set of ten strong electrolytes was synthesized as test analytes to evaluate the utility of HMBCD and PEMEDA-BCD. The advantages of these new sulfated analytes are that they are permanently charged, and can be used at both low and high pH background electrolytes (BE). A series of neutral, acidic, basic and ampholytic enantiomers were also separated in aqueous BEs. It was observed that HMBCD complexed with the analytes weakly, leading to poor resolution of the enantiomers. Strong complexation was observed at low PEMEDA-BCD concentrations with the analytes.

Using HMBCD for separation of anionic analytes at high pH, it was observed that the effective mobilities decreased with increasing HMBCD concentration. The anionic effective mobility decreased from -29×10^{-5} cm^{2} V^{-1}s^{-1} to 1.3×10^{-5} cm^{2} V^{-1}s^{-1} for the multiply, positively charged HMBCD, indicating weak complexation between the analytes and HMBCD. Poor separation selectivities were observed for the enantiomers of these analytes with HMBCD. This poor separation selectivity behavior may have been caused by the steric hindrance from the multiple morpholinio substituents on the CD rim.

The utility of PEMEDA-BCD as a chiral resolving agent was first tested at low pH BE with the newly synthesized strong electrolytes. The effective mobilities decreased from –29 x 10^{-5} cm^2 $V^{-1}s^{-1}$ to 9 x 10^{-5} cm^2 $V^{-1}s^{-1}$ at 20 mM PEMEDA-BCD concentration. This is an indication of strong binding between the dicationic PEMEDA-BCD and the analytes. Excellent separation selectivies were observed for the enantiomers of the strong electrolytes and PEMEDA-BCD. Over the concentration range of PEMEDA-BCD studied in the low pH, the electroosmotic flow mobility (μ_{EOF}) ranged from –4.0 x 10^{-5} cm^2 $V^{-1}s^{-1}$ to 7.0 x 10^{-5} cm^2 $V^{-1}s^{-1}$, most of the weak acids were fully undissociated, and therefore behaved like neutral analytes. Similar separation behavior was observed for both weak acid and neutral analytes in low pH BE. Strong complexation between the nonionic analytes and PEMEDA-BCD was observed based on their cationic effective mobilities which increased with increase in PEMEDA-BCD concentration, and reached a maximum of 13.0 x 10^{-5} cm^2 $V^{-1}s^{-1}$, which is close to the effective mobility of 14.5 x 10^{-5} cm^2 $V^{-1}s^{-1}$ for the uncomplexed PEMEDA-BCD. The enantiomers of some of the nonionic analytes were resolved, but due to the low μ_{EOF} longer analysis times were observed. For the cationic analytes, no complexation was observed with the PEMEDA-BCD probably due to repulsion between the two.

In the high pH aqueous PEMEDA-BCD BE all of the weak acids were fully dissociated, and the ampholyte analytes were negatively charged. The μ_{EOF} ranged from –2 x 10^{-5} cm^2 $V^{-1}s^{-1}$ to10 * 10^{-5} cm^2 $V^{-1}s^{-1}$. The conditions favored the complexation of these analytes with PEMEDA-BCD that resulted in excellent separation of the anionic enantiomers at very low concentration of PEMEDA-BCD. In general, three types of separation trends were observed for the anionic analytes in the high pH BE. (1) For the strongly binding analytes the anionic mobilities decreased and crossed the zero mobility line and became cationic at below 3 mM PEMEDA concentration. (2) For the moderately strongly binding analytes the anionic effective mobilities crossed the zero mobility line at about 10 mM PEMEDA-BCD concentration. (3) For the weakly binding analytes the anionic effective mobilities decreased but did not cross the zero mobility line in the PEMEDA-BCD concentration range studied. This observed separation behavior is in agreement with the predicted behavior of separation of anionic enantiomer with charged chiral resolving agents reported in ref. 49. For the nonionic analytes in the high pH PEMEDA-BCD BE the observed behavior resembled that seen with PEMEDA-BCD in the low pH aqueous BE: the cationic effective mobilities increased with an increase in the PEMEDA-BCD concentration. However, shorter analysis time for the same concentrations of PEMEDA-BCD was observed in high pH than in low pH BE due to an increase in the μ_{EOF} at high pH. In comparison, better separation selectivities were seen for the high pH BE than for the low pH BE in all groups of analytes studied because of the favorable β values.

Based on the number of charges, one would have thought that the HMBCD would bind the analytes more strongly than the PEMEDA-BCD. Contrary to the predictions, PEMEDA-BCD, having fewer positive charges, showed stronger complexation with the anions then HMBCD, and offered excellent enantioresolution.

This observed trend could only be attributed to the difference in the number of substituents on the cyclodextrin rim. Because only one glucose unit is substituted on PEMEDA-BCD and the substitution on the HMBCD is on seven glucose units, the area around the CD cavity is less crowded in PEMEDA-BCD than in HMBCD. Since the CD cavity is essential for enantioresolution [98], steric hindrance by the substituents would lead to poor enantioresolution.

REFERENCES

[1] S. C. Stinson, Chem. Eng. News 72 (1994) 38.

[2] E. Thall, J. Chem. Ed. 73 (1996) 481.

[3] J. Alasandro, J. Pharm. Biomed. Anal. 14 (1996) 807.

[4] W. Lindner, Chromatographia, 24 (1987) 97.

[5] D. Armstrong, Anal. Chem. 59 (1987) 84A.

[6] K. G. Lynam, E. C. Nicolas, J. Pharm. Biomed. Anal. 11 (1993) 1197.

[7] S. Birmbaum, S. Nilsson, Anal. Chem., 64 (1992) 2872.

[8] A. Berthod, S. Chang, D. Armstrong, Anal. Chem. 64 (1992) 395.

[9] S. Han, Y. Han, D. Armstrong, J. Chromatogr. 441 (1986) 128.

[10] J. Snopek, I. Jelinek, E. Smolkova-Keulemansova, J. Chromatogr. 438 (1988) 211.

[11] M. Gazdag, G. Szepesi, L. Huszar, J. Chromatogr. 351 (1986) 128.

[12] I. E. Valko, H. Siren, M. L. Riekkola, J. Microcol. Sep. 11 (1999) 199.

[13] J. H. Knox, I. H. Grant, Chromatographia 24 (1987) 135.

[14] B. Chankvetadze, J. Chromatogr. A 792 (1997) 269.

[15] B. Chankvetadze, Trends Anal. Chem. 18 (1999) 485.

[16] A. Rizz, Electrophoresis 22 (2001) 3079.

[17] D. W. Armstrong, Y. Tang, T. Ward, M. Nicholas, Anal. Chem. 65 (1993) 1114.

[18] W. L. Hinze, T. E. Reihi, D. W. Armstrong, J. of Chromatogr. B 686 (1996) 103.

[19] H. Nishi, J. Pharm. Biomed. Anal. 13 (1995) 1483.

[20] G. Blaschke, B. Chankvetadze, J. Chromatogr. A 875 (2000) 3.

[21] S. Fanali, J. of Chromatogr. A 875 (2000) 89.

[22] M. Fillet, P. Hubert, J. Crommen, J. Chromatogr. A 875 (2000) 123.

[23] B. Koppenhoefer, X. Zhu, A. Jakob, S. Wuerthner, B. Lim, J. Chromatogr. A 875 (2000) 135.

[24] Cyclobond Handbook-A Guide to Using Cyclodextrin Bonded Phases, Advanced Separation Technologies, Whippany, NJ. 8 1995.

[25] C. Dette, S. Ebel, S. Terabe, Electrophoresis 15 (1994) 799.

[26] J. Szeman, K. Ganzler, A. Salgo, J. Szejtli, J. Chromatogr. A 728 (1996) 423.

[27] A. P. Croft, R. A. Butsch, Tetrahedron 39 (1983) 1417.

[28] D. W. Armstrong, W. Li, C. D. Chang, J. Pitha, Anal. Chem. 62 (1990) 914.

[29] K. H. Gahm, A. M. Stalcup, Anal. Chem. 67 (1995) 19.

[30] C. Desiderio, S. Fanali, J. Chromatogr. A 716 (1995) 183.

[31] B. Chankvetadze, G. Endresz, G. Blaskchke, J. Capil. Electrophor. 5 (1995) 235.

[32] G. M. Janini, G. M. Muschik, H. J. Isaaq, Electrophoresis 17 (1996) 1575.

[33] B. Chankvetadze, G. Endresz, G. Blaskchke, Chem. Soc. Rev. 25 (1996) 141.

[34] G. Weseloh, H. Bartsch, W. A Konig, J. Microcolumn. Sep. 7 (1995) 355.

[35] J. B. Vincent, G. Vigh, J. Chromatogr. A 816 (1998) 233.

[36] J. B. Vincent, G. Vigh, J. Chromatogr. A 817 (1998) 105.

[37] S. Terabe, Trends Anal. Chem. 8 (1989) 129.

[38] G. Galaverna, R. Corradini, A. Dossena, R. Marchelli, G. Vecchio, Electrophoresis 18 (1997) 905.

[39] J. B. Vincent, D. M. Kirby, T. V. Nguyen, Gy. Vigh, Anal. Chem. 69 (1997) 4419.

[40] H. Cai, T. V. Nguyen, Gy. Vigh, Anal. Chem. 70 (1998) 580.

[41] W. Zhu, Gy. Vigh, Electrophoresis 22 (2001) 1394.

[42] W. Zhu, Gy. Vigh, Anal. Chem. 72 (2000) 310.

[43] M. B. Busby, O. Maldonado, Gy. Vigh, Electrophoresis 23 (2002) 456.

[44] D. K. Maynard, Gy. Vigh, Carbohydr. Res. 328 (2000) 277.

[45] S. Li, G. Vigh, Electrophoresis 24 (2003) 2487.

[46] S. Li, G. Vigh, Electrophoresis 25 (2004) 1201.

[47] S. Li, G. Vigh, Electrophoresis 25 (2004) 2657.

[48] M. B. Busby, G. Vigh, Electrophoresis 26 (2005) 1978.

[49] B. A. Williams, G. Vigh, J. Chromatogr. A 777 (1997) 295.

[50] Y. Matusi, O. Okimoto, Bull. Chem. Soc. Jpn. 51 (1978) 3030

[51] R. C. Petter, J. S. Salek, J. Am. Chem. Soc. 109 (1987) 7897.

[52] R. C. Petter, J. S. Salek, T. Sikorski, G. Kumaravel, F. T. Lin, J. Am. Chem. Soc. 112 (1990) 3860.

[53] H. Yamamura, Y. Yamada, R. Miyag, K. Kano, S. Araki, M. Kawai, J. Incl. Phenom. and Macrocyclic Chemistry 45 (2003) 211.

[54] Y. Matsui, A. Okimoto, Bull. Chem. Soc. Jpn. 51 (1978) 3030.

[55] K. Hamasaki, H. Ikeda, A. Nakamaru, A. Ueno, F. Toda, I. Suziki, T. Osa, J. Am. Chem. Soc. 115 (1993) 5035.

[56] K. Kano, T. Kitae, H. Takashima, J. Incl. Phenom. and Molecular Recognition in Chemistry 25 (1996) 243.

[57] F. Lelievre, C. Gueit, P. Gareil, Y. Bahaddi, H. Galons, Electrophoresis 18 (1997) 891.

[58] T. Kitae, H. Takashima, K. Kano, J. Incl. Phenom. and Macrocyclic Chemistry, 33 (1999) 345.

[59] T. L. Wang, L. L. Yuan, S. F. Li, J. Chromatogr. A 1013 (2003) 19.

[60] A. M. Abushoffa, M. Fillet, A. C. Servais, P. Hubert, J. Crommen, Electrophoresis 24 (2003) 343.

[61] R. Sebesta, M. Salisova, Enantiomer 4 (1999) 271.

[62] P. Mikus, D. Kaniansky, R. Sebesta, M. Salisova, Enantiomer 4 (1999) 279.

[63] R. Ivanyi, L. Jicsinszky, Z. Juvancz, N. Roos, K. Otta, J. Szejtli, Electrophoresis 25 (2004) 2675.

[64] H. Yamamura, A. Akasaki, Y. Yamada, K. Kano, T. Katsuhara, S. Araki, M. Kawai, T. Tsuda, Electrophoresis 22 (2001) 478.

[65] V. Cucinotta, A. Giuffrida, D. La Mendola, G. Maccarrone, A. Puglisi, E. Rizzarelli, G. Vecchio, J. Chromatogr. B 800 (2004) 127.

[66] G. Galaverna, S. Sforza, T. Tedeschi, R. Corradini, A. Dossena, R. Marchelli, Electrophoresis 24 (2003) 2698.

[67] V. Cucinotta, A. Giuffrida, G. Grasso, G. Maccarrone, G. Vecchio, Analyst 128 (2003) 134.

[68] R. Breslow, M. F. Czarnbiecki, J. Emert, H. Hamaguchi J. Am. Chem. Soc. 102 (1980) 762.

[69] A. Nardi, A. Elisev, P. Bocek, S. Fanali, J. Chromatogr. 638 (1993) 247.

[70] U. B. Nair, D. W. Armstrong, Microchemical Journal 57 (1997) 199.

[71] G. Galaverna, M. C. Paganuzzi, R. Corradini, A. Dossena, R. Marchelli, Electrophoresis 22 (2001) 3171

[72] R. P. Bonomo, V. Cucinotta, F. D'Alessandro, G. Impellizzeri, G. Maccarrone, G. Vecchio, E. Fizzarelli, Inorg. Chem. 30 (1991) 2708.

[73] B. Di Blasio, S. Galdiero, M. Saviano, G. De Simone, E. Benedetti, C. Pedone, W. A. Gibbons, R. Deschenaux, E. Rizzarelli, G. Vecchio, Supramol. Chem. 7 (1996) 47.

[74] G. Galaverna, R. Corradini, A. Dossena, R. Marchelli, G. Vecchio, Electrophoresis 18 (1997) 905.

[75] G. Galaverna, R. Corradini, A. Dossena, R. Marchelli, Electrophoresis 20 (1999) 2619.

[76] H. Yamamura, Y. Kawase, M. Kawai, Y. Butsugan, Bull. Chem. Soc. J. 66 (1993) 585.

[77] A. Gadelle, J. Defaye, Angew. Chem. Int. Ed. Engl. 30 (1991) 78.

[78] W. Tagaki, H. Yamamoto, Tetrahedron Lett. 32 (1991) 1207.

[79] H. M. Parrotlopez, C. C. Ling, P. Zhang, A. Baszkin, G. Albrecht, C. Derango, A. W. Coleman, J. Am. Chem. Soc. 114 (1992) 5479.

[80] K. Kano, T. Kitae, Y. Shimofuri, N. Tanaka, Y. Mineta, Chemistry – A European J. 6 (2000) 2705.

[81] O. Zerbinati, F. Trotta, Electrophoresis 24 (2003) 2456.

[82] N. Budanova, E. Shapolova, S. Lopatin, V. Varlamov, O. Shpigun, Electrophoresis 25 (2004) 2795.

[83] J. L. Haynes, S. A. Shamsi, F. O'Keefe, R. Darcey, I. M. Warner, J. Chromatogr. A. 803 (1998) 261.

[84] D. Lee, S. A. Shamsi, Electrophoresis 23 (2002) 1314.

[85] Y. Tanaka, S. Terabe, J. Chromatogr. 781 (1997) 151.

[86] F. Wang, M. G. Khaledi, Electrophoresis 19 (1998) 2095.

[87] D. H. Russell, R. D. Edmundson, J. Mass Spectrom. 32 (1997) 263.

[88] W. K. Russell, D. H. Russell, M. B. Busby, A. Kolberg, S. Li, D. K. Maynard, S. Sanchez-Vindas, W. Zhu, G. Vigh, J. Chromatogr. A 914 (2001) 325.

[89] H. H. Baer, A. V. Berenguel, Y. Y. Shu, J. Defaye, A. Gadelle, F. S. Gonzalez, Carborhydr. Res. 228 (1992) 307

[90] P. R Ashton, R. Koniger, J. F. Stoddart, D. Alker, V. D. Harding, J. Org. Chem. 61 (1996) 903

[91] F. O'Keeffe, S. A. Shamsi, R. Darcy, P. Schwinte, I. M. Warner, Anal. Chem. 69 (1997) 4773.

[92] B. L. May, S. D. Kean, C. J. Easton, S. F. Lincoln, J. Chem. Soc.-Perkin Trans. 1 (1997) 3157.

[93] N. Zhong, H. Byun, R. Bittman, Tetrahedron Lett. 39 (1998) 2919.

[94] S. Lalwani. E. Shaves, H. C. Fleisher, K. Nzeadibe. M. B. Busby, G. Vigh, Electrophoresis 25 (2004) 2128.

[95] S. Fanali, E. Camera, Chromatographia 43 (1996) 247.

[96] F. Lelievre, P. Gariel, A. Jardy, Anal. Chem. 69 (1997) 385.

[97] S. Li, G. Vigh, Electrophoresis 25 (2004) 2657.

[98] B. A. Williams, G. Vigh, Anal. Chem. 69 (1997) 4445.

[99] B. A. Williams, G. Vigh, Anal. Chem. 68 (1996) 1174.

[100] Q. Liu, T. Inoue, J. R. Kirchhorff, C. Huang, L. M. V. Tillekeratne, K. Olmstead, R. A. Hudson, J. Chromatogr. A. 1033 (2004) 349.

[101] S. A. C. Wren, R. C. Rowe, J. Chromatogr. A 603 (1992) 235.

APPENDIX

SYNTHESIS PROTOCOL FOR SINGLE-ISOMER QUATERNARY AMMONIUM CYCLODEXTRINS

Synthesis of Heptakis(6-deoxy-6-iodo)- β-cyclodextrin

1. Dry native β-cyclodextrin in the vacuum oven at 90°C to a constant weight.
2. Dissolve 40.1 g of $(C_6H_5)_3P$ in 160 mL of DMF at room temperature while stirring. Set the reaction flask in an oil bath at room temperature.
3. Slowly add 40.5 g of I_2 into the flask. This process is exothermic, so do not let the temperature go above 50 °C.
4. Slowly add 11.6 g of dry β-cyclodextrin into the flask. This process is very exothermic, so do not let the temperature rise above 50 °C during the addition.
5. Maintain the heat to the flask in the oil bath at 70 °C for 18 hours.
6. Prepare a 3 M sodium methoxide solution by carefully dissolving 4.2 g of sodium in 60 mL of methanol with cooling.
7. After 18 hours, evaporate the reaction mixture down to 100 mL, using a high vacuum pump connected to the rotavap.
8. Slowly add the 3 M solution of sodium methoxide to the reaction flask with cooling and stirring. Continue stirring for 15 min.
9. Pour the reaction mixture into 800mL of methanol.
10. Filter off the precipitate that is formed, and collect in a beaker.
11. Dissolve the solid material in approximately 100 mL of DMF, and slowly add to it deionized water until cloudiness appears. Allow the mixture to stand, and more solids will form, leaving a clear supernatant liquid. Filter the solids out, and keep the filtrate for additional product recovery.

12. Repeat step 11 and monitor the purity of the product by normal phase HPLC, using methanol:water 95:5 mobile phase, at a flow rate of 2.0 mL / min. Typical purity > 99%.

Synthesis of Heptakis(6-deoxy-6-morpholino)-β-cyclodextrin

1. Dissolve Heptakis(6-deoxy-6-iodo)-β-Cyclodextrin (dried to a constant weight in the vacuum oven at 75 °C) in morpholine in the ratio of 1 g of CD to 17 mL of morpholine with stirring.
2. Place the flask in the oil bath and set the temperature at 65 °C for 24 hours.
3. Monitor the progress of the reaction by indirect UV-detection CE, using a 20 mM acetic acid buffer titrated to pH 4.55 with imidazole as the BE, with the UV-detector placed at the cathode.
4. The reaction is judged complete when the normalized relative peak area of the fastest migrating component is > 98%. Note: this peak migrates very close to the unreacted morpholine peak.
5. Remove the flask from the oil bath and evaporate off the excess morpholine on the high vacuum rotovap.
6. Dissolve the resulting solid in a small amount of deionized water.
7. Precipitate the solids with acetone, filter by suction using number one filter paper, and collect the solids.
8. Suspend the solids in ethanol using 1g of solids to 7mL of ethanol.
9. Digest the suspension by gentle heating to remove the brownish color.

10. Repeat steps 8 and 9 and monitor the purification by CE until the solids are white. Typical purity is about 98%.

Synthesis of Heptakis(6-deoxy-6-morpholinio)-β- cyclodextrin Iodide

1g scale

1. Dissolve 1 g of heptakis(6-deoxy-6-morpholino)-β-CD (dried to a constant weight in the vacuum oven at room temperature) using 5mL of dry 1-methyl-2- pyrrolidinone (NMP) in 25 mL, 3-neck, round bottom flask.
2. Place a small stir bar into the flask and clamp the flask in the oil bath. Attach a condenser to the flask.
3. Connect the condenser to a recirculating coolant.
4. Maintain the temperature of the oil bath at 45 °C.
5. Dropwise add 3 mL of iodomethane into the reaction flask.
6. Add 10 mg of sodium carbonate
7. Monitor the reaction by ^{1}H NMR, using D_2Oas the solvent and 500 MHz NMR as the instrument, and observe the anomeric ^{1}H around δ 5.2 ppm.
8. The reaction is judged complete when the multiple peaks in the NMR spectrum at about 5.2 ppm have disappeared leaving only one doublet for the anomeric proton.
9. Evaporate the reaction solvent under reduced pressure at 60°C to obtain a brownish paste that dissolves readily in water.

10. Precipitate the off-white solids from the aqueous solution with acetone, and subsequently recrystallize them from a methanol-ethanol mixture (~ 10 mL/g) to obtain the pure product.
11. Check the purity of the final product by indirect UV-detection CE, using 20 mM formic acid/aniline buffer, pH = 3.6, positive to negative polarity. Typical purity is about 98%.

Synthesis of Heptakis(6-deoxy-6-morpholinio)-cyclomaltoheptaose Chloride (HMBCD)

1. For a 5 g sample, use a 46 mL volume of a strong anion exchange resin.
2. Wash the anion exchanger in a beaker several times with deionized water until the wash water is clear.
3. Slowly pack the anion exchange resin in a suitable glass column.
4. Prepare 40 mL each of 1 M HCl and 1 M NaOH solutions.
5. Pour the NaOH solution into the column and using deionized water elute it at a rate of 1 mL/min.
6. Check the pH of the effluent with pH paper.
7. Continue the water wash until the effluent is neutral by pH paper. For a 5 g scale, elute another 20 mL of water after the pH paper first appeared neutral.
8. Repeat steps 5 to 7 with the acid solution.
9. Prepare another NaOH solution and repeat steps 5 to 7.
10. Dissolve the sample in a minimum amount of water and elute through the column.

11. Wash the column with deionized water until the effluent is neutral. Combine all the effluent. Collect extra 20 mL of effluent and add it to the sample.
12. Titrate the collected solution with HCl to neutral pH.
13. Evaporated the water under reduced pressure at 50 °C to obtain the pure solid product.

Synthesis of *p*-Toluenesulfonyl Anhydride (Ts_2O)

1. Add 500 mL CH_2Cl_2 into a 500 mL flask.
2. Dissolve 80 g (0.43 mol) of TsCl and 20 g (0.11 mol) of $TsOH.H_2O$ in the 500 mL CH_2Cl_2.
3. Stir the mixture for 24 hours.
4. Pour about 250 g of silica gel into a Buchner funnel, and wash with dichloromethane, using suction. Slowly filter the reaction mixture through the silica gel.
5. Reduce the volume of the solution down to 50% by evaporation.
6. Slowly add hexane to the solution to precipitate pure Ts_2O.

Synthesis of Mono(6-*O*-tosyl)-β-cyclodextrin

1. Suspend 11.5 g (10 mmol) of native β-CD and 4.9 g (15 mol) of the freshly made Ts_2O in 250 mL deionized water in a reaction flask.
2. Stir the suspension for 2 hours.
3. Add a solution of NaOH (5.0 g in 50 mL of deionized H_2O).

4. After 10 min, filter off the unreacted Ts$_2$*O* using a sintered glass funnel.
5. Add 13.4 g of NH_4Cl to the solution to bring its pH to about 8.
6. Allow the solids to precipitate out overnight at 4 °C.
7. Siphon off the supernatant liquid.
8. Wash the solids 2 times by adding 250 mL each of deionized water into the beaker containing the product. Stir the material for a few minutes and allow it to settle. Then remove the supernatant liquid. Repeat the water wash 2 times to be sure that all the salts are have been removed.
9. Repeat the washing procedure with acetone.
10. Filter and collect the white product using number one filter paper.
11. Check the purity of the material by TLC using (1) aluminum-backed Silica 60 plates and n-propanol : water : ethylacetate : ammonium hydroxide; 5:3:1:1 as the running solvent, giving an $R_f = 0.68$, and (2) an isocratic normal phase HPLC separation, using a 4.6 mm I. D. × 250 mm Zorbax silica column and a 30 : 70, ethylacetate : methanol binary mobile phase at 2.0 mL / min, at ambient temperature. Typical purity is about 98%.

Synthesis of Mono(6-deoxy-6-pyridinium)-β-cyclodextrin (CDP)

1. Add 10g (7.8 mmol) of mono(6-*O*-tosyl)-β-CD (dried to a constant weight at room temperature) into 100 mL of dry pyridine in a 500 mL flask.
2. Flush the reaction flask with dry nitrogen.
3. Place the flask on a heating mantle and raise the temperature to 70 °C.

4. Monitor the progress of the reaction by direct UV-detection CE, using a 50 mM phosphoric acid buffer titrated with lithium hydroxide to pH 2.13 as the BE, with the UV-detector placed at the cathode.
5. The reaction is judged complete when the peak area of the major component >98%.
6. Remove unreacted pyridine by evaporation, using the high vacuum rotovap.
7. Dissolve the residue in deionized water, and filter off the undissolved solids.
8. Collect the filtrate and concentrate it to about 30% of its original volume by evaporation.
9. Precipitate the solid material from the aqueous solution by slow addition of the equal volume of acetone, and collect the precipitate by filtration.
10. Repeat the precipitation procedure 3 times, or until the product becomes white, check the purity by CE. Typical purity > 98%.

Synthesis of Mono(6-deoxy-6-*N,N,N',N',N'*-pentamethylethylenediamino)- β-cyclodextrin

For a 1g scale

1. In a 3 neck ,50 mL round bottom flask, add 1.0 g (0.78 mmol) of dry mono(6-*O*-tosyl)-β-CD, and 10 mL of N,N,N'-trimethylethylenediamine. Place the reaction flask in the oil bath and stir at 60°C. Progress of the reaction can be monitored by two complementary methods; (i) indirect UV-detection CE, using a 20 mM acetic acid solution, titrated to pH 4.55 with 10 mM imidazole as the BE, and (ii) direct UV-detection CE, using 25 mM phosphoric acid titrated to pH 2.55 with lithium

hydroxide as the BE to follow the disappearance of the mono-tosylated β-CD that shows as a negative peak close to the neutral marker peak.

2. The reaction is stopped after the mono(6-*O*-tosyl)-β-CD peak has completely disappeared from the electropherogram obtained using the second monitoring procedure, which is about 12 hours.
3. Evaporate the reaction mixture to dryness under reduced pressure.
4. The resulting solids are dissolved in a minimum volume of water, and precipitated by slow addition of ethanol. Repeat the purification procedure 3 times. Check the purity by CE. Typical purity > 98%. Dry the product in a vacuum oven at room temperature.

Synthesis of Mono(6-deoxy-6-*N,N,N',N',N'*-pentamethylethylenediammonio)-β-cyclodextrin Iodide.

1. Dissolve 1 g of mono(6-deoxy-6-*N,N,N'*-trimethylethylenediamino)-β-CD in 10 mL of DMF and obtain a clear solution in a reaction flask.
2. Slowly add 5 mL of iodomethane into the reaction flask.
3. Place the flask in the oil bath. Attach a condenser to the flask, and connect the condenser to a recirculating coolant. Raise the temperature to 45 °C.
4. Monitor the progress of the reaction by indirect UV-detection CE, using a 20 mM acetic acid solution, titrated to pH 4.55 with 10 mM imidazole as the BE.
5. The reaction is judged complete when the relative area of the major component with a mobility of about 13×10^{-5}cm / Vs is greater than 98%.

6. Evaporate the reaction solvent under reduced pressure, and redissolve the residue in a minimum volume of deionized water. Slowly add acetone, about 2 times the volume of the aqueous solution, to precipitate the solid product. Collect the solids by suction filtration.
7. Repeat this procedure until the brownish solids turn to off-white. Check purity by CE. Typical purity >98%.

Synthesis of Mono(6-deoxy *N,N,N',N',N'*-6-pentamethylethylenediammonio)-cyclomaltoheptaose Chloride (PEMEDA-BCD)

1. For a 1 g sample, pour 8 mL of the anion exchange resin into the column and rinse the column with deionized water.
2. Dissolve 1 g of NaOH in 20 mL of deionized water, and elute through the column with deionized water.
3. Wash the column with more deionized water until the effluent pH is neutral pH paper.
4. Repeat steps 4 and 5 with HCl.
5. Then repeat steps 4 and 5 with NaOH.
6. Dissolve the 1 g of mono(6-deoxy-6-*N,N,N',N',N'*-pentamethylethylenediammonio)-β-cyclodextrin Iodide in 2 mL of deionized H_2O, and pour the solution into the column. Elute through the column with deionized H_2O until the effluent is neutral by pH paper. Allow 5 mL extra deionized H_2O to elute into the collection beaker after the effluent was observed to be neutral.

7. Check for the disappearance of iodide by direct UV-detection CE analysis, using a 25 mM phosphoric acid solution titrated to pH 2.55 with lithium hydroxide as the BE, and the detector at 214 nm. Run the separation with negative to positive polarity.
8. Titrate the basic solution with HCl to pH ~ 7.0
9. Evaporate water from the solution to obtain the final product.
10. Analyze the product by MALDI-TOF-MS.

Synthesis of Anionic Analytes

1. Add 1 g of the starting alcohol and 1.5 mL of DMF into a 25 mL reaction flask with stir bar.
2. Carefully add 1.25 g of sulfur trioxide pyridine complex (98%) into the reaction flask, and allow the mixture to stir at room temperature.
3. Monitor the progress of the reaction by direct UV-detection CE, using a BE containing 20 mM boric acid titrated to pH 9.0 with LiOH. The reaction is stopped when there is no more increase in the peak area of the target component.
4. Evaporate the reaction mixture to a viscous liquid at less than 50 °C.
5. Redissolve the product in small amount of deionized water, and add a 1 M NaOH solution to bring the pH 12 to 12. Immediately add the solution to an equal volume of acetone.
6. Filter off the sodium salts, using number one filter paper.

7. Evaporate the liquid from the solution at not more than 50 °C to collect the final product.

VITA

Kingsley C. I. Nzeadibe obtained his B.S. degree in Chemistry from the University of Oklahoma, Norman, Oklahoma, in December 1992, and his M.S. degree in Chemical Engineering from Louisiana Tech University, Ruston, Louisiana, in February 1997. In 2000 Kingsley received the College of Science Dean's Graduate Scholar award from Texas A&M University, College Station, Texas, where he obtained his Ph.D. in Chemistry in May 2006.

During Kingsley's career at Texas A&M University, his work produced one publication in the *Electrophoresis* and materials for more publications, a dissertation, and a patent. Kingsley also presented his research at both local and international conferences. At the 2005 IUCCP symposium, Kingsley received an award for an Outstanding Oral Presentation in the Graduate Research in Pharmaceutical Chemistry Symposium.

Kingsley can be reached at Department of Chemistry, TAMU 3255, College Station, TX 77843.